MICROSTRUCTURE AND MECHANICAL PROPERTIES OF AN AS-HOT ROLLED CARBON MANGANESE FERRITE-BAINITE SHEET STEEL.

By

Bruno Debray

A Thesis Submitted to the Faculty of Graduate Studies

and Research in Partial Fulfillment of the Requirements

for the Degree of Master of Engineering

Department of Mining and Metallurgical Engineering

McGill University

Montreal, Canada

May 1993

MICROSTRUCTURE AND PROPERTIES OF A FERRITE-BAINITE SHEET STEEL.

ABSTRACT

By means of torsion testing, the microstructures and mechanical properties produced in a 0 14%C-1 18%Mn steel were investigated over a wide range of hot rolling conditions, cooling rates and coiling temperatures The reheating temperature was varied between 800°C and 1050°C, and strains between 0 and 0 8 were applied. This led to austenite grain sizes ranging from 10 to 150μm Two cooling rates, 55°C/s and 90°C/s, were applied and cooling was interrupted at coiling temperatures ranging from 550°C to 300°C

Optical microscopy and TEM were used to study the microstructures. High cooling rates and fine austenite grain sizes produced a mixture of a first phase consisting of polygonal and/or acicular ferrite and a second phase composed of lath-like bainite and/or ferrite containing a fairly high density of carbides When the cooling rate was decreased, the second phase was replaced by pearlite A coarse austenite grain size before accelerated cooling resulted in a strongly acicular ferrite associated with a second phase composed of lath-like bainite and carbide-bearing ferrite

The mechanical properties were studied by means of tensile testing. It was found that, for a fine austenite grain size before cooling, the coiling temperature had little influence on the mechanical properties, in opposition to the cooling rate, which induced an increase of approximately 30MPa in the tensile and yield strengths when it was increased from 55°C/s to 90°C/s When a coarse austenite grain size was present before cooling, the influence of coiling temperature was increased The amount of strain was found to have little influence at the cooling rate studied, 90°C/s. This was attributed to the saturation of nucleation site density as a result of the supercooling.

A method developed by IRSID for deducing the transformation kinetics from the cooling data was adapted to the present context and used successfully to interpret the observed influence of the process parameters For fine austenite grain sizes, it was shown that the transformations were completed at temperatures above 500°C, resulting in the negligible influence of the coiling temperature Very coarse austenite grain sizes lead to considerable transformation delays, displacing the end of transformation to much lower temperatures and resulting in a strong influence of the coiling temperature.

RESUME

Les microstructures et propriétés mécaniques produites dans un acier 0.14%C-1.18%Mn sous différentes conditions de laminage et de refroidissement ont été étudiées à l'aide d'essais de torsion à chaud. Les températures de réchauffage utilisées étaient comprises entre 800°C et 1050°C pour des déformations allant de 0 à 0.8. Ces conditions se traduisaient par des tailles de grain austénitiques avant refroidissement variant entre 10µm et 150µm. Deux vitesses de refroidissement ont été utilisées, 55°C/s et 90°C/s, pour des températures de bobinage comprises entre 550°C et 300°C.

Des examens aux microscopes optique et électronique à transmission ont permis d'étudier les microstructures. Une vitesse de refroidissement élevée associée à une taille de grain austénitique fine produit une microstructure composée de ferrite polygonal et/ou aciculaire et une seconde phase composée de bainite à lattes et de ferrite contenant une densité élevée de carbures. Lorsque la vitesse de refroidissement diminue, la seconde phase est remplacée par une perlite classique. Une microstructure austénitique très grossière avant le refroidissement conduit à une ferrite très aciculaire et une seconde phase composée de bainite et de ferrite contenant une densité élevée de carbures.

Des test de traction ont été effectués. On a ainsi pu montrer que la température de bobinage avait peu d'influence sur les propriétés mécaniques lorsque la taille de grain austénitique avant le refroidissement était fine. En revanche, une augmentation de la vitesse de refroidissement de 55°C/s à 90°C/s entraine une augmentation de la résistance maximale à la traction et de la limite d'élasticité d'environ 30MPa. Une taille de grain austénitique grossière mène à un effet important de la température de refroidissement. Pour une vitesse de refroidissement de 90°C/s, on a montré que la déformation n'avait pas d'influence sur les propriétés mécaniques. Ceci a été attribué à la forte germination à l'intérieur des grains.

Une méthode de calcul des cinétiques de transformation à partir des données du refroidissement développée par l'IRSID a été adaptée au contexte de cette étude et utilisée pour interpréter les résultats obtenus. On a ainsi montré que, pour une taille de grain austénitique fine avant le refroidissement, les transformations avaient toutes lieu à des températures supérieures à 500°C. Ceci explique la faible influence de la température de bobinage. En revanche, lorsque une taille de grain grossière est présente à l'origine, les transformations se trouvent reportées vers des températures plus basses, résultant en un effet accru de la température de bobinage.

ACKNOWLEDGMENTS

I would like to express my sincere gratitude to Professor J J Jonas for giving me the opportunity to work in his research team at McGill University and for his constant encouragement

I am also very grateful to the French company SOLLAC, Flat Products Division of USINOR-SACILOR, for its financial support, and particularly to M G Rigaut, director of the Centre de Recherche des Produits à Chaud, for his trust and encouragement.

Special thanks are due to Edwin Fernandez, who, by the outstanding quality of his work in preparing the specimens and building equipment, played a great part in the success of this study He also was responsible to a considerable degree for the good atmosphere prevailing in the group

I would like to thank Dr Christine Roucoules, Prof. Paulo Cetlin and Dr Terrence Maccagno for their constant and friendly assistance.

I am grateful to Lorraine Mello and Carol Rousseau for their help regarding administrative problems

I would also like to thank my fellow graduate students, as well as the research associates and professors alongside whom I worked these eighteen months, for their friendship and the pleasant moments we shared

Enfin, je voudrais remercier mon épouse, Rose, et mes deux filles, Marina et Caroline, pour leur patience infinie et leur constant soutien au cours de ce travail.

TABLE OF CONTENTS

Table of contents

LIST OF FIGURES

LIST OF TABLES

CHAPTER I

INTRODUCTION

The present study was undertaken to respond to industrial concerns about a new type of sheet steel produced directly on hot strip mills The French company SOLLAC, the flat products division of USINOR-SACILOR, was at the origin of this project It is currently producing a high strength, high formability ferrite-bainite steel directed towards the car wheel market. Over the past few years, the demand for lighter car bodies and parts has increased, together with growing concerns about the environment and energy consumption This has resulted in the development of new high strength steels However, classical strengthening mechanisms are detrimental to the formability of steel For this reason, new solutions are being investigated One of these is based on a mixture of a soft phase, ferrite, and a hard phase, martensite for dual-phase steels, or bainite for the so-called ferrite-bainite steels Both techniques have been shown to lead to considerable increases in strength associated with good formability. However, the manufacture of dual phase steels is considerably more difficult than that of the ferrite-bainite steels. As a result, ferrite-bainite metallurgy has been chosen at SOLLAC as the basis for a new family of high strength, high formability steels.

Until now, there has been little information available on the metallurgy of ferrite-bainite steels with chemical compositions similar to the ones produced by SOLLAC. In particular, the nature of the bainite has not been investigated. Also, the effect of the various process parameters, such as finish rolling temperature, cooling rate and coiling temperature, on the properties of the steels is not known precisely. This knowledge is necessary for good control of steel quality to be achieved and for the improvement of process stability The aim of this study was thus to simulate physically the hot rolling and

accelerated cooling of ferrite-bainite steel HR55 in order to provide this missing information.

The torsion machine available in the Department of Metallurgical Engineering at McGill University is a very powerful tool for the simulation of hot rolling However, the complete process in a hot strip mill also involves accelerated cooling after hot rolling, followed by very slow cooling, which corresponds to the cooling of the steel coil at the end of the process The first objective of this work was thus to develop a technique to simulate these two cooling steps after hot deformation on the torsion machine Once this was done, the method was used to investigate the behavior of the SOLLAC HR55 ferrite-bainite steel, which contains 0 14% C and 1 2% Mn Various cooling conditions were employed to reveal the influence of cooling rate and coiling temperature The influence of deformation prior to cooling, i e., the state of the austenite before transformation, was studied by varying the reheating temperature and the amount of deformation

A literature review is first presented in Chapter II in order to clarify the context of this thesis and to evaluate the work that has been done In Chapter III, the experimental method is described In the first part, the development of the cooling device is outlined Focus is placed on the reproducibility as well as on the reliability of the temperature measurements In the second part, the choice of the experimental conditions, such as the reheating temperatures, amounts of deformation, cooling rates, and coiling temperatures, is justified In the last part, the methods used for evaluation of the mechanical properties and for the microstructural investigations are described

In Chapter IV, the results of this study are presented and they are discussed and evaluated in Chapter V In the latter chapter, a new method is developed for determining the transformation kinetics from the cooling data This method is used to interpret the observed role of the coiling temperature Finally, general conclusions are drawn in Chapter VI.

CHAPTER II

LITERATURE REVIEW

The aim of this literature review is to clarify the context of this study and to show that its objectives are of real interest in the field of the physical metallurgy of hot rolled steels As the steel studied is produced in a hot strip mill, and as the experimental work consisted of simulations of hot rolling and of the accelerated cooling taking place in such a production unit, the hot strip mill will be introduced in the first part of this review. The metallurgical events taking place in the mill and the traditional ways of strengthening steel will be discussed next Then, a closer look will be taken at the specific requirements for the steel used to manufacture car wheels This will serve as an introduction to a description of the historical development of ferrite-bainite steels The definition of bainite will be discussed, together with the role it plays in the strengthening of ferrite-bainite steels Finally, basic features of the production of ferrite-bainite steels will be examined. Previous publications regarding the influence of production parameters will be discussed and the results of this discussion will be used to bring out the achievements of this project.

II.1. The Hot Strip Mill

II.1.1. General Description

The hot strip mill can be divided into five parts· the reheating furnace, the roughing stands, the finishing stands, the accelerated cooling unit and the coiler. In what follows, the numerical data correspond to the SOLLAC-FOS hot strip mill, on which the steel studied is currently being produced according to reference 1 A schematic diagram of this mill is shown in Figure 2 1

HOT STRIP MILL

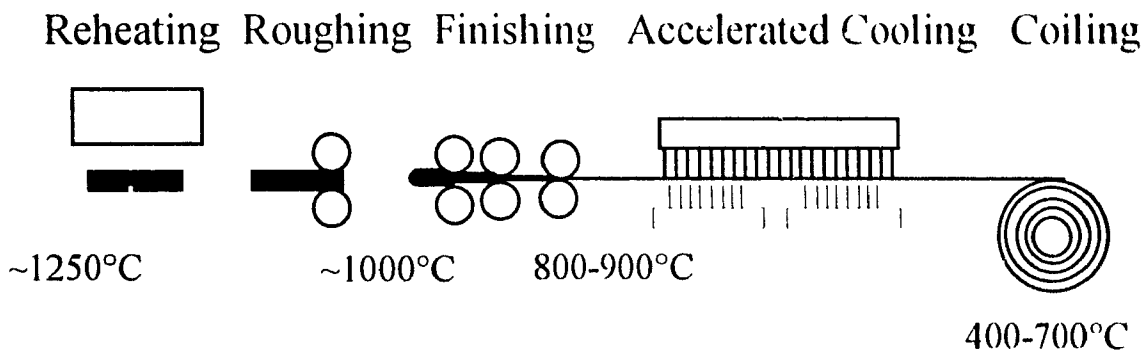

Figure 2 1 Schematic representation of a hot strip mill

In the reheating furnace, slabs are brought up to temperatures of about 1200°C[12], with the primary objective of providing a temperature high enough to permit easy deformation Roughing occurs at temperatures between 1200°C and 1100°C It involves the thickness reduction of the slab to a transfer bar 30 to 50 mm thick through five successive, independent passes in 2-high and 4-high stands Finishing takes place at temperatures between 1100°C and 800°C in seven successive finishing stands located 6 m from one another The final thickness can range from 1 5 to 15 mm During this operation, the steel is deformed simultaneously in the seven stands The temperature decreases continuously from the beginning to the end of the finishing operation The temperature of the last pass is usually called the finishing temperature

The rolling schedule in the finishing stands, i e the amount of reduction applied in each pass, depends on the final thickness Usually, the largest deformations are employed during the few first passes, leaving the last two passes for thickness and shape adjustment An example of a rolling schedule is given in reference 3 The reductions are as follows first pass, 50%, second pass, 40%, third pass, 40%, fourth pass, 35%, fifth pass, 15 %, and sixth pass, 10%. SOLLAC also provided the rolling schedule used for the type of steel

studied in the present work first pass, 60%, second pass, 53%, third pass, 47%, fourth pass, 41%, fifth pass, 28%, sixth pass, 13% and seventh pass, 6%

After the last reduction, the steel enters the runout table, where it is cooled by laminar water jets The cooling rate is determined by the strip thickness and the flow rate of the laminar sprays This can be varied continuously by computer control to provide the desired temperature at the end of the runout table This temperature is called the coiling temperature, for it corresponds to the temperature at which the steel strip is coiled During accelerated cooling, the cooling rate is not controlled However, as the temperatures at the beginning and end of the runout table are controlled, the overall cooling rate is well determined Once the steel is coiled, it cools very slowly (about 20°C/hour).

II.1.2 Metallurgical events taking place in the hot strip mill.

The final mechanical properties of a strip steel are the result of a complex transformation process which takes place in the hot strip mill and which involves strain accumulation, recrystallization, phase transformation, and sometimes precipitation, when microalloying elements are present This review will deal more particularly with C-Mn steels, leaving aside the microalloyed and other steels Only the general case will be considered, for which the steel is in the austenitic state during the complete deformation process and for which the transformation to other phases occurs on the runout table

During reheating, the main event is the growth of the austenite grains as well as general diffusion of the alloying elements Strain hardening and recrystallization take place in the rolling mill, during and after the deformation passes Phase transformations take place during accelerated cooling or in the coil.

II 1 2 a Events taking place in the deformation zone

Strain hardening is the first event occurring during deformation It corresponds to the continuous increase in flow stress with increasing strain This phenomenon is related to the generation and movement of the dislocations associated with deformation As more and more dislocations are created, interactions occur, mainly with other dislocations or grain boundaries, which limit their movement [4] The stress level necessary for this movement to occur increases accordingly The stress-strain relationship has been shown to depend mainly on temperature and strain rate [5], the stress level increasing with decreasing temperature or increasing strain rate

Restoration processes are the mechanisms by which a strained material recovers a soft or dislocation-free microstructure They are of two types dynamic processes and static processes Dynamic restoration takes place during deformation When a certain strain level is reached, dynamic recovery occurs first The rearrangement of dislocations leaves dislocation-free areas frequently called subgrains. If the strain keeps increasing, dynamic recrystallization can take place, leading to the formation of new grains The strain at which dynamic recrystallization begins is called the critical strain for dynamic recrystallization When this happens, the flow rate decreases to a steady state level, as illustrated by Figure 2 2 [6] On this graph, it can also be seen that the steady state stress as well as the peak stress and peak strain depend on the strain rate The temperature is also an influential factor In fact, it was shown by C M Sellars[7] that the peak strain can be expressed as:

$$\varepsilon_p = 6.97 \times 10^{-4} d_0^{0.3} Z^{0.17} \quad (1)$$

where

$$Z = \dot{\varepsilon} \exp(312000/RT) \quad (2)$$

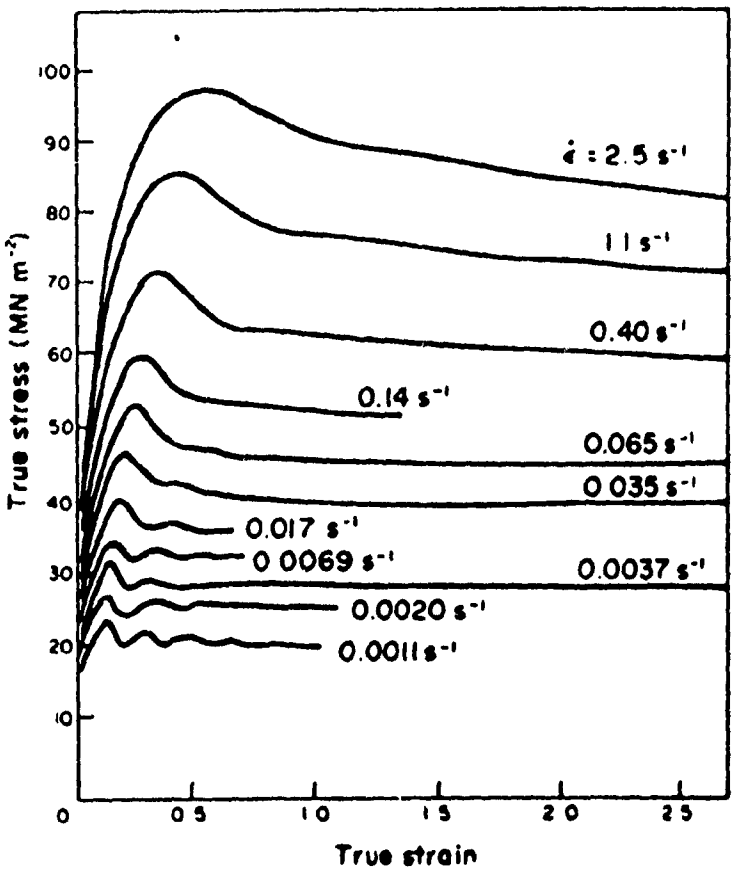

Figure 2 2: Flow curves representative of the dynamic recrystallization produced during hot torsion testing of a 0.25%C steel in the austenitic condition at 1100°C.[6]

Z being the Zener-Hollomon parameter, d_0 the initial grain size, T the temperature and $\dot{\varepsilon}$ the strain rate

The static restoration processes include recovery, static recrystallization and post-dynamic recrystallization They all occur after the end of deformation Recovery is the reorganization of the dislocations, leading to the formation of subgrains and to softening of the material. Static recrystallization involves the formation of new, dislocation-free grains It takes place when the pre-strain is less than 0 8 times the peak strain ε_p It has been shown to follow a nucleation and growth mechanism, whose kinetics can be relatively well described by the Avrami equation[8]

$$X = 1 - \exp[-0\ 693(t / t_{0.5})^k] \tag{3}$$

where X is the volume fraction recrystallized after time t. $t_{0.5}$ is the time for half recrystallization For C-Mn steels, it can be expressed as

$$t_{0.5} = 2\ 5\times 10^{-19} d_0^2 \varepsilon^{-1} \exp(300000/RT) \tag{4}$$

where ε is the applied strain

Metadynamic recrystallization occurs after dynamic recrystallization It has been extensively studied recently[9]. It was shown to differ to a large extent from static recrystallization in terms of its kinetics, which are very dependent on strain rate, instead of on strain as for static recrystallization As an example, for a Mo steel, the time for 50% recrystallization was found to obey the following equation

$$t_{50\%} = 6\ 66\times 10^{-6} \dot{\varepsilon}^{-0.61} \exp(123000/RT) \tag{5}$$

The final result of all these events is refinement of the austenite grain size and a change in the state of the austenite (i e whether it is recrystallized or not) The austenite grain size after recrystallization was modeled by various workers[10,11] Sellars gave the following equations for the rec.ystallized grain size d_{rex}, which take into account the possibility that static, dynamic or metadynamic recrystallization occurs.

$$d_{rex} = 0\,5 d_0^{0.67} \varepsilon^{-1} \quad \text{for} \quad \varepsilon \le \varepsilon^* \tag{6}$$

$$d_{rex} = 1\,8 \times 10^3 Z^{-0.15} \quad \text{for} \quad \varepsilon \ge \varepsilon^* \tag{7}$$

$$\text{where } \varepsilon^* = 2.8 \times 10^{-4} d_0^{0.67} Z^{0.15} \tag{8}$$

where Z and d_0 are the same as for equations (1) to (5)

The grain size and state of the austenite are determinant parameters for the subsequent transformations and the final properties From the previous equations, it can be seen that temperature as well as strain and strain rate play a predominant role in the conditioning of austenite However, on the hot strip mill, the strains and strain rates cannot be modified easily The main process parameter is therefore the temperature.

II 1 2 b Events taking place on the runout table

The major topic of this thesis is the transformation taking place during cooling of the steel on the runout table Figure 2 3 shows a continuous-cooling-transformation (CCT) diagram for a typical C-Mn steel It can be seen that, for low cooling rates, ferrite transformation occurs first, followed by pearlite transformation When the cooling rate is increased, the pearlite is replaced by bainite When still higher cooling rates are used, the proportion of bainite increases to the point where it completely replaces the ferrite An additional increase results in the formation of martensite The mechanisms involved are complex and, therefore, a detailed examination is not possible here. The accent will be put instead on how the process parameters can affect them

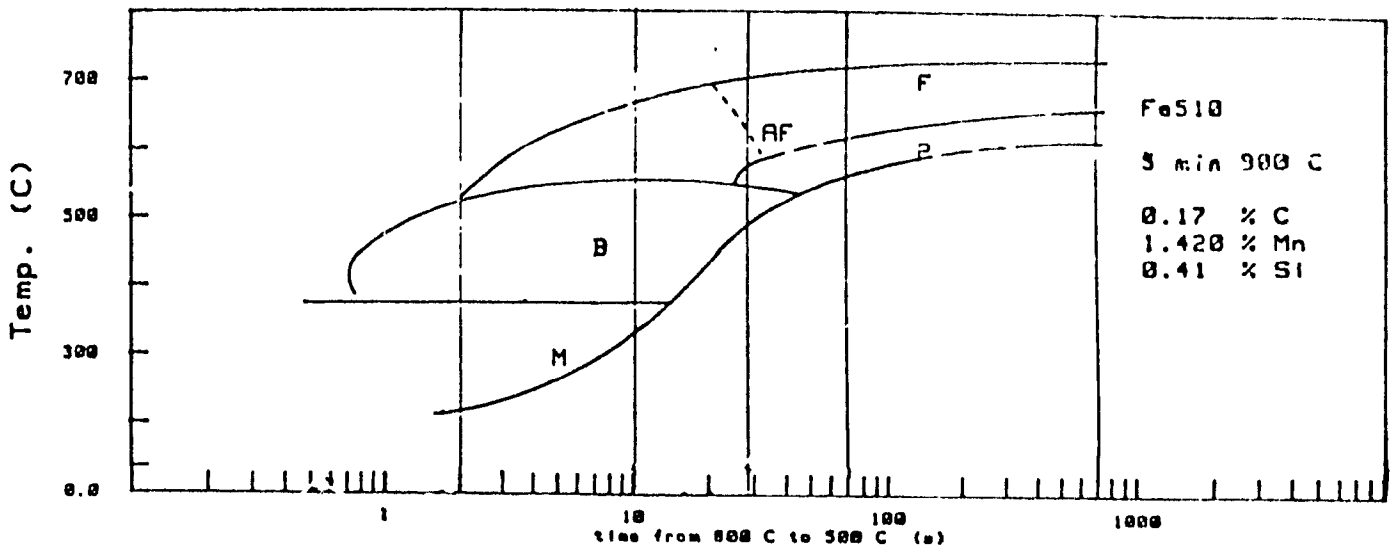

Figure 2.3: CCT diagram for a C-Mn steel (Fe 510)[12].

Ferrite transformation

The transformation from austenite to ferrite is a nucleation and growth process. The nucleation rate is affected by several parameters The classical nucleation theories [13] show that the nucleation rate increases when the temperature decreases because of an increase in the energy difference between the two phases Consequently, when the cooling rate increases, the nucleation rate also increases The nucleation of ferrite being heterogeneous, the state of austenite also greatly affects the nucleation rate For example, K. Amano et al.[14] have shown that increasing the deformation in the austenite range in a 0.15% C-1 3% Mn steel leads to an increase in the number of ferrite nuclei formed during isothermal transformation This is illustrated in Figure 2.4. The same study showed that the nucleation sites change from grain boundaries at low strains and limited supercooling to mostly grain interiors at large strains and high degrees of supercooling

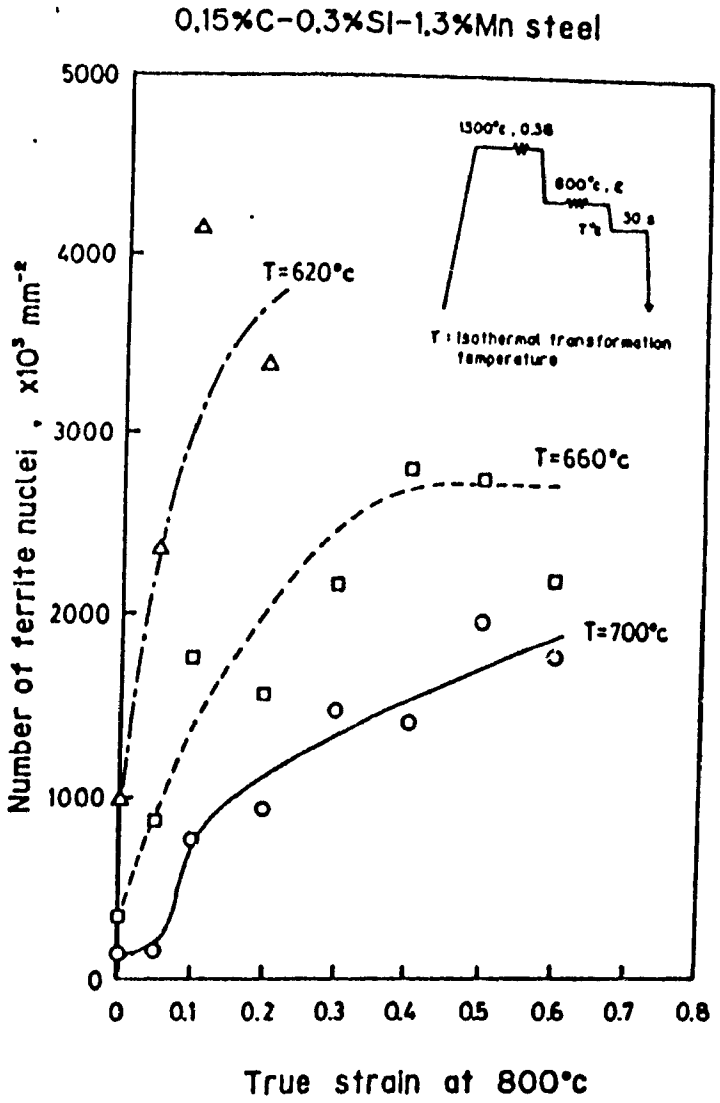

Figure 2.4 Relation between number of ferrite nuclei per unit area and true strain at 800°C as a function of isothermal transformation temperature in a 0.15%C-1.3%Mn steel [14]

This transition occurs even though the frequency of nucleation at grain boundaries is also enhanced

The nucleation sites in the grain interiors were found to be located mostly along deformation bands and twin boundaries The influence of cooling rate on ferrite nucleation was studied indirectly by investigating the evolution of ferrite grain size It was shown by the same authors that increasing the cooling rate results in a significant decrease in the final ferrite grain size, which reveals that the nucleation rate has been increased The relationship between nucleation rate and ultimate grain size was clarified by Umemoto et all[15] Complex calculations led to the following expression for the final grain size

$$d_\alpha = \left(\frac{2}{\pi}\right)^{-\frac{1}{6}} \left(\frac{\sqrt{I_s}}{\alpha}\right)^{-\frac{1}{3}} d_\gamma^{\frac{1}{3}} \tag{9}$$

where I_S is the nucleation rate, α the parabolic growth rate, and d_γ the previous austenite grain size When the relation between nucleation rate and cooling rate is taken into account, these same authors obtain the following relation

$$d_\alpha = \alpha\, d_f^{-b}\, C_r^{-c} \tag{10}$$

where C_r is the cooling rate Similar results were obtained experimentally at IRSID[16]

The growth rate α is controlled by the diffusion of carbon away from the interphase boundary This diffusion occurs because of the much lower solubility of carbon in ferrite as compared to austenite The following expression is given [6] for the growth kinetics of ferrite in austenite

$$s = \alpha t^{1/2} \qquad \alpha = (C_\gamma^{\gamma\alpha} - C_0) \sqrt{\frac{D_C^\gamma}{(C_0 - C_\alpha^{\alpha\gamma})(C_\gamma^{\gamma\alpha} - C_\alpha^{\alpha\gamma})}} \tag{11}$$

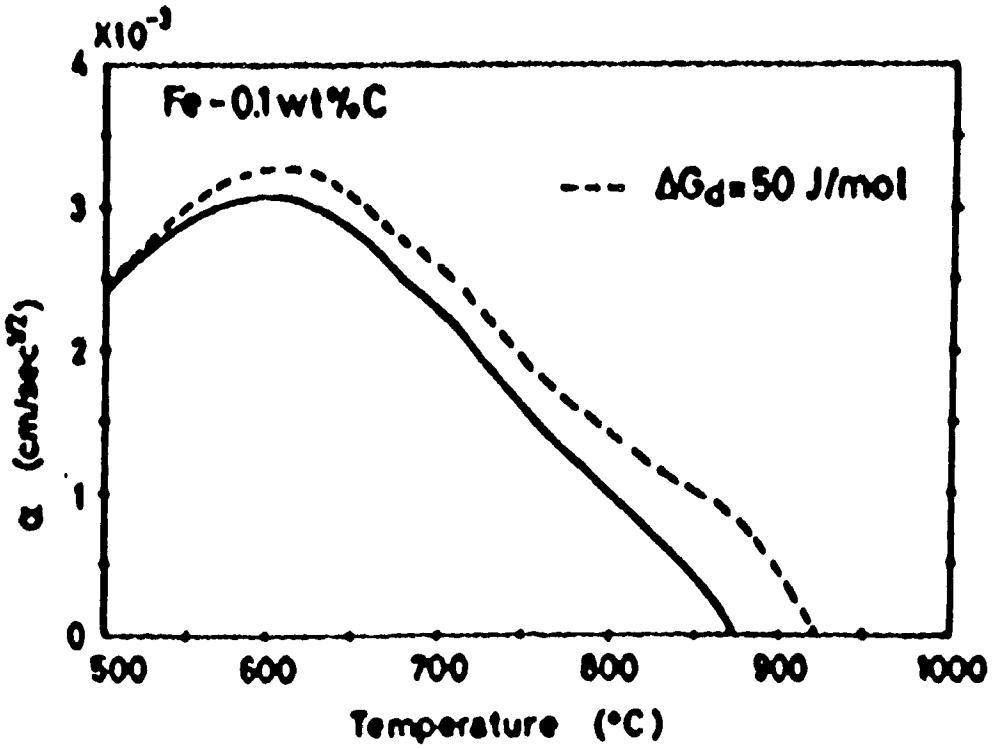

Figure 2.5: Dependence of parabolic growth rate on temperature for deformed (----) and undeformed (____) austenite. [17]

where s is the half-thickness of the ferrite grains, D_c^{γ} is the diffusivity of carbon in the austenite, $C_{\gamma}^{\gamma\alpha}$ and $C_{\alpha}^{\alpha\gamma}$ are the concentrations of carbon at the interface in the austenite and in the ferrite (equilibrium concentrations), and C_0 is the average concentration in the austenite. Despite the decrease in diffusivity, the growth rate increases with decreasing temperature because of the larger difference between the equilibrium concentration and the average concentration in the austenite. However, this increase in growth rate does not compensate for the increase in nucleation rate when the temperature is decreased. Figure 2.5.[17] shows the dependence of growth rate on temperature.

Second phase formation

When austenite is transforming into ferrite, carbon segregation occurs, leading to a higher concentration in the austenite. In the case of slow cooling, the concentration of

carbon in the austenite eventually reaches the eutectoid composition at which the pearlite transformation occurs When the cooling rate is slow enough, this transformation takes place at the A_{c1} temperature. At faster cooling rates, the critical composition is reached at a lower temperature A_{r1}. However, if the cooling rate is increased further, the critical composition is no longer attained at a temperature at which the rate of carbon diffusion is sufficiently high to permit a truly pearlitic transformation. In this case, other phases form, even before the critical composition is reached [18]

Like pearlite, they are composed of ferrite and cementite, but these are no longer arranged in a lamellar structure For intermediate cooling rates, degenerate pearlite is obtained When the cooling rate is increased further, bainites are obtained, which can have various morphologies, depending on the temperatures at which they form The transformation from austenite to pearlite is dictated by the eutectoid composition, which is independent of temperature, the bainite transformation is triggered by cooling to the B_s temperature, below which the transformation begins, for a given instantaneous composition of the austenite For this reason, if the ferrite transformation is delayed to very low temperatures, either because of a large austenite grain size or because of a fast cooling rate, completely bainitic structures can be obtained. However, if the cooling rate is too high, the bainite transformation is inhibited and the transformation to martensite takes place instead

The influence of deformation on the formation of second phases has been the object of several studies C.M Vlad [19] showed that increasing the deformation of austenite before transformation accelerates of the kinetics of ferrite formation The concentration of carbon in the austenite increases more rapidly when it is deformed (by means of pipe diffusion), leading to the formation of pearlite instead of bainite at high cooling rates When several types of second phases are present, an increase in the strain leads to the replacement of the harder phases, formed at low temperatures, by softer

phases formed at higher temperatures This same study showed that when the deformation of austenite is increased, the B_S temperature is decreased This is in contradiction to the results of another study by Sun Benrong et al., [20] in which it was reported that all the characteristic temperatures are increased by deformation However, both sets of authors agree that increasing the strain is detrimental to the bainite transformation, which tends to be replaced by the pearlite transformation

II.2. History of the development of ferrite-bainite steels.

In the last few years, environmental concerns have led to a demand for lighter and more efficient vehicles This has led car manufacturers to increase the fuel mileage of their cars There are several ways of achieving this objective Improving the engines is one, and decreasing the overall weight of cars is another It also turns out that decreasing the weight of rotating parts results in savings 1 2 to 1 3 times greater than those that can be achieved for translating parts For this reason, manufacturers are trying to find ways of reducing the thickness of the steels being used for wheels This can be done by using stronger steels However, the complex manufacturing process employed for making wheels imposes some restrictions on the properties of these steels In particular, the steel has to be weldable, which limits the carbon level, and formable, which imposes a minimum elongation Recently, the shapes of wheels have become more complicated, mainly for aesthetic reasons. This has further increased the demand for good formability Among the service properties of wheels, the fatigue resistance is the most important [21] Fortunately, it is generally recognized that the fatigue resistance increases with increasing tensile strength

Several types of steels have been tried for the manufacture of car wheels. Originally, plain carbon-manganese steels were used [22] These had microstructures of ferrite plus pearlite The main strengthening mechanisms were the reduction of grain size and the increase in pearlite content The former was brought about by decreasing the

rolling and coiling temperatures It was also limited by the characteristics of the hot strip mill being employed The latter was produced by increasing the carbon level The potential of this technique was limited by weldability requirements Using both methods for strengthening, the highest tensile strength previously obtained was 500 MPa

HSLA steels containing strengthening precipitates were also tried However, the heat affected zones of the welds obtained with these steels usually contained softened regions, which were considered to be detrimental The next real improvement involved the application of dual-phase steels to the manufacture of wheels Dual-phase steels are composed of ferrite and martensite They display, at the same time, high strength and a ductility that is superior to that of ferrite-pearlite steels of similar strength levels Several studies [23,24] of the microstructure-properties relationship have shown that the strengths of dual phase steels can be related directly to the volume fractions of martensite in their microstructures The strength levels obtained are due to the great hardness of martensite as opposed to that of pearlite or bainite The ductility comes from the fact that martensite is deformed together with the ferrite matrix when large plastic deformations are applied, whereas pearlite is not In the case of a ferrite-pearlite steel, the cementite was shown to fracture at large deformations, leading to ultimate failure

In terms of mechanical properties, dual-phase steels seemed to offer a better solution for the manufacture of wheels However, in terms of production, they had several drawbacks To obtain the required mixture of ferrite and martensite, the steel manufacturers either used off-line heat treatments or complex cooling patterns on the runout table of the hot strip mill [25] The off-line heat treatments involved intercritical annealing in the austenite plus ferrite domain followed by quenching into the martensite region This process therefore resulted in high manufacturing costs Furthermore, the compositions used for these steels were often enriched in costly alloying elements such as Mo, Cr or V

The other process route involved hot rolling followed by slow cooling on the runout table in order to promote the formation of ferrite Once the desired proportion of ferrite was obtained, the steel was cooled quickly to temperatures below the M_s temperature Several steel producers have successfully produced such steels, using this direct method [26,27] In Japan, intercritical rolling is used in addition to the processes described above to increase the rate of the austenite to ferrite transformation[28]. All these steps require excellent control of the production process as well as particular facilities for low temperature coiling This is why the manufacture of dual-phase steels is considered to be difficult and can present major problems for quality control Steel manufacturers have therefore tried to find other solutions

Stretch flangeability is one of the main desired properties for steels for the manufacture of wheels The disk fabrication process involves the press forming of a pierced blank Stretch flangeability is the ability to apply large deformations to such parts This property is usually measured by the hole expansion test This test is performed by expanding a hole with a conical punch until fracture occurs The expansion ratio λ is then calculated as the fractional increase in diameter [29]

$$\lambda = \frac{d_b - d_i}{d_i} \times 100(\%) \qquad (12)$$

where d_i is the initial diameter of the hole and d_b is the diameter at rupture In ref 29, it is shown that λ can be directly related to the reduction of area measured during a tensile test

In the beginning of the eighties, studies at Kobe Steel by Sudo et al showed the beneficial effect of bainite on the stretch flangeability of dual-phase steels [30,31] The same authors also tested a new niobium-bearing ferrite-bainite steel and showed that they could obtain still better stretch flangeabilities and better fatigue strengths with this mixture than with dual-phase steels, for comparable levels of strength [32] Later studies carried out in

Germany confirmed that bainite could improve the ductility without significantly decreasing the tensile strength of dual-phase steels [33] The positive effect of bainite was attributed to its higher ductility The total elongation was increased much more than the uniform elongation, which means that it is mainly the deformation during necking or the total reduction of area that was affected by the presence of bainite In other studies, it was reported that good strength-elongation combinations were obtained with the mixtures of ferrite and very fine pearlite or bainite produced by low temperature coiling [34,35,36]

II.3 Conditions for the manufacture of ferrite-bainite high strength sheet steels.

II.3.1 Composition

In the various studies described above [29 35], different compositions and process conditions were examined Their influence on the microstructures formed was discussed, together with the mechanical properties obtained. The compositions studied are listed in Table 2.1. The composition of the steel employed in the present study is presented in the last row of the table so that the reader can compare it with the ones employed in the previous investigations Except for reference 29, the steels studied contained more than 0.1% Si and most of them actually had more than 0 2% All the steels in reference 31 contain chromium in association with high silicon levels All the steels in reference 32 contain niobium except for the one which contains molybdenum Only the steels in reference 29 are somewhat similar to SOLLAC HR55

The differences in composition induce differences in steel behavior through the transformation This is well illustrated by the formulae which express the characteristic transformation temperatures, A_{r3}, M_s and B_s, as a function of composition For example, A_{r3} is given by Ouchi et al [37] as

$$A_{r3}=910 -310C-80Mn-20Cu-15Cr-80Mo \qquad (13)$$

Table 2 1 Steel compositions for references 29 to 35 (wt %)

reference	C	Si	Mn	P	S	Al	Nb	Cr	Mo	N
29 A	0 05	0 03	1 01	0 01	0 003	0 049				
29 B	0 1	0 04	1 01	0 01	0 004	0 055				
29 C	0 15	0 01	0 68	0 011	0 006	0 044				
29 D	0 15	0 01	1 01	0 005	0 004	0 034				
29 E	0 15	0 04	1 48	0 009	0 004	0 056				
29 I	0 3	0 04	1 07	0 009	0 005	0 059				
29 G	0 06	0 03	1 04	0 01	0 003	0 055	0 018			
31 A	0 05	0 02	1 5			0 036		0 049		
31 B	0 04	0 51	1 5			0 032		0 01		
31 C	0 05	0 49	1 56			0 032		0 48		
31 D	0 05	0 52	1 52			0 031		1 03		
31 I	0 06	0 5	1 55			0 029		1 43		
31 I	0 04	0 97	1 52			0 035		0 02		
31 G	0 05	0 97	1 55			0 037		0 51		
31 H	0 05	1 01	1 55			0 04		1 02		
32A	0 05	0 49	1 6	0 004	0 006	0 033	0 025			
32B	0 07	0 49	1 59	0 005	0 003	0 03	0 038	0 51		
32C	0 06		1 73	0 008	0 005	0 02			0 3	
32D	0 06		1 83	0 01	0 004	0 035	0 026		0 29	
32E	0 06		1 74	0 011	0 004	0 035	0 088		0 3	
32I	0 05	0 57	1 09	0 008	0 005	0 025	0 018			
32G	0 07	0 78	1 66	0 012	0 005	0 038	0 023			
33A	0 09	0 21	1 02	0 003	0 004	0 016				0 0051
33B	0 12	0 18	0 96	0 004	0 002	0 014				0 0051
33C	0 15	0 19	1	0 004	0 004	0 041				0 005
33D	0 18	0 2	1 01	0 004	0 004	0 043				0 005
33E	0 11	0 15	1 06	0 003	0 005	0 014	0 03			0 0053
33F	0 15	0 28	1 26	0 013	0 001	0 039				0 0112
33G	0 13	0 13	1 38	0 003	0 004	0 017				0 0052
34A	0 08	0 4	1 5			0 04				0 0072
34B	0 08		0 8			0 02				
34C	0 14	0 1	0 8			0 06				
34D	0 06	0 1	0 05			0 05				0 007
34I	0 15	0 28	1 26			0 03				
34F	0 15	0 3	1 3							
34G	0 14	0 1	1 08			0 02				0 0062
Sollac Hr55	0 14	0 06	1 18			0 04		0 03		0 0040

at a cooling rate of 1°C/s This means that an increase in the carbon concentration by 0 05 % depresses the A_{r3} temperature by 15°C and an increase in the manganese content by 0 5% decreases A_{r3} by 40°C The same type of equation can be obtained for B_s [38]

$$B_s = 719\text{-}127(C\%)\text{-}50(Mn\%)\text{-}31(Ni\%)\text{-}27(Cr\%)\text{-}61(Mo\%) \quad (14)$$

Again, one can see the strong influence of Mn and Cr, which vary over a wide range in the studies described above Similar formulae are available for M_s

Depending on where the critical temperatures are located, the cooling rate, coiling temperature and even the strain can have very different influences on the behavior of the steel This is illustrated in Figure 2 6 In diagram a), the B_s and B_f temperatures are low, so that the coiling temperature has a strong effect on the type of bainite formed Also, the transformations are delayed to longer times, which means that variations in cooling rate have little effect In diagram b), the B_s and B_f temperatures are high and the transformations occur early during cooling In this case, the cooling rate plays an important role, whereas the coiling temperature has a more limited effect as soon as the temperature has dropped below 500°C. In both cases, though, the final microstructure is of the ferrite-bainite type

From the preceding, it is evident that the composition can have a strong influence on the role played by the various process parameters, even if the same kind of microstructure is obtained at the end of the process This means that, while the general behaviors of steels can be deduced from the studies referred to above, a detailed study of the characteristics of Sollac Hr55 is still necessary if the processes to be used on this composition are to be carefully controlled

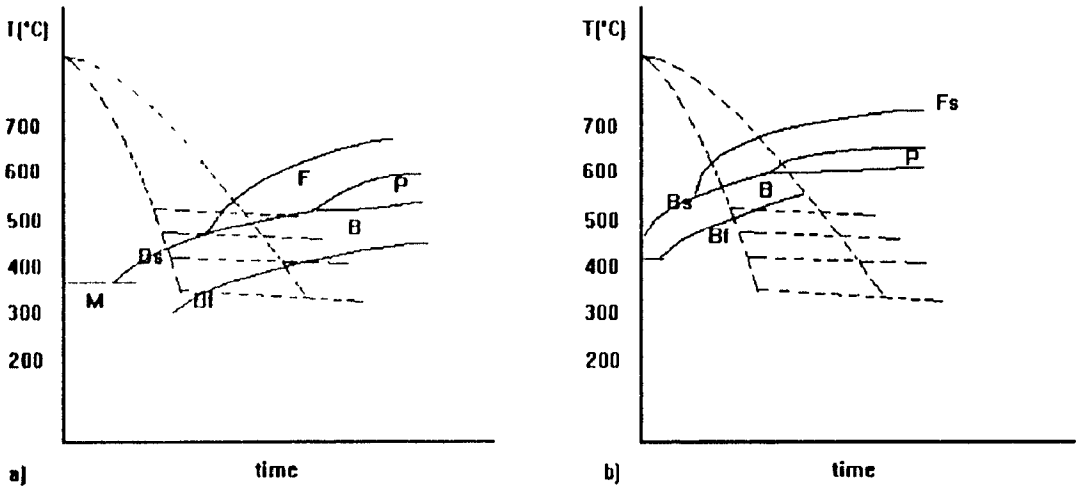

Figure 2 6 Schematic illustration of the effect of changes in the characteristic temperatures on the influence of cooling rate and coiling temperature

II.3.2 Coiling temperature.

The coiling temperature is the parameter that has been studied by all the authors cited in refs 30-35 The temperatures chosen are generally 650°C, 500°C, 300°C and room temperature. All the authors found that the coiling temperature has a strong influence on the mechanical properties as well as on the microstructure In ref. 35, K. Kunishige made the distinction between three coiling temperature regimes. Regime I is defined by coiling temperatures above 500°C The corresponding microstructures are composed of ferrite and pearlite. The strengthening of ferrite by solute carbon or nitrogen is absent In regime II, characterized by coiling temperatures between 500°C and 300°C, the microstructure is composed of ferrite and fine pearlite or bainite At these temperatures, the precipitation of AlN is inhibited, which induces strengthening by solute nitrogen Below 300°C, in regime III, the second phase becomes martensite and solute carbon is retained in the ferrite, which induces additional strengthening.

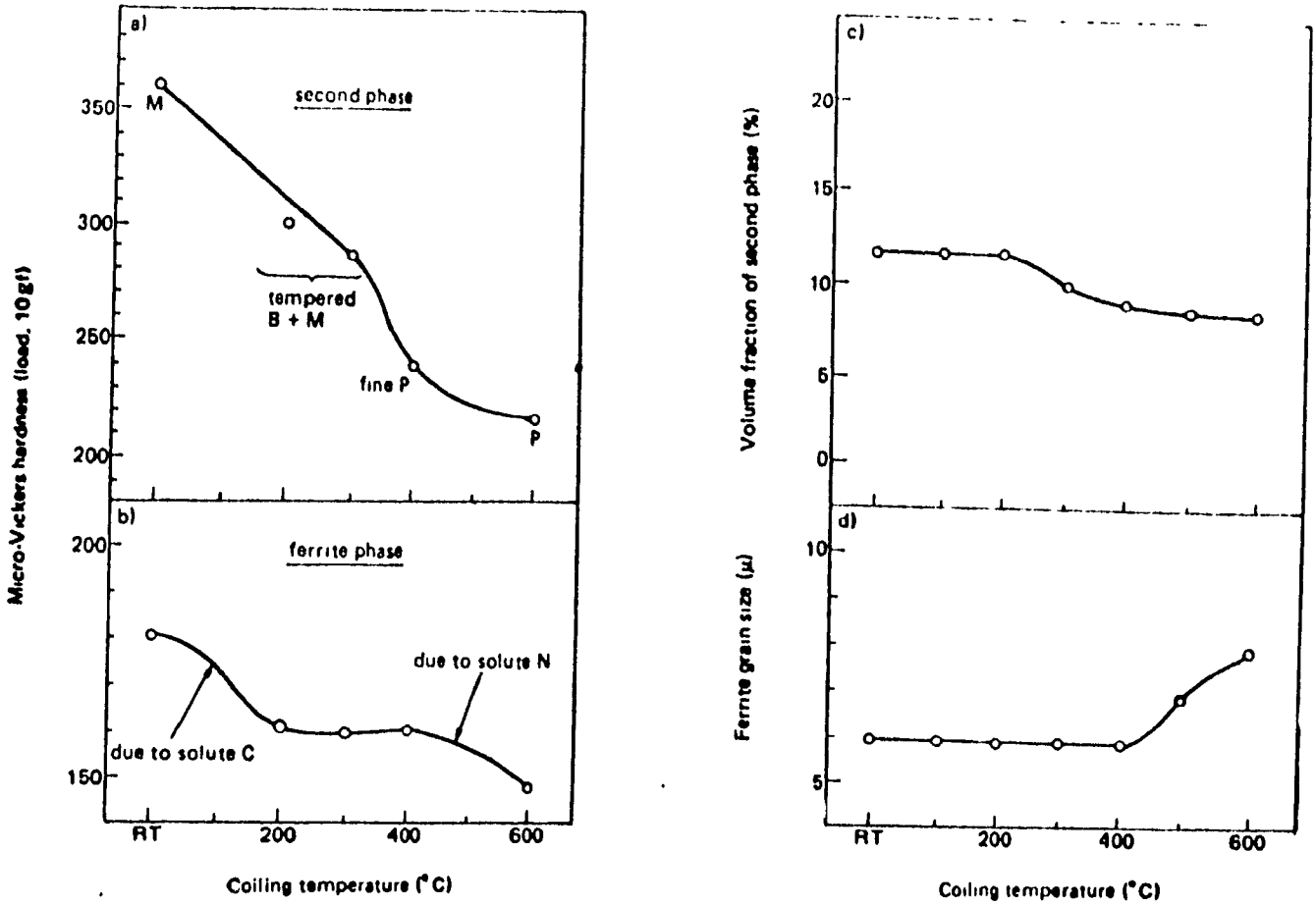

Figure 2.7: Change in strengthening factors with coiling temperature for a steel containing 0.08%C, 0.4%Si, 1.5%Mn, 0.04%Al and 0.0072%N. [35]

These results are interesting because they show that coiling temperature not only affects the final microstructure but also the state of the ferrite by its effect on the solute elements. This aspect of the influence of coiling temperature is related to the quasi-isothermal holding that follows the end of accelerated cooling during which AlN precipitation can take place. Figure 2.7 shows the changes in strengthening factor with coiling temperature that apply to a steel containing 0 08%C, 0 4%Si, 1 5%Mn, 0 04%Al, and 0.0072%N [34].

The other authors [29-32] also observed a strong influence of coiling temperature on the second phase and on the mechanical properties, but they did not study the influence on

the solute content of the ferrite The general conclusion is that the second phase evolves from pearlite for coiling temperatures over 600°C, to bainite for intermediate temperatures, and eventually to martensite for temperatures below 200°C. This leads to an increase in the tensile strength with decreasing temperature The yield strength also increases until the second phase becomes martensite At this point it decreases considerably, which is responsible for the excellent yield ratio of dual phase steels. In reference 29, Hashimoto et al found that the effect of coiling temperature on the mechanical properties was increased when the Mn content of the steel was increased.

These studies were all aimed at showing the positive effect of the presence of bainite as the second phase The authors did not focus on variations in the mechanical properties or of the microstructure over narrower ranges of coiling temperature Now that ferrite-bainite steels are being produced industrially, it is of interest to know what property changes can be induced by small variations around the usual manufacturing conditions

II.3.3 Cooling rate

Although cooling rate plays an important role in determining the microstructure and mechanical properties of multi-phase steels [19], its effect on the microstructure and properties of ferrite-bainite steels has not been extensively studied. Only two investigations [34, 31] have involved changes in cooling rate The other publications on the subject were carried out with constant cooling rates usually around 40 to 60°C/s

In both references 31 and 34, the cooling patterns used were of two different types continuous or controlled cooling, for which two different cooling rates were applied successively In both studies, continuous cooling was performed at a single cooling rate, which means that no information is available on the effect of cooling rate in this case However, indirect information can be obtained from the experiments on controlled cooling When the first cooling rate, corresponding to the austenite-to-ferrite transformation range, was increased, the proportion of ferrite decreased, leading to an

increase in tensile strength in reference 31, where a Cr and Si bearing steel was used By contrast, there was little variation in mechanical properties in the case of reference 34, where a C-Mn steel was employed In this last case, it was shown that an increase in primary cooling rate led to the formation of Widmanstatten ferrite instead of the polygonal ferrite obtained at lower cooling rates Increasing the secondary cooling rate led to an increase in the volume fraction of the low temperature products as well as to the formation of martensite instead of bainite in the work of reference 31 In the case of the C-Mn steels used in reference 34, the changes in secondary cooling rate had no effect at all on the microstructure or on the mechanical properties

II.3.4 Deformation

The influence of deformation was studied by Sudo et al in ref 31 by varying the finishing temperature. They showed that increasing the finishing temperature led to an increase in tensile strength because of an increase in the proportion of low temperature products This type of result has also been reported by Vlad and by Sun Benrong et al Depending on the CCT diagram of the steel, the influence of deformation can be more or less crucial If the transformations are very fast or, on the contrary, very slow, the small variations associated with hot strip mills may not have a very strong effect On the other hand, if the transformation rate is intermediate, i e if the nose of the C curve is crossed during accelerated cooling at the rates currently used on the hot strip mill, changes in the reduction or related variations, such as in finishing temperature or strain rate, can have a strong influence on the nature of the phases formed and on the mechanical properties As no information is available on the transformation kinetics for the type of composition used by SOLLAC for the manufacture of HR55, this topic will be one of the issues of this thesis

II.4 Nature of the bainite

As bainite was mentioned several times in this bibliographic study and as it will be the major topic of this investigation, the definition of bainite will be discussed briefly here, together with its various morphological features

Unlike pearlite or martensite, which have very well defined morphological characteristics, bainite has never been clearly delineated In fact its definition varies with the author and is still a matter of controversy This probably arises from the fact that the bainite transformation has never been completely understood or, at least, has never been the subject of wide agreement There are three different ways of characterizing bainite·

i) By its microstructure Sinha [6] gives the following definition Bainite is a nonlamellar two-phase product of eutectoid decomposition in which diffusional and sequential precipitation and noncooperative growth of the low temperature phases occurs

ii) By the kinetics of the bainite transformation In this definition [6], bainite is the phase that forms at temperatures below that of the pearlite transformation and that displays a separate C-curve on a TTT diagram The maximum bainite start temperature, the kinetic B_S, lies considerably below the eutectoid temperature

iii) By surface relief effects In this definition, bainite (1) consists simply of plates which differ in composition from its parent phase, (2) grows slowly, and (3) exhibits a martensite-like surface relief when formed at a free surface

For the present work, the microstructural definition is certainly the most convenient, because the other two definitions require special experimental techniques, either to study free surfaces, before and after transformation, or to perform isothermal

transformations However, the definition given by Sinha does not provide an easy way to identify bainite as a final microstructural component because it involves notions about the mechanism of transformation, which is not readily identified in most cases The definition given by Bramfitt and Speer [39] will therefore be preferred It was proposed in order to describe the microstructures formed during the continuous cooling of steels, as opposed to the ones obtained through isothermal transformation, for which the first definitions had been created For Bramfitt and Speer, the term bainite designates any of the following morphological characteristics

(1) acicular ferrite associated with the intralath precipitation of iron carbide,

(2) acicular ferrite associated with interlath particles or interlath films of cementite and/or austenite, and

(3) acicular ferrite associated with a constituent consisting of discrete islands or blocky regions of austenite and/or martensite or pearlite

The classical theories about bainite, based on isothermal transformation products, distinguish between two types of bainite Upper bainite forms at high temperatures and is characterized, in its most usual form, by interlath precipitates of cementite Lower bainite appears at low temperatures and contains no interlath precipitates In this case, precipitation takes place inside the ferrite laths, usually at a constant angle from the longitudinal direction of the lath When continuous cooling is employed, this classification is no longer valid because hybrid forms of bainite can appear and the temperature domains in which the constituents can be found are not clearly delimited For these reasons, Bramfitt and Speer [39] proposed a new classification, which avoids the reference to temperature and permits the description of more complex microstructures They first define three main classes of microstructure

class 1 bainite (B_1) incorporates an intralath constituent,

class 2 bainite (B_2) incorporates an interlath particle or film constituent; and

class 3 bainite (B_3) incorporates discrete regions of a retained parent phase or secondary transformation product

Subclasses can then be defined For example, a bainite containing interlath and intralath precipitates in the same area is designated as $B_{1,2}$ type bainite On the other hand, a microstructure containing discrete areas of B_1 and B_2 bainite can be described as B_1+B_2 bainite

Influence of bainite morphology on the mechanical properties

From preceding discussion, it is evident that the morphology of bainite can vary. One should expect the different types of bainite to have different behaviors In terms of strength, it appears that the intralath carbides present in B_1 type bainite have a strong strengthening effect, whereas the interlath carbides found in B_2 bainite have no visible influence on strength [40] Other properties may also depend on the type of bainite formed For this reason, efforts should be made to identify the type of bainite present in a microstructure In the case of ferrite-bainite steels, both types of bainite were found for different compositions and cooling conditions However, the evolution of bainite morphology with the cooling conditions was not explicitly studied This will be one of the objectives of this thesis

CHAPTER III

EXPERIMENTAL PROCEDURE

In this chapter, the experimental procedure will be presented In the first part, a description will be given of how the torsion machine was adapted to the simulation of accelerated cooling in hot strip mills The quality of the simulation will be assessed through the computer modeling of sample cooling Then, in a second part, the choice of the different experimental parameters will be described Computer modeling will again be used to determine the state of the austenite at the end of rolling in the hot strip mill From these results, the rolling and reheating conditions will be chosen The cooling rates and coiling temperatures will also be discussed. In the last part, the methods employed for microstructural examination and mechanical testing will be presented

III.1. Adaptation of the torsion machine to simulate the hot strip mill.

III.1.1 Objectives

The torsion machine is a tool that has been successfully used to simulate hot rolling on various hot deformation units including hot strip mills However, as discussed in the literature review, the complete process of hot strip rolling involves accelerated cooling on the runout table. The primary objective was thus to adapt the torsion machine in order to simulate accelerated cooling To achieve our objective and to provide good reproducibility, the cooling device had to obey the following requirements

i) It should be possible to cool a specimen just after the end of deformation at a cooling rate that is representative of the cooling rates used in hot strip mills

ii) The cooling rate should be reproducible and adjustable so as to be able to handle the large range achieved on actual production units (typically 10°C/s to 120°C/s as measured in the austenite range;

iii) The temperature measurements should be accurate enough to allow accelerated cooling to be stopped at the desired temperature, within an acceptable error They should also provide acceptable data for the calculation of cooling rates. Control over the flow rate of the cooling medium should also be accurate enough for the same reasons

iv) The specimens should be cooled as uniformly as possible in order to produce uniform microstructures and mechanical properties If this cannot be attained, the structure and property gradients should be evaluated

III.1.2 Presentation of the equipment

III 1 2 a The Torsion Machine

The equipment used for this research was a servohydraulic, computer-controlled MTS torsion machine mounted on a lathe bed (Figure 3 1). On the left hand side, a hydraulic servovalve (1) controlled the flow of oil to a hydraulic motor (2), which transmitted the rotational force to the rotating torsion bar (3) The rotational displacement was measured by a 50 turn potentiometer (4) On the other side, the specimen (5) was screwed into the stationary grip (6) The torque was measured by a 113 N-m torque cell (7) The ensemble on the right side could be translated in order to permit the installation and removal of the specimen, which was only fitted into a slot in the rotating grip. The grips were made of inconel in order to be able to withstand high temperatures

The displacement, torque and temperature were recorded continuously by a data acquisition unit and a microcomputer The MTS TestStar system was used for data acquisition and the control of the hydraulic servovalve This system provided a very user-

friendly and flexible interface with the torsion machine The deformation schedules were entered as a series of steps, including different operations such as data acquisition or displacement. The parameters (displacement, interval between data readings, speed of displacement) were all easily adjustable wide ranges

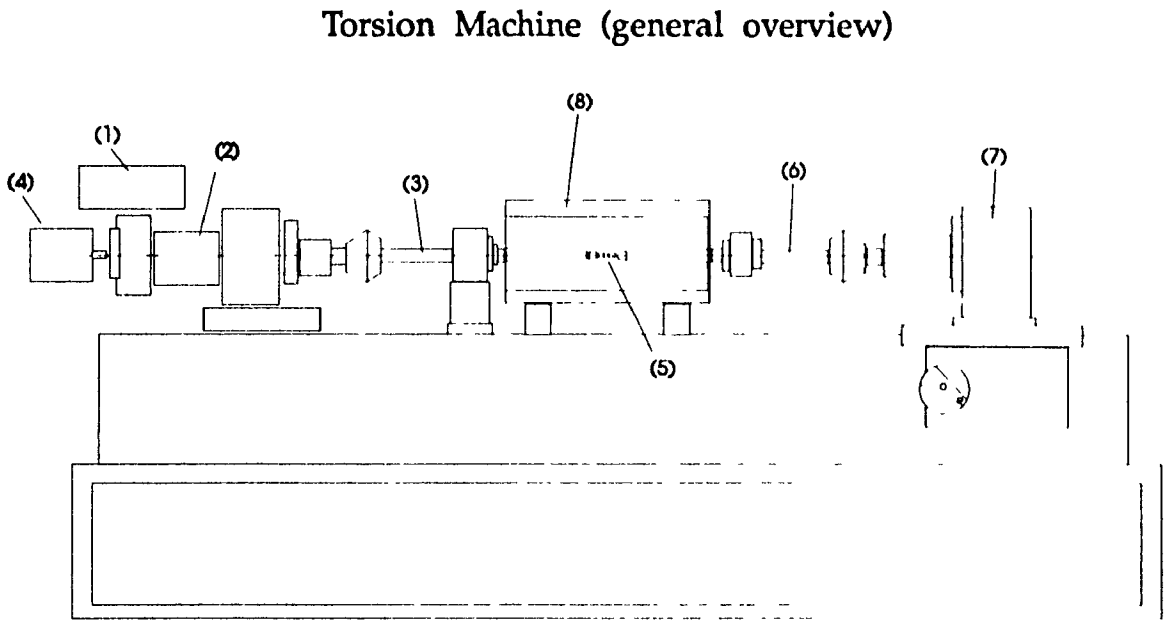

Figure 3.1 The torsion machine

II.1 2 b The radiation furnace

Reheating was performed in a four-element radiant furnace manufactured by Research Inc. The temperature was controlled by an Electromax process controller coupled to a Leeds and Northrup 1300 process programmer Temperature readings were taken every 0.5 second through a type K thermocouple in contact with the specimen surface. The signal was processed by the controller and the power input to the furnace was adjusted continuously to maintain the current set point defined by the programmer An analog signal was also sent to the TestStar system from the controller The latter

system had no control over the furnace The temperatures were acquired only as data which could be used to command the torsion machine if desired

The specimen was placed at the centre of the furnace chamber in a quartz tube sealed at both ends An argon atmosphere was constantly circulated to prevent oxidation of the specimens and tools

III 1 2.c Specimen geometry

The geometry of the most commonly used torsion specimen is shown in Figure 3 2 The gage length has a diameter of 6 4 mm and a length of 21 mm The shoulders have diameters of 15 8 mm At one end, a thread is machined to permit the specimen to be screwed into the grip. At the other end, a flat is machined to fit into a slot in the grip. The thermocouple for furnace control was usually placed with the open end in contact with the gage length as close as possible to the shoulder

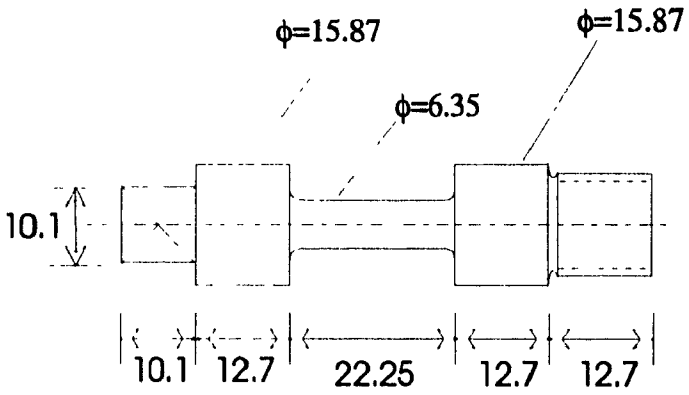

Figure 3 2 Standard torsion specimen

III.1.3 The cooling system

III 1 3 a Heat exchange in hot strip mills.

The thermal behavior of strip on a runout table is not perfectly known. Most steel plants have their own cooling systems, involving various types of water jets or sprays Most of the time, heat transfer is simply expressed as the total temperature drop, which depends on the number of water banks used[41] In other cases, a Newtonian law is

assumed with a constant heat transfer coefficient [42] or with a coefficient that depends to some extent on the temperature[43] For the present study, it was assumed that cooling on the runout table can be represented by a Newtonian law of the following type

$$\text{Heat flux} = \lambda(T-T_W)$$

where λ is a constant, T is the surface temperature of the strip, and T_W is the temperature of the water

III.1.3.b Development of the cooling system

As mentioned at the beginning of this chapter, one of the objectives of this research was to develop a cooling system that could provide a cooling pattern similar to that of a hot strip mill. This implies that the heat transfer taking place be of the Newtonian type One solution would be to use water sprays However, the development of an easily controllable cooling system based on water sprays would have taken a very long time Water sprays also possess other disadvantages, such as the possible heterogeneity of cooling due to the difficulty of controlling the spray shape and rate of flow. For all these reasons, gas cooling was preferred It provides Newtonian heat transfer and is also easy to set up and operate.

In a first stage, compressed air was tried It was blown towards the specimen through the two nozzles usually used for water quenching The temperature was measured using a thermocouple placed on the outside of the specimen The cooling obtained by means of this technique was found to be very heterogeneous. The temperature measured during cooling decreased in a very erratic manner and very rapidly, although the microstructures observed after the test were more representative of slow cooling, containing large grain sizes and coarse lamellar pearlite It was concluded that the thermocouple was not reading the actual temperature of the specimen because the tip of

the thermocouple cooled more quickly than the specimen itself To avoid this problem, it was decided that a second thermocouple would be placed inside the specimen. The slow cooling was attributed to the poor heat transfer coefficient of air. Helium, which has a thermal conductivity about 5 times higher than air (see Figure 3.3) was chosen to replace the latter. The problem of inhomogeneity was partially solved by designing a new cooling device.

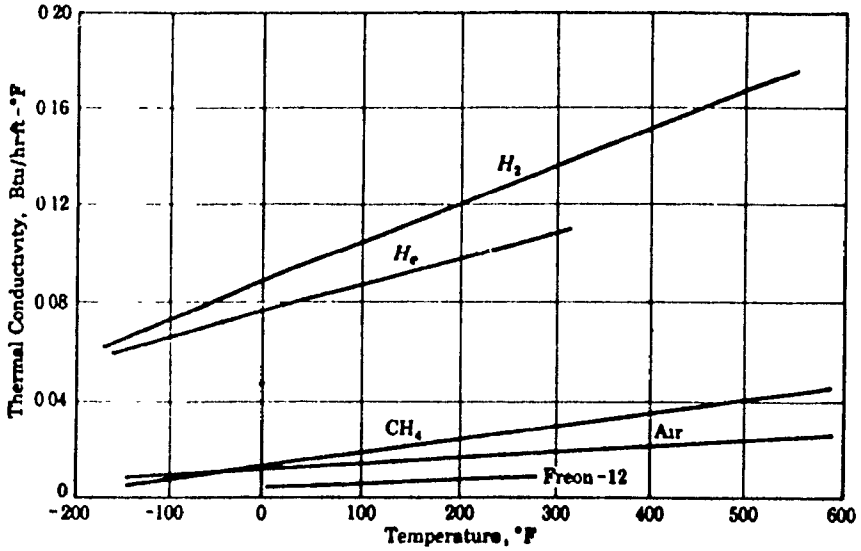

Figure 3 3 Thermal conductivity of various gases as a function of the temperature.[44]

III.1.3.c Description of the cooling system

The new cooling device is shown in Figure 3.4 together with the new specimen geometry. The position of the cooling device on the torsion machine is shown in Figure 3.5. The cooling device was composed of a torus with a rectangular cross section. The internal wall was pierced with three rows of four holes at 90° from one another for the helium outlet. The helium was introduced into the cooling device under pressure through two inlets on the external wall. The helium pressure was controlled by means of a two-stage pressure regulator, which provided good reproducibility and permitted close regulation of the cooling rate

The torsion specimens were modified to permit temperature readings to be taken at the interiors of the specimens. A 2.4 mm hole was drilled along the specimen axis, as

can be seen in Figure 3 4 The thermocouple was introduced through the grip so that its tip contacted the center of the gage length A second thermocouple was also placed on the outside diameter of the specimen for control of the radiant furnace The signal from the internal thermocouple was acquired by the computer through an analog amplifier, which permitted very fast acquisition

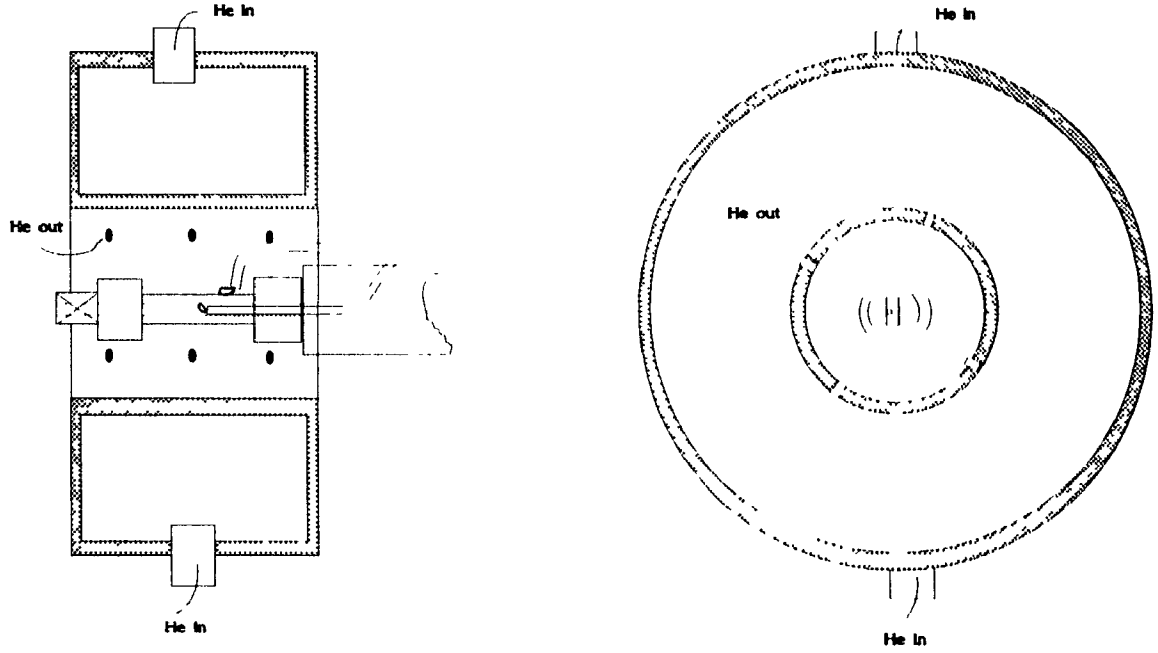

Figure 3.4 Cooling device with specimen in cooling position

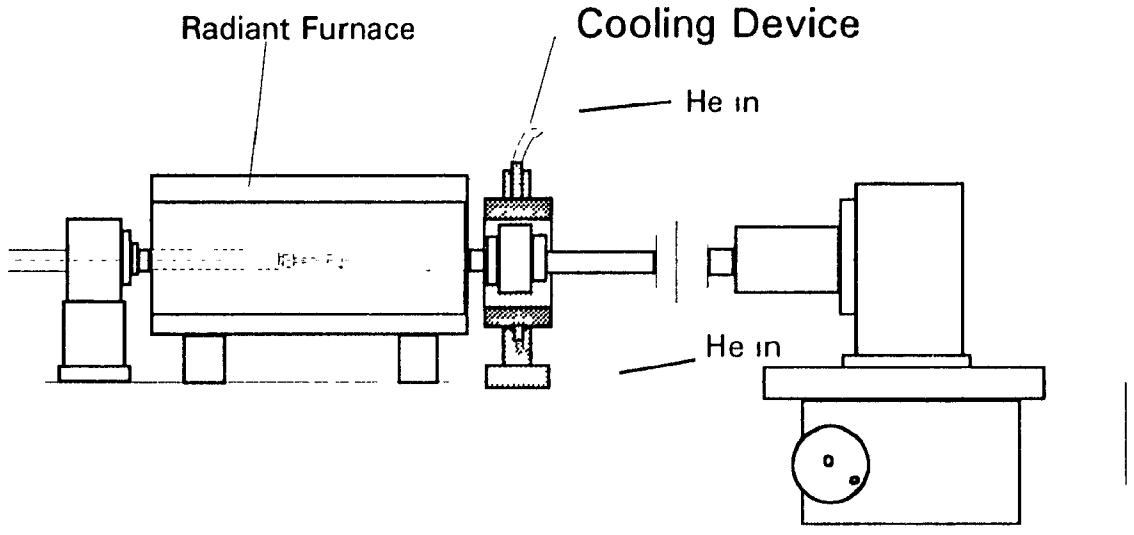

Figure 3 5. Position of the cooling device on the torsion machine

III 1 3 d Evaluation of the uniformity of cooling

As mentioned above, the temperature readings were carried out at the centers of the specimens In the next part of this study, the microstructures were studied a few hundreds of micrometers below the surfaces of the specimens This point corresponds to the region where the deformation is a maximum Tensile tests, to measure the mechanical properties, were also performed They provided results that were relative to the overall gage length or to areas somewhat removed from the center For these reasons, it was necessary to know the representativity of the temperature reading at the center of the specimen In order to assess the temperature gradients present in the specimens, a finite difference computer simulation of the cooling was performed. For this purpose, a computer program was written in Pascal The listing is given in Appendix I

The program was based on the following assumptions.

i) heat transfer at the surface follows a Newtonian law of the type

$$\Phi=-\lambda(T-T_{gas})$$

where Φ is the heat flux at the specimen surface, λ is a constant, T is the temperature of the surface and T_{gas} is the temperature of the gas,

ii) λ is independent of the surface orientation with respect to the gas flow,

iii) the general laws of heat conduction can be applied inside the specimen;

iv) the grip remains at approximately the same temperature during cooling;

v) no transformation occurs during cooling

As the specimen has rotational symmetry around the torsion axis, it was divided into a net of circular cells, as illustrated in Figure 3.6. Depending on its position, each cell receives different amounts of heat from the surrounding cells, either by conduction or by

convection for the cells in contact with the surface Four different heat fluxes (q_i, i =1, ,4) can be defined, one for each side of the cell The temperature change dT of the cell is given by the following equation[45]·

$$\sum q_i . dt = \rho\, Cp\, dT$$

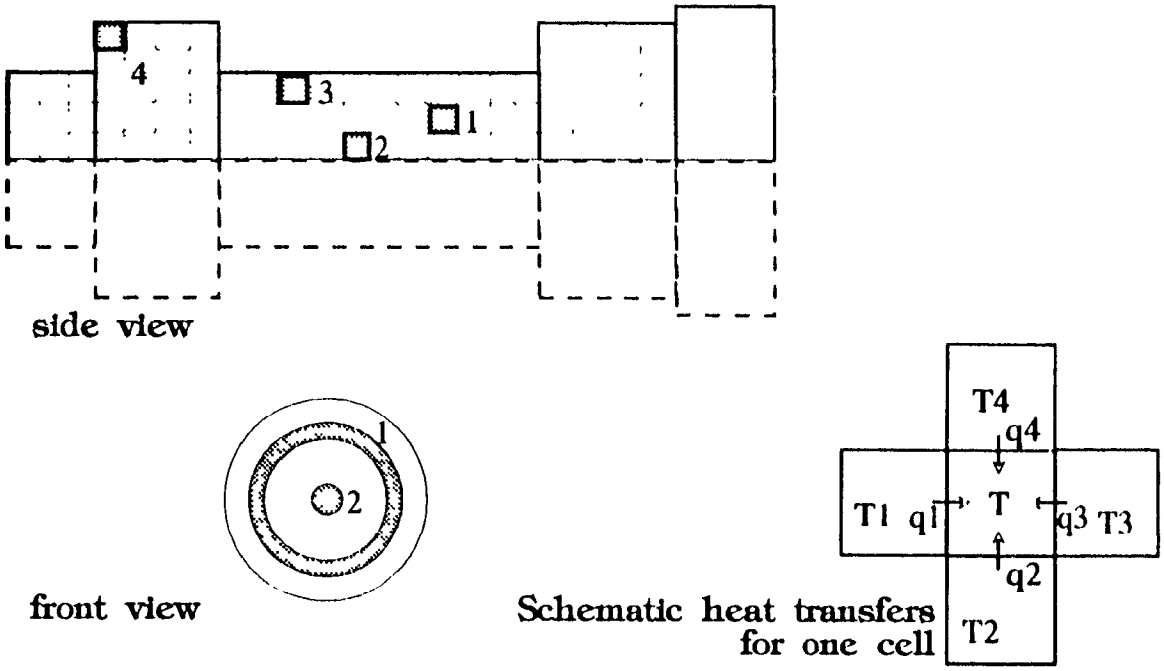

Figure 3.6 Cell division of the specimen for the cooling simulation

A few examples of possible calculations are given below The cell types refer to the numbers in Figure 3 7

Type 1 cell: Only conduction takes place from the surrounding cells

$$\begin{cases} q_i = -k\ s_i \dfrac{T - T_i}{r - r_i} \\ i = 1,2,3,4 \end{cases}$$

where T_i is the temperature of one of the neighboring cells, s_i is the cross-sectional area of the interface between the two cells, and k is the conduction coefficient

Type 2 Center cell, no heat comes from the center because of symmetry

$$q_2 = 0 \qquad \text{and} \qquad \begin{cases} q_i = -k\ s_i \dfrac{T - T_i}{r - r_i} \\ i = 1,3,4 \end{cases}$$

Type 3 Surface cell, convection takes place on one side.

$$q_4 = \lambda\ s_4\ (T - T_\infty) \text{ and } \begin{cases} q_i = -k\ s_i \dfrac{T - T_i}{r - r_i} \\ i = 1,2,3 \end{cases}$$

Type 4 Corner cell, convection takes place on two sides

$$q_3 = q_4 = \lambda\ s_i (T - T_\infty) \text{ and } \begin{cases} q_i = -k\ s_i \dfrac{T - T_i}{r - r_i} \\ i = 1,2 \end{cases}$$

The program flow chart is given in Figure 3 7. The value of λ was adjusted so that the various cooling rates used for this research could be obtained Figure 3.8 gives examples of the calculated temperatures after 1 second and 4 seconds of cooling at 90°C/s The numbers correspond to the temperature of the cell at the same location as in the specimen It can be seen that large longitudinal gradients are developed in the specimen However, the region effectively studied is shorter than the actual gage length, which reduces the effect of these large temperature gradients. It also appears that the cooling rates, which are disparate at the beginning, become relatively uniform over the gage length (cf Figure 3 8) after some stabilization time. In any case, special care will be taken in the interpretation of these results in the continuation of this work

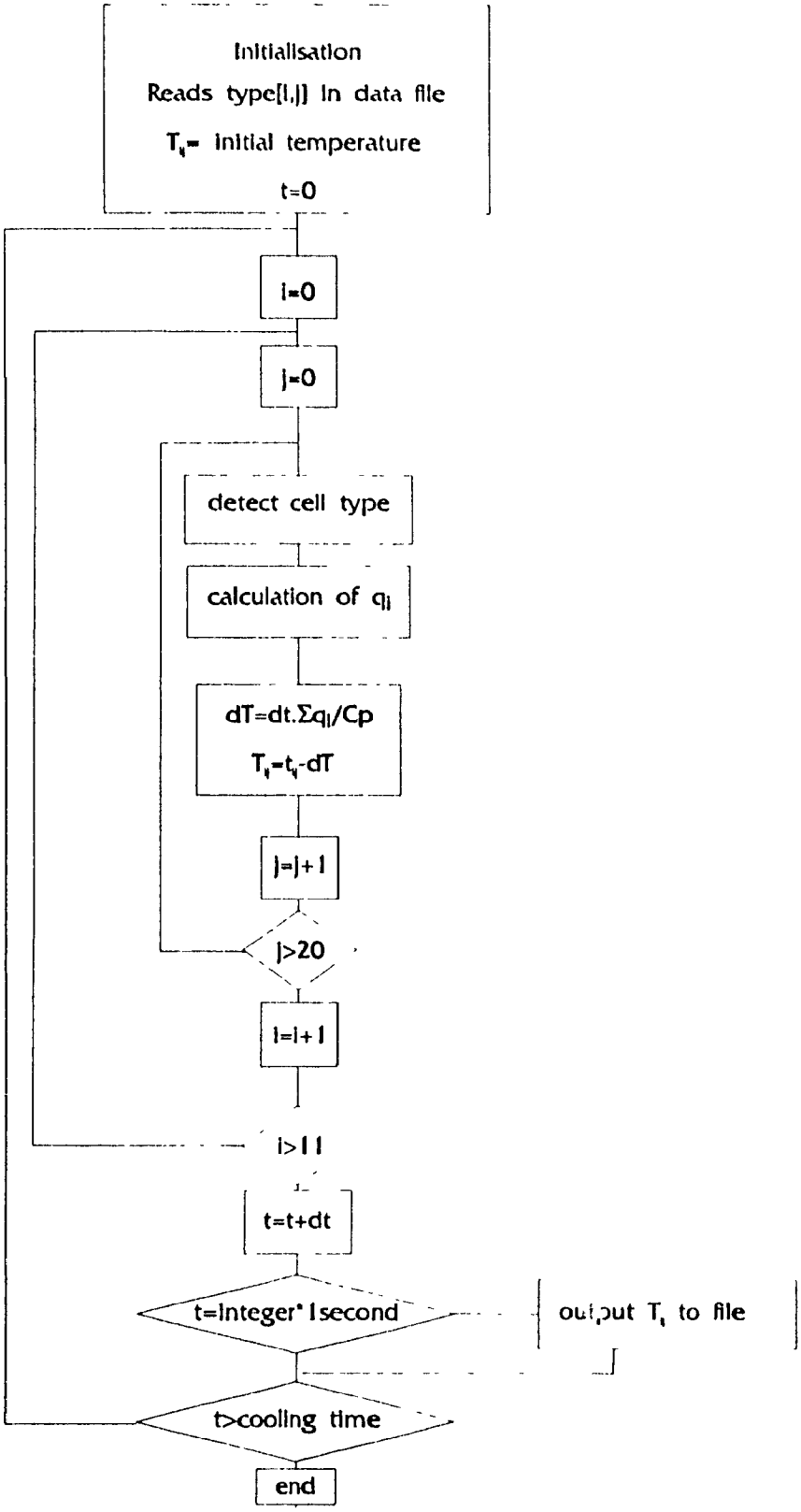

Figure 3 7 Flow chart for the computer simulation of cooling

Figure 3 8 Temperature distribution in the specimen after 1 second at 70°C/s (initial cooling rate) Only half the specimen is shown here

792	816	825	836	841	839	825	795	786	784	784	784	786	795	825	840	844	846	850
788	812	821	833	840	838	822	788	779	778	777	778	779	788	822	838	842	845	850
781	804	814	829	836	834	817	776	767	765	765	765	767	776	817	835	840	843	850
770	794	804	821	831	829	810								810	830	835	839	850
756	779	790	811	824	822	801								801	823	829	834	850
			797	814	813	791								791	814	820	827	850
			783	801	800	779								779	802	808	816	850
			768	786	786	764								765	787	793	803	850

Temperature distribution in the specimen after 4 seconds at 70°C/s (initial cooling rate). Only half the specimen is shown here

628	664	691	712	724	718	689	640	612	599	595	599	612	642	697	737	769	805	850
624	660	687	709	721	715	686	635	606	594	590	594	607	637	694	734	767	803	850
618	654	681	703	716	710	682	625	597	584	581	584	598	627	690	730	762	800	850
610	645	671	695	709	704	675								684	724	756	795	850
599	633	659	684	700	696	667								676	715	748	789	850
			671	690	686	658								667	705	738	781	850
			658	678	674	647								655	694	726	770	850
			644	664	660	634								643	680	712	757	850

Cooling rate distribution in the specimen after 1 second

58	34	25	14	9	11	25	55	64	66	66	66	64	55	25	10	6	4
62	38	29	17	10	12	28	62	71	72	73	72	71	62	28	12	8	5
69	46	36	21	14	16	33	74	83	85	85	85	83	74	33	15	10	7
80	56	46	29	19	21	40								40	20	15	11
94	71	60	39	26	28	49								49	27	21	16
			53	36	37	59								59	36	30	23
			67	49	50	71								71	48	42	34
			82	64	64	86								85	63	57	47

Cooling rate distribution in the specimen after 4 seconds

47	47	44	42	42	42	44	47	51	54	56	54	51	46	40	34	25	13
47	47	44	42	42	42	44	46	51	53	55	54	50	45	40	34	25	13
47	46	43	42	42	42	43	46	50	53	54	53	49	45	38	33	25	13
46	45	43	41	41	42	42								37	33	25	13
45	45	42	40	41	41	42								37	33	25	13
			39	40	40	40								35	32	24	13
			38	39	40	39								35	31	24	13
			38	39	39	38								34	31	24	12

III.2. Experimental conditions

III.2.1 Steel composition

The steel composition is given in Table 3 1 It was taken from a bar being transferred from the roughing to the finishing stands at the SOLLAC Fos hot strip mill This grade is currently used to make the high strength, high formability steel sheet known as HR55

Table 3 1 Steel Composition (in wt %)

C	Mn	Si	Al	Ni	Cr	N
0 14%	1 18%	0 06%	0 04%	0 02%	0 03%	0 004%

III.2.2 Deformation conditions

The objective of this work was to determine the effects of the various production parameters on the final properties and microstructure of the steel In order to achieve this purpose, thermomechanical processing was performed on the steel so as to 1) produce the same state of austenite as at the end of the finishing operation, and 2) simulate variations of the rolling conditions In the case of a C-Mn steel containing no microalloying elements, only the history of deformation influences the final grain size No additional phenomena such as precipitation take place during the deformation of such steels For this reason, processing that leads to the same final austenite grain size and the same final state of recrystallization as on the hot strip mill should be sufficient

SOLLAC provided the rolling schedule for one coil of HR55 The thicknesses after the various passes are given in Table 3 2, together with the corresponding strains, temperatures and interpass times The velocity of the strip at the exit of the last finishing stand was also given It was 9 5 m/s This information made possible the exact calculation of the strain rates and interpass times Assuming a constant volume and knowing the speed

v_1 and thickness h_1 of the strip at the entrance to the rolling stand, one can calculate the strain rate $\dot{\varepsilon}$ in the rolling mill for a given instantaneous thickness h (see Figure 3 9) One obtains

$$\dot{\varepsilon} = \frac{1}{h}\frac{dh}{dt} = -\frac{2\sqrt{-h_1^2 - h^2 - 4rh_1 + 4rh + 2h_1h}}{h^2(2r + h_1 - h)}$$

Table 3 2 Thicknesses, strains, temperatures and interpass times during finishing

Pass number		1	2	3	4	5	6	7
Thickness at the exit (mm)	39 88	21 22	12 4	7.74	5.14	3 88	3.38	3.16
Strain		0 631	0 537	0 471	0.409	0 281	0.138	0 067
Temperature (°C)		1032	992	954	917	882	848	816
Interpass Time (s)		4 24	2 47	1 54	1 02	0 77	0 67	0.63

Figure 3 10 shows the evolution of strain rate as the thickness of the strip is reduced For the rest of this work, the average pass strain rates are used They are also given in Figure 3.11

A computer program was written, using the equations developed by Sellars that were mentioned in the literature review They were used to calculate the fraction recrystallized and the grain size at the beginning of each pass and at the entrance to the runout table These results are presented in Table 3 3. The last line corresponds to the state of the austenite at the entrance to the runout table. It can be seen from this simulation that the final grain size is around 12μm, with an accumulated strain approaching 27% This can be attributed to the low finishing temperature associated with the small reductions in the last passes, which lead to little recrystallization

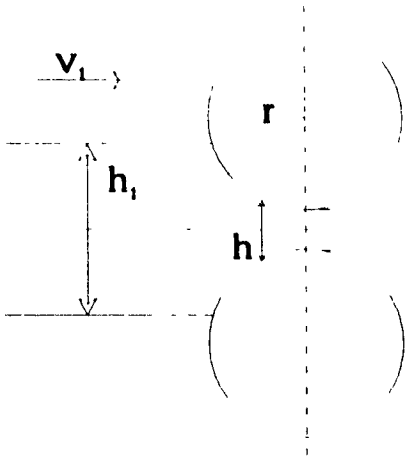

Figure 3 9 Definition of the parameters in the calculation of the strain rate

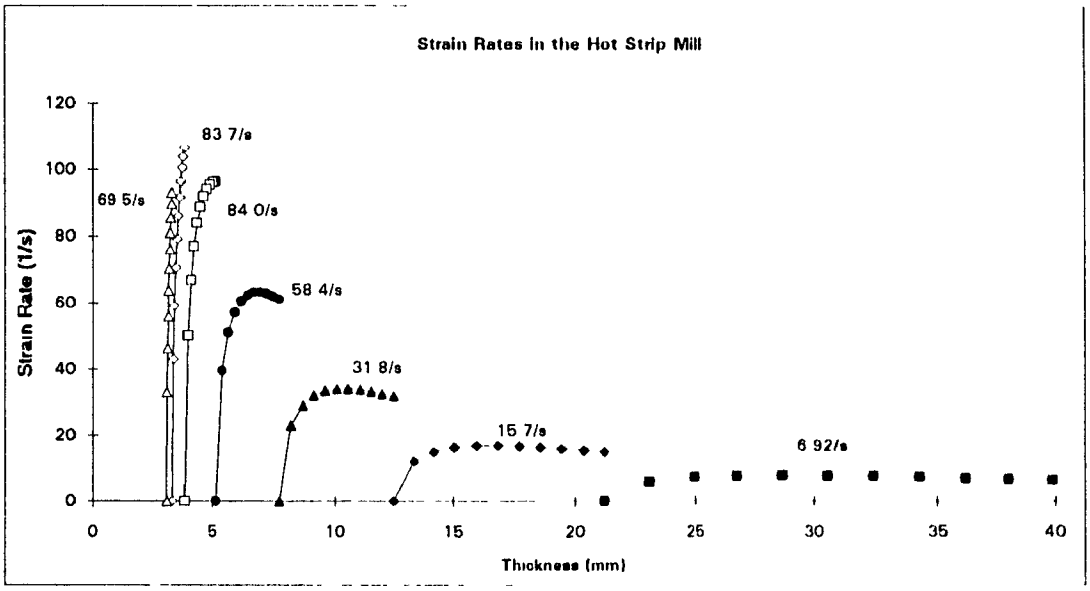

Figure 3.10 Strain rates in the hot strip mill Figures beside the curves are the average strain rate for the corresponding pass

Table 3.3 Microstructural evolution during finishing

Pass #	grain size at entrance (μm)	ε	ε_{cumul}	interpass time (s)	$\dot{\varepsilon}$ (s^{-1})	ε_{peak}	$t_{50\%}$ (s)	fraction Rx	ε_{res}	ε^*
1	50	0 631	0 631	4 245	6.9	0.38	0.14	1	0	0.421
2	49 25	0 537	0 537	2 473	15.7	0.49	0 12	1	0	0 542
3	35.53	0.471	0 471	1 545	31.8	0.53	0.11	1	0	0.556
4	25.6	0 409	0 409	1 025	58.4	0.57	0.16	1	0	0.566
5	17.85	0 281	0 281	0.77	84 0	0 58	0 92	0.414	0.165	0.545
6	14.51	0 138	0 303	0 675	83.7	0.61	1 17	0.263	0 223	0.55
7	12 51	0.067	0 291	0 63	69 5	0 64	2 7	0.075	0.269	0.563
	12 1		0 269							

The reheating and deformation conditions were chosen in order to finish the steel in the same range of temperature (around 850°C), with a total deformation equivalent to the strain in the last passes of the finishing process The reference testing conditions were chosen to be 850°C and a strain of 0.2. These conditions were used to study the influence of cooling and coiling on the microstructure and mechanical properties Quenching tests performed just after deformation showed that the resulting austenite grain size was approximately 13μm

In the second part of this work, the reheating temperature and amount of deformation were changed in order to study the effect of austenite state on the subsequent transformation and on the final properties The various reheating and deformation conditions considered for this study are given in Table 3 4 Reheating at 1050°C was used in order to produce a very large austenite grain size, which led to the formation of low temperature products This was done with the objective of identifying these phases so as to be able to recognize them

Table 3.4. Reheating and deformation conditions

Reheat temperature	Strain used for study of the cooling conditions	Strains used for study of the effect of deformation
1050°C (10 min)	0	-
900°C (15 min)	0	0, 0 2, 0 4, 0 6, 0 8
850°C (10 min)	0 20	0, 0 2, 0 4, 0 6, 0 8
800°C (10 min)	0.20	0, 0.2, 0 4, 0 6, 0 8

III.2.3 Cooling and coiling conditions

From the information transmitted by SOLLAC on the industrial cooling conditions it was deduced that the cooling rate on the runout table is close to an average of 60°C/s This means that the cooling rate when the steel is still in the austenitic state should be above 100°C/s. For the present work, this type of cooling rate was aimed at In the first stage, however, only 55°C/s in the austenite was achieved This was used for a first set of experiments. In the second set, modifications to the helium pressure regulator permitted the attainment of 90°C/s in the austenitic range

As mentioned in the literature review, coiling corresponds to the very slow cooling of the steel from the coiling temperature to room temperature For the present study, the configuration of the grips prevented removal of the specimen at the end of cooling without a large decrease in temperature On the other hand, the radiant furnace was generally much hotter than the specimen, which prevented its use for the simulation of coiling Therefore, when the coiling temperature was reached, the helium flow was stopped and the specimen was left to cool in air, resulting in a cooling rate of approximately 3°C/s The coiling temperatures investigated were all in the range corresponding to regime III of coiling, as defined by Kunishige[36] Table 3 5 recapitulates the cooling rates and coiling temperature used for this study

Figure 3 11 shows the cooling curves obtained in four tests performed at a cooling rate of 90°C/s in the austenite, with different coiling temperatures The cooling rate was measured in the first portion of the curve, where it is a maximum The first inflexion point corresponds to the beginning of the austenite-to-ferrite transformation The corresponding decrease in cooling rate to approximately 30°C/s is due to the change in heat capacity and to the heat generated by the transformation

Table 3 5 Cooling Conditions

Cooling rate in the austenite	Coiling temperatures
55°C/s	550, 500, 450, 400 and 300°C
90°C/s	500, 450, 400 and 300°C

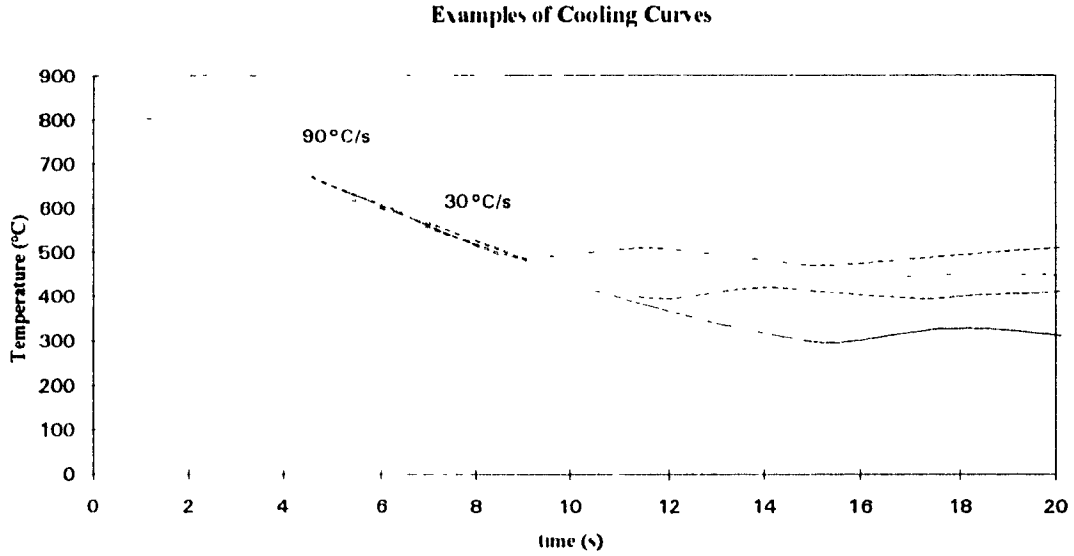

Figure 3 11 Examples of cooling curves.

III.3 Evaluation of the final properties.

III.3.1 Microstructure

III 3 1 a Austenite microstructure

The austenite microstructures were obtained by quenching just after deformation The specimens were cut at the intersection with the shoulder and mounted in bakelite for grinding with the torsion axis parallel to the surface to be observed The samples were ground using 240, 400 and 600 grit silicon carbide papers Polishing was then performed with 6μm diamond paste and 0 5μm alumina powder Etching was carried out in a solution of saturated picric acid containing 8 drops of HCl for 100 ml of solution and 3 drops of Teepol The solution was heated to approximately 80°C. This etchant reveals the prior austenite grain boundaries in the martensite microstructure formed on quenching.

The grain size was measured in the microscope using the method described in ASTM standard E112

III 3.1.a Final microstructure.

Optical microscopy

The same procedure was used for the observation of the final microstructures The etchant used in this case was Le Pera's reagent [46] This etchant is used to distinguish between ferrite, bainite and martenstite in dual phase steels It reveals the ferrite as a light tan phase, the bainite as a brown phase and the martensite as a bright white phase Pearlite was revealed as bainite when the lamellar structure was too fine to be seen using optical microscopy.

To measure the proportion of second phase, a grid with 25 intercepts was placed in the objective The number of intercepts falling in second phase grains was counted and

divided by 25 to give the volume fraction This was repeated over 10 fields or more for each specimen

Electron Microscopy

To make the thin foils, thin slices were cut from the surface of the optical microscopy samples They were ground down to a thickness of 70μm using 600 grit silicon carbide paper A Struers Tenupol 2 was then used for jet thinning with a solution containing 6% perchloric acid in methanol. The voltage was set at 30 V and the flow rate at 3 Liquid nitrogen was used to cool the solution down to -20°C

III.3.2 Measurement of the mechanical properties

To measure the mechanical properties of the final material, the tested torsion specimens were used directly as tensile specimens in an MTS servohydraulic tensile testing apparatus, as illustrated in Figure 3.11. As little material was available for this study, only one test was performed for each experimental condition A crosshead speed of 1mm/min was employed. The crosshead displacement as well as the force were registered continuously Engineering stress was calculated by dividing the force by the cross-sectional area of the specimen (i.e the gage cross-sectional area minus the center hole area) The yield stress was given by the intersection between a line parallel to the elastic region shifted by 0.2% and the stress-strain curve. The elongation was approximated by the crosshead displacement The percent elongation was corrected so that the results would be compatible with ASTM standards[47]

The total elongation e_f of the specimen is equal to the uniform elongation e_u plus the necking elongation The uniform elongation is independent of the geometry of the specimen On the other hand, it has been shown[48] that, for a given material, the necking elongation is proportional to the square root of the cross-section A_0, divided by the gage length L_0

$$e_f = \beta \frac{\sqrt{A_0}}{L_0} + e_u$$

For the tensile testing of flat specimens, the ASTM standard requires that the ratio L_0/A_0 be 4 5. In order to be able to compare the elongations obtained with results in the literature, a corrected elongation was calculated as follows

$$e_{corr} = e_u + 4\ 5\beta$$

$$\text{with } \beta = \left(\frac{e_f - e_u}{\sqrt{A_0}} \right) L_0$$

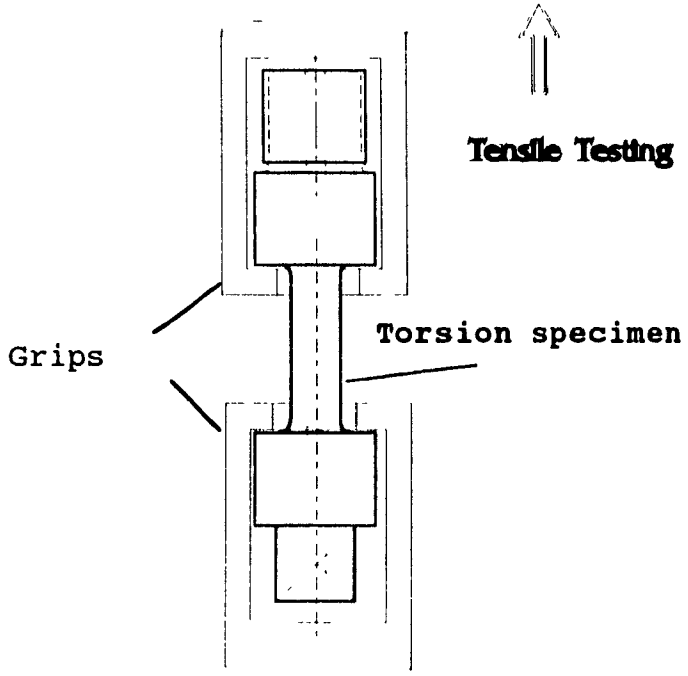

Figure 3.11 Use of the torsion specimen as a tensile specimen

CHAPTER IV

RESULTS

As underlined in the literature review, little is known about the details of C-Mn ferrite-bainite microstructures Most of the work on this subject was performed on compositions that have varied over a wide range, usually including alloying elements such as Cr or Mo Close examination of the bainite has seldom been performed For this reason, the first objective of this work was to identify the microstructures formed under standard rolling and cooling conditions As a second objective, the evolution of this microstructure and of the associated mechanical properties was studied for various process parameters.

This chapter will be divided in the following manner In the first part, the influence of the reheating and deformation parameters on the state of the austenite will be discussed. This will lead to some clarification of the experimental conditions and of the metallurgical meaning of the various process parameters In the second part, optical micrographs of the final microstructures will be presented as pertaining to the various rolling and cooling conditions A closer look will be taken at the bainite morphology through a TEM examination of a few particular cases Then, in the last part, the mechanical properties will be studied

IV.1 Initial microstructures

In order to compare the state of the austenite produced by the conditioning performed on the torsion machine with the states encountered on hot strip mills, the austenite microstructure was fixed by quenching specimens just after deformation for a few characteristic cases

Figure 4 1 shows the austenite microstructure obtained after reheating at 850°C for 10 minutes followed by a deformation of 20% (equivalent strain) The corresponding grain size was measured to be approximately 13μm, which is relatively close to the final grain size obtained from the computer simulation of hot rolling on the hot strip mill

In order to determine the influence of a coarser austenite grain size on the subsequent transformations, reheating at 900°C was performed, without deformation The resulting microstructure is shown in Figure 4 2 A grain size of 20μm was measured

The effect of deformation was also studied at these two reheating temperatures for strains ranging between 0 and 80%, applied in one single pass The microstructures obtained after a deformation of 80% at temperatures of 850°C and 900°C are shown in Figures 4 3 and 4 4, respectively The corresponding grain sizes were found to be 10μm for a temperature of 850°C and 15μm for 900°C

In order to produce even smaller grain sizes, specimens were reheated at 800°C for 10 minutes and then deformed to various strains However, because of the relatively low temperature or because of insufficient reheating time, incomplete austenitization was achieved For a deformation of 20%, the microstructure consisted of a mixture of fine (10-12μm) austenite and coarse (25μm) ferrite grains (Figure 4 5) For a strain of 80%, a band microstructure was developed, with elongated ferrite grains alternating with areas of fine recrystallized austenite, as shown in Figure 4 6 Even if this case cannot be related directly to conventional hot strip mill practice, it is of interest because of its extreme character In

fact, with ferrite already present and a very fine austenite grain size, this microstructure is expected to lead to high temperatures of transformation from austenite to other phases.

The final treatment was intended to produce very coarse austenite in order to promote low temperatures of transformation Reheating was carried out at 1050°C for ten minutes without deformation The resulting microstructure had a grain size of 150μm and is shown in Figure 4 7

Figure 4 1 Austenite microstructure after reheating at 850°C for 10 minutes followed by a deformation of 20%

Figure 4 2 Austenite microstructure after reheating at 900°C for 15 minutes

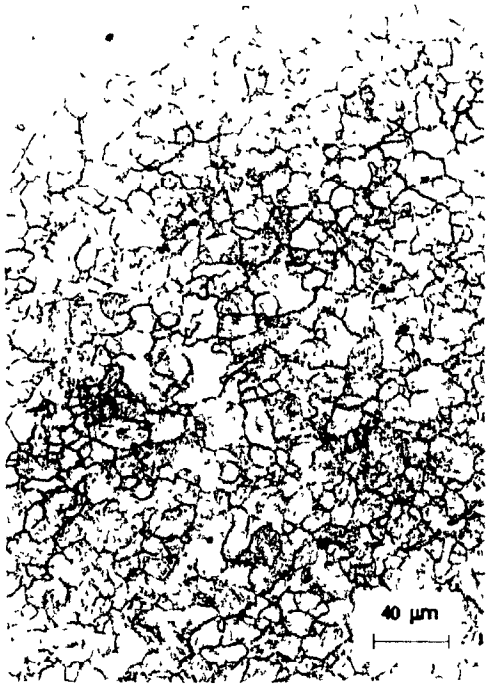

Figure 4.3. Austenite microstructure after reheating at 850°C for 10 minutes followed by a deformation of 80%

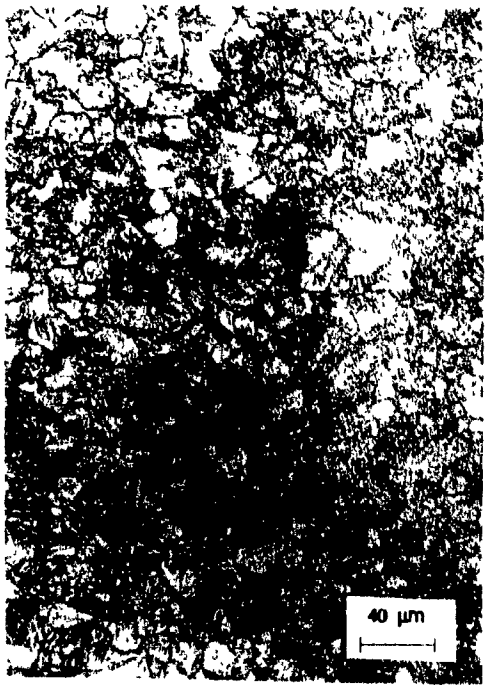

Figure 4 4 Austenite microstructure after reheating at 900°C for 15 minutes followed by a deformation of 80%

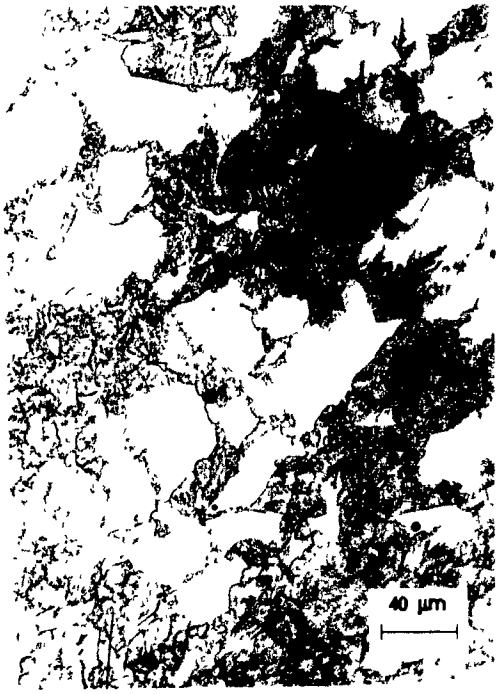

Figure 4 5 Austenite microstructure after reheating at 800°C for 10 minutes followed by a deformation of 20%

Figure 4 6 Austenite microstructure after reheating at 800°C for 10 minutes followed by a deformation of 80%

Figure 4 7 Austenite microstructure after reheating at 1050°C for 10 minutes (no deformation)

IV.2 Final microstructures

IV.2.1 Reference state

IV 2 1.a Optical microscopy

As mentioned above, the austenite microstructure produced by reheating at 850°C followed by a deformation of 20% is close to the microstructure observed on hot strip mills For this reason, the results obtained for this initial condition were considered as reference results They were the object of greater attention

Optical micrographs of the microstructures obtained after reheating at 850°C and applying a deformation of 20% followed by cooling at 90°C/s to coiling temperatures of 300°C, 400°C and 500°C are presented in Figure 4 8 No differences could be observed between the specimens coiled at different temperatures The microstructures were composed of a ferrite matrix, the light phase on the micrograph, and a second phase, in which the lamellar structure is not readily resolved by means of optical microscopy The proportions were approximately 52 % ferrite, 48% second phase The ferrite often had an acicular shape, with the elongated grains separated from one another by elongated second phase grains TEM investigation was necessary to identify the second phase positively These results will be discussed later In all cases, the mean grain size was approximately 5µm However, large second phase grains were also observed with a size of 15µm

When a lower cooling rate was used (55°C/s), the same type of microstructure was obtained (Figure 4 9) The proportion of second phase dropped to about 35% Again, it was not possible to identify firmly the second phase by means of optical microscopy No significant differences were observed between the optical microstructures of the specimens coiled at different temperatures

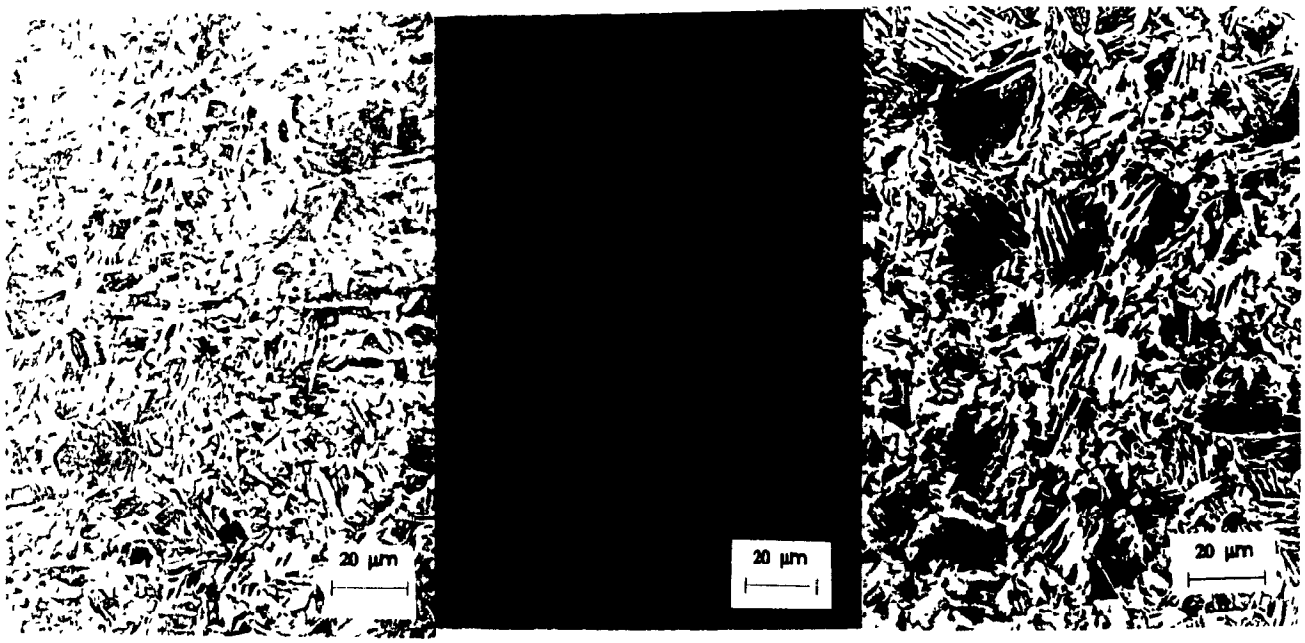

a) b) c)

Figure 4 8 Microstructure of samples reheated at 850°C, deformed 20% and cooled at 90°C/s to a) 500°C, b) 400°C and c) 300°C

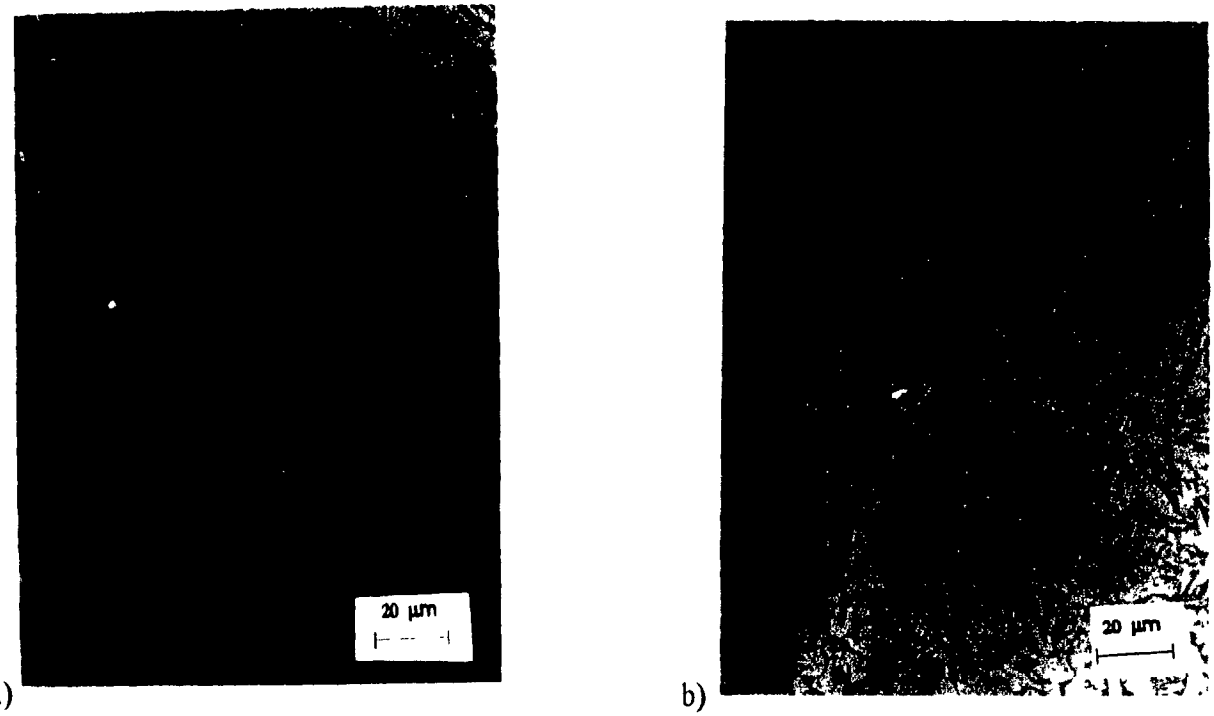

a) b)

Figure 4 9 Microstructure of samples reheated at 850°C, deformed 20% and cooled at 55°C/s to a) 500°C and b) 300°C

IV.2.1.b Electron microscopy

One of the main objectives of this work was to identify the second phase formed during accelerated cooling of the HR55 grade It was mentioned above that optical microscopy did not have high enough resolution for this purpose, TEM had to be used

Specimens cooled at 90°C/s

In Figure, 4 10 the microstructure of a specimen cooled at 90°C/s and coiled at 300°C is shown under low magnification It can be observed that the microstructure is relatively complex One can distinguish four main components i) polygonal grains of ferrite (A), ii) large acicular ferrite grains, iii) blocks of acicular ferrite with or without interlath carbides (B), iv) grains of ferrite with a dense but non-uniform distribution of iron carbides and, often, a high dislocation density (C) It is probable that the last two constituents correspond to the dark second phase on the optical micrographs, whereas the first two are related to the white phase The blocks of acicular ferrite containing interlath carbides correspond well with the definition of upper or B_2 bainite in Bramfitt and Speer's nomenclature[39] The other second phase constituent cannot be named so easily The size of the carbides and the frequent high dislocation density may be the mark of a low temperature phase related to lower bainite Figure 4 11 gives examples of this unusual microstructure

At a higher coiling temperature (450°C), the same type of microstructure was obtained, with clear B_2 bainite blocks (Figure 4 12) in addition to polygonal ferrite, acicular ferrite, and the other second phase component An example of the latter, where the very fine carbides are aligned and surrounded by agglomerations of dislocations, is presented in Figure 4 13 It was not possible to see any clear influence of coiling temperature on the final microstructure from the TEM examinations

Figure 4 10 TEM micrograph of a specimen reheated at 850°C, strained 20%, and cooled at 90°C/s to 300°C (A) polygonal ferrite grain, (B) bainite, (C) carbide-bearing second phase component

Figure 4 11 Carbides-containing ferrite second phase in a specimen reheated at 850°C, deformed 20% and cooled at 90°C/s to 300°C

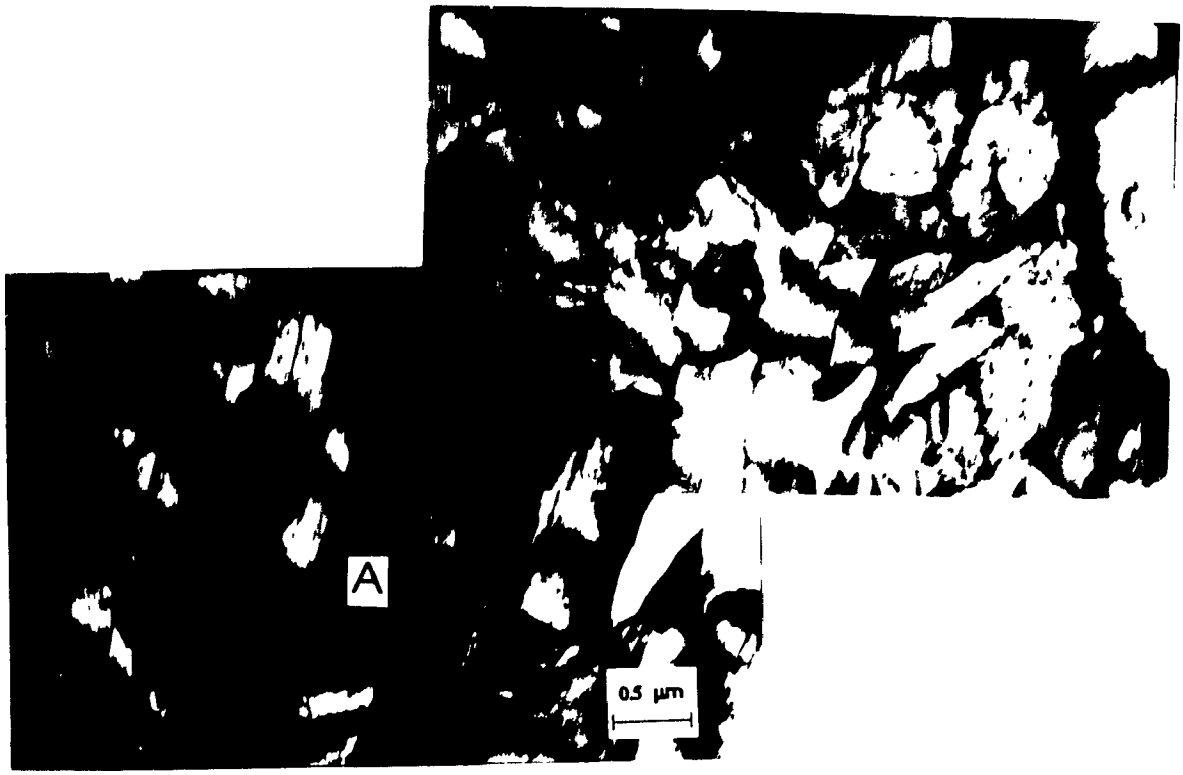

Figure 4.12 B_2 bainite (A) in a specimen reheated at 850°C, deformed 20% and cooled at 90°C/s to 450°C.

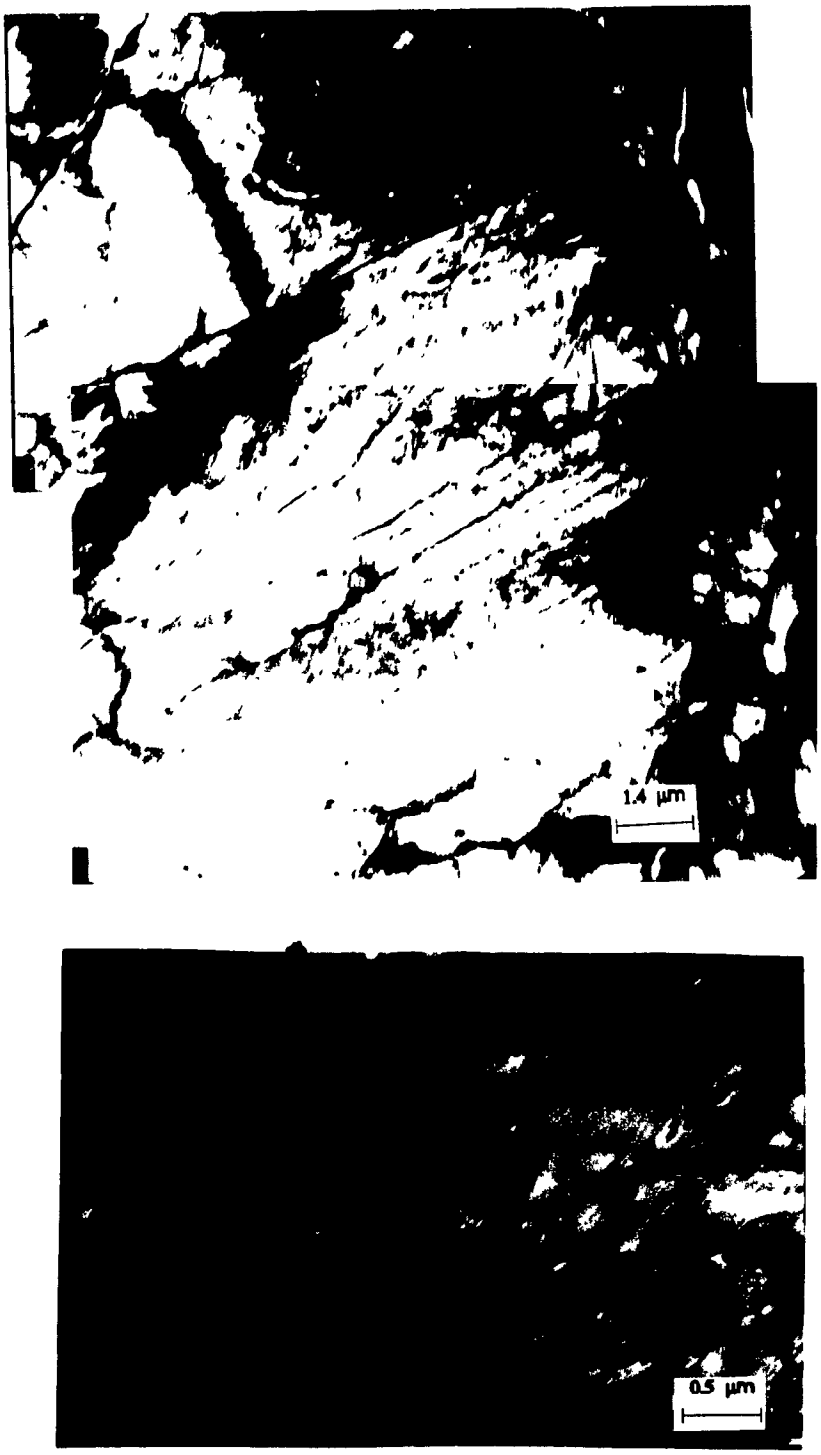

Figure 4 13 Aligned carbides in ferrite in a specimen reheated at 850°C, deformed 20% and cooled at 90°C/s to 450°C

Specimens cooled at 55°C/s

When a lower cooling rate (55°C/s) was used, the second phase had, most of the time, a clear lamellar pearlite structure (A) (Figure 4.14). Sometimes, however, this structure was degenerate (B). In Figure 4.14, grains of ferrite with an acicular shape can be seen. Again, the TEM observations did not reveal any difference between the specimens coiled at different coiling temperatures.

IV.2.2 Influence of the initial microstructure of the austenite

IV.2.2.a Reheating at 900°C

Specimens cooled at 90°C/s

An optical micrograph of a specimen reheated at 900°C for 15 minutes (austenite grain size 20μm), cooled at 90°C/s and coiled at 450°C is presented in Figure 4.15. This microstructure is similar to the microstructures observed in the specimens reheated at 850°C and strained 20% (austenite grain size 10μm). The volume fraction of second phase was approximately the same as for the previous case. TEM investigation revealed the same type of microstructural elements as for the specimens reheated at 850°C and strained 20%. Figure 4.16 shows a region of a specimen reheated at 900°C, cooled at 90°C/s and coiled at 300°C. In this case, bainitic ferrite without apparent carbides (A) or with interlath carbides (B) can be seen, in addition to non-uniformly distributed carbides inside a ferrite grain (C).

Specimens cooled at 55°C/s

The specimens reheated at 900°C and cooled at 55°C/s were found to have microstructures identical to the one found in the standard state at the same cooling rate.

Figure 4 14 Fine pearlite in an acicular ferrite matrix in a specimen reheated at 850°C, deformed 20% and cooled at 55°C/s to 350°C.

Figure 4 15 Microstructure of a specimen reheated at 900°C and cooled at 90°C/s to 450°C.

Figure 4 16 Bainites in a specimen reheated at 900°C and cooled at 90°C/s to 300°C

IV 2 2 c Specimens strained 80%

In order to obtain additional information about the influence of the initial austenite microstructure on the final microstructure, specimens were strained to an equivalent strain of 0 8 (80%) cooled at 90°C/s and coiled at 400°C after reheating at two temperatures (850°C and 900°C) The microstructure associated with a reheating temperature of 850°C is shown in Figure 4 17 It displays the same characteristic features as the microstructures observed in the specimens strained 20% The portion of second phase was 51%, which is identical to that found in the reference specimens The average grain size was finer than for the reference state (3 5μm) This seems to be due mainly to the smaller size of the second phase grains (10μm instead of 16μm)

IV 2 2 d Intercritically rolled specimens

A series of specimens was deformed in the intercritical range (austenite plus ferrite) at 800°C to various levels of strain These were subsequently cooled at 90°C/s to 400°C The microstructure produced by applying a strain of 20% is presented in Figure 4 18 It is composed of large areas of ferrite, which correspond to the ferrite present before accelerated cooling, and of a dense mixture of ferrite and a second phase which has replaced the former austenite At high magnification, the second phase displays a resolved lath structure (Figure 4 19), which indicates that it is bainite The fraction of second phase is around 44% for an initial austenite content of 62%, which means that 70% of the prior austenite transformed into the second phase

The same type of result was obtained for the specimens strained 80% before cooling (Figure 4 20) The measured proportion of second phase was 41%

Figure 4.17 Microstructure of a specimen reheated at 850°C, deformed 80% and cooled at 90°C/s to 400°C

Figure 4 18 Microstructure of a specimen reheated at 800°C (in the intercritical range), deformed 20% and cooled at 90°C/s to 400°C

Figure 4 19 Same as 4 18 The second phase possesses an acicular structure

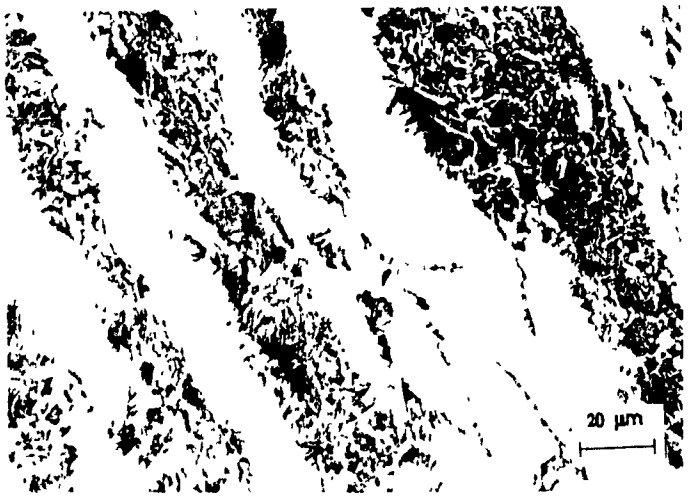

Figure 4.20 Microstructure of a specimen reheated at 800°C (intercritical range), deformed 80% and cooled at 90°C/s to 400°C.

IV 2 2 e Specimens reheated at 1050°C

A series of specimens was reheated at 1050°C for 10 min, leading to a coarse (150µm) austenite grain size Such a microstructure was produced in order to delay the austenite-to-ferrite transformation by decreasing drastically the number of ferrite nucleation sites The intention was to promote the formation of low temperature transformation products and to compare them with the phases identified in the previous cases The cooling rate used for these experiments was 55°C/s.

Optical micrographs of specimens coiled at 500, 400 and 300°C are presented in Figure 4 21 Optical microscopy does not reveal any dependence of the microstructure on coiling temperature It is composed of acicular ferrite and 30% of a second phase TEM examination revealed the nature of the second phase. When the coiling temperature was high, it was formed of bainite, with a well defined lath structure in addition to fine pearlite and ferrite grains containing non-uniformly distributed carbides (Figure 4 22). At a lower temperature (450°C), the proportion of ferrite grains containing carbides increased. The carbides were smaller and often aligned (Figure 4 23) At very low coiling temperatures, (300°C), martensite clusters were identified, in addition to the components present in the other specimens

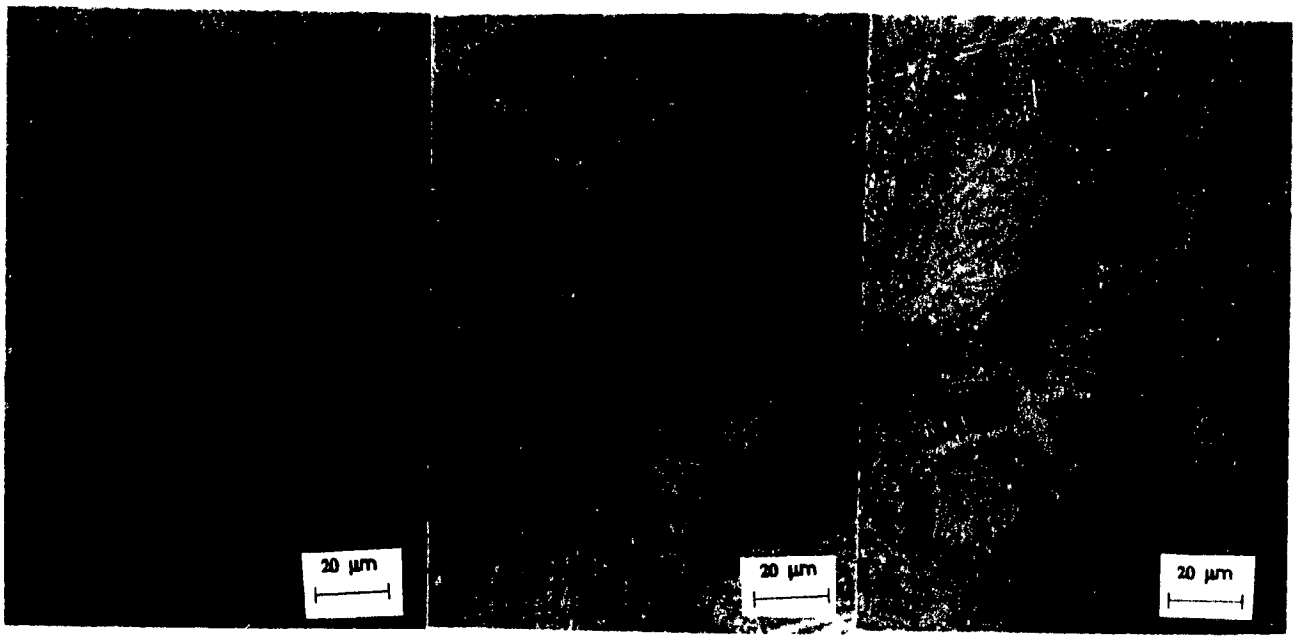

Figure 4.21 Microstructure of specimens reheated at 1050°C and cooled at 55°C/s to a) 500°C, b) 400°C and c) 300°C.

Figure 4 22 Carbides in ferrite in a specimen reheated at 1050°C and cooled at 55°C/s to 500°C

Figure 4 23 Aligned carbides in a specimen reheated at 1050°C and cooled at 55°C/s to 400°C

IV.3 Mechanical properties

IV.3.1 Influence of coiling temperature and cooling rate

IV 3 1 a Yield strength and tensile strength

The influence of coiling temperature on the tensile strength associated with various initial conditions and cooling rates is illustrated in Figure 4 24. The yield stress data are presented in Figure 4 25

Three different behaviors can be identified in Figure 4 24 The tensile strength of the first group of specimens is centered around 520 MPa and increases slightly with decreasing coiling temperature, from a low of 510 MPa for a coiling temperature of 530°C to 540 MPa for a coiling temperature of 300°C A second group is characterized by a stable level of tensile strength centered around 560MPa The third group displays a strong dependence on coiling temperature, with the tensile strength increasing from 515 MPa to 617 MPa

Reheating at 850°C and 900°C and cooling at 55°C/s

The first group of data correspond to specimens cooled at the lowest cooling rate, 55°C/s, from reheating temperatures of 850°C and 900°C It also includes the specimens deformed in the intercritical region and cooled at 90°C/s For the specimens reheated at 850°C and strained 20%, the tensile strengths ranged from 510 to 535 MPa, increasing slightly with decreasing coiling temperature. The yield strength was contained between 360 and 380 MPa For the specimens reheated at 900°C, the tensile and yield strengths were slightly higher (between 512 and 540 MPa for the tensile strength and between 375 and 396 MPa for the yield strength)

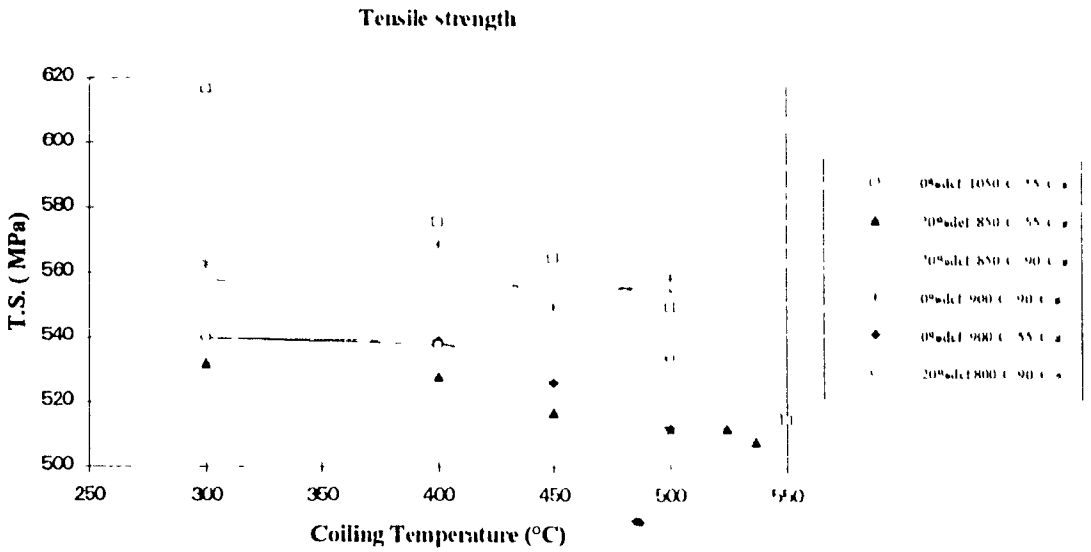

Figure 4 24 Evolution of the tensile strength with coiling temperature

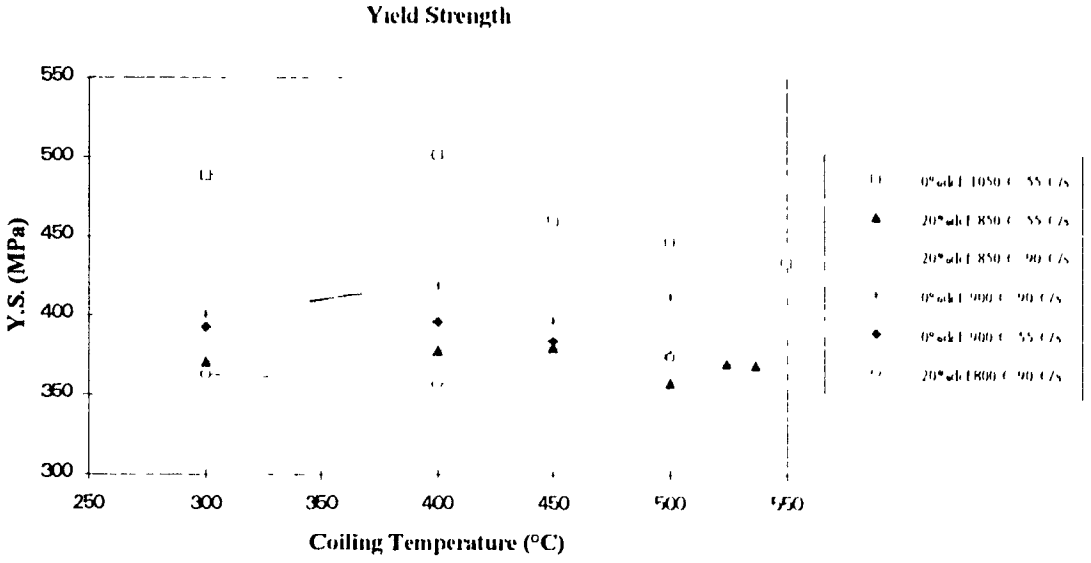

Figure 4 25 Evolution of the yield strength with coiling temperature

Although the yield and tensile strengths increase with decreasing coiling temperature, the magnitude of the variations is limited (20 MPa). As only one test was performed for each condition, the small trends observed can be attributed to normal experimental scatter For this reason, it can be concluded that coiling temperature has little influence on the tensile and yield strength of specimens reheated at 850°C, as well as of those reheated at 900°C when the cooling rate is 55°C/s

Deformation in the intercritical range and cooling at 90°C/s

The specimens deformed in the intercritical range at 800°C and cooled at 90°C/s also had tensile strengths at the same level, between 534 and 540 MPa, and relatively low yield strengths, between 357 and 363 MPa. The coiling temperature does not seem to have much influence on the mechanical properties under these conditions.

Reheating at 850°C and 900°C and cooling at 90°C/s

The second group of data concerns specimens cooled at 90°C/s from 900°C and 850°C The tensile strengths were around 555 MPa for reheating at 850°C and lay between 550 and 569 MPa for reheating at 900°C. The yield strengths fell between 395 and 414 MPa for both treatments The coiling temperature does not seem to have any influence on either the tensile or the yield strength at this cooling rate.

Reheating at 1050 and cooling at 55°C/s.

The last group of data is composed of the specimens reheated at 1050°C without deformation and cooled at 55°C/s In this case, the coiling temperature has a strong influence on the tensile strength, which increases continuously from 515 MPa to 617 MPa with decreasing coiling temperature The yield strength also increases from 433 MPa at a coiling temperature of 550°C to 502 MPa at 400°C, the value for a coiling temperature of 300°C being lower at 489 MPa

IV 3.1 b Elongation and yield ratio

The total elongations determined in these experiments are presented in Figure 4 26 The corrections necessary to match the ASTM standards as well as the possible inaccuracies due to the shape of the specimens make these results ambiguous The separate influences of cooling rate, coiling temperature and austenite state before cooling cannot be identified on this graph Only the specimens reheated at 1050°C display an elongation appreciably lower than for the other conditions

The uniform elongations (Figure 4 27) are probably more representative This is due to the fact that it is an intrinsic property of the material, and is independent of specimen shape In Figure 4.27, the same three groups of data can be identified as for the tensile strength. Specimens cooled at 55°C/s from a reheating temperature of 850°C or 900°C display the highest elongations, together with the specimens rolled in the intercritical range and cooled at 90°C/s Intermediate values are obtained for specimens cooled at 90°C/s from reheating temperatures of 900°C and 850°C Low values are observed for the specimens reheated at 1050°C No clear influence of coiling temperature could be observed on the uniform elongation

The uniform elongation and yield ratio (ratio of the yield strength to the ultimate tensile strength) are considered as the most important properties for the press forming of steels The yield ratio is illustrated in Figure 4 28 Very low yield ratios, between 0 66 and 0 70, were obtained for the specimens deformed in the intercritical range Yield ratios for the specimens reheated at 850°C or 900°C all fall between 0 70 and 0 75, independently of the cooling rate The highest yield ratios, between 0.80 and 0 85, were obtained for the specimens reheated at 1050°C

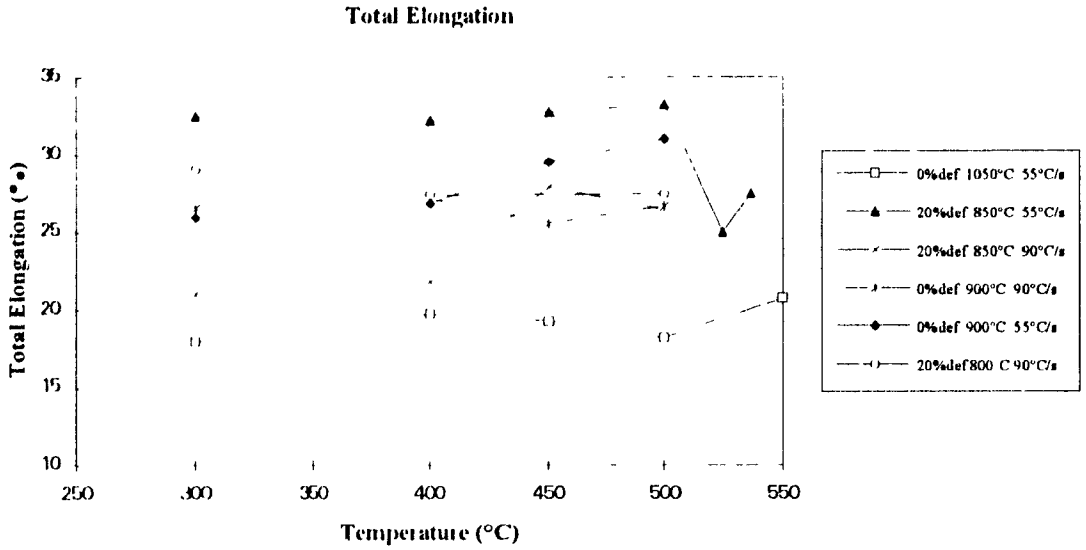

Figure 4 26 Evolution of the total elongation with coiling temperature.

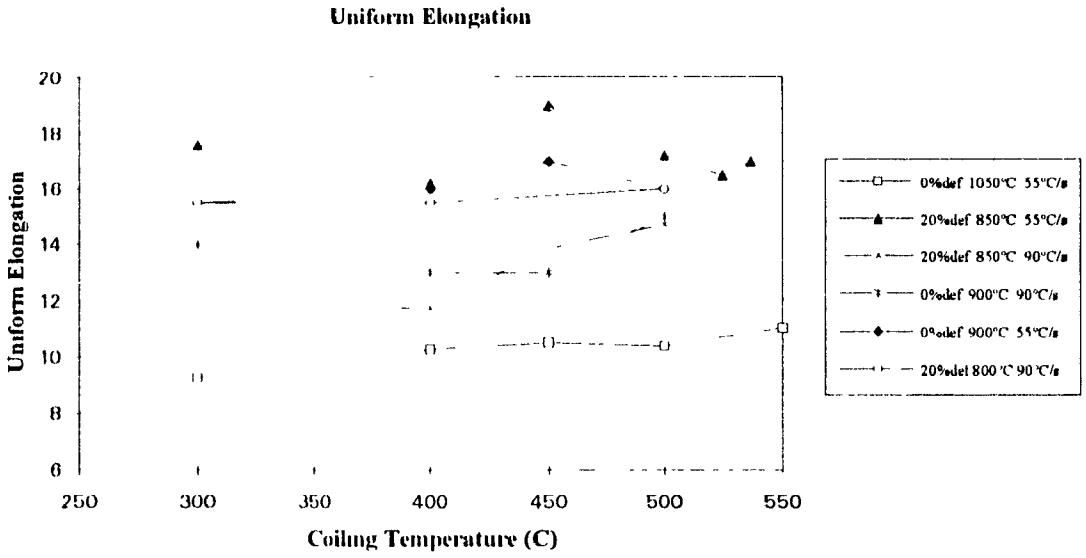

Figure 4 27 Evolution of the uniform elongation with coiling temperature.

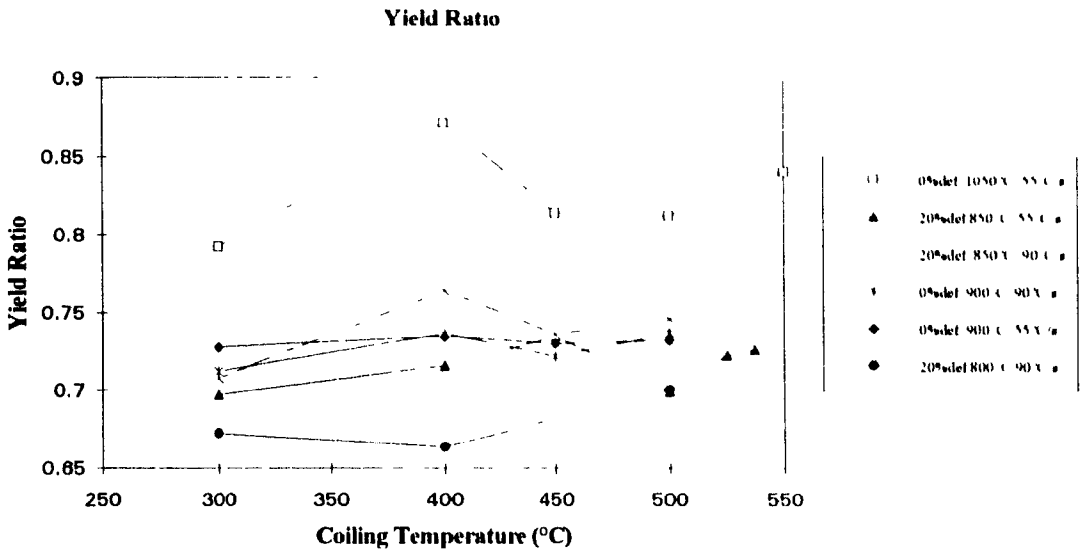

Figure 4 28 Evolution of the yield ratio (Y.S /U.T S) with coiling temperature

IV.3.2 Influence of strain

The first series of results on mechanical properties was intended to show the possible influence of coiling temperature, of cooling rate and to some extent of the state of the austenite before cooling. Additional information regarding the influence of the amount of strain will now be presented. Specimens were reheated to three different temperatures (800°C, 850°C and 900°C), subsequently strained to equivalent strains of 0 2, 0 4, 0 6 and 0.8, and cooled at 90°C/s The results are shown in Figure 4 29 for the yield and tensile strengths, in Figure 4.30 for the uniform elongations, and in Figure 4 31 for the yield ratio From these graphs, no influence of strain can be detected The yield ratios of the specimens deformed in the intercritical range are still the lowest

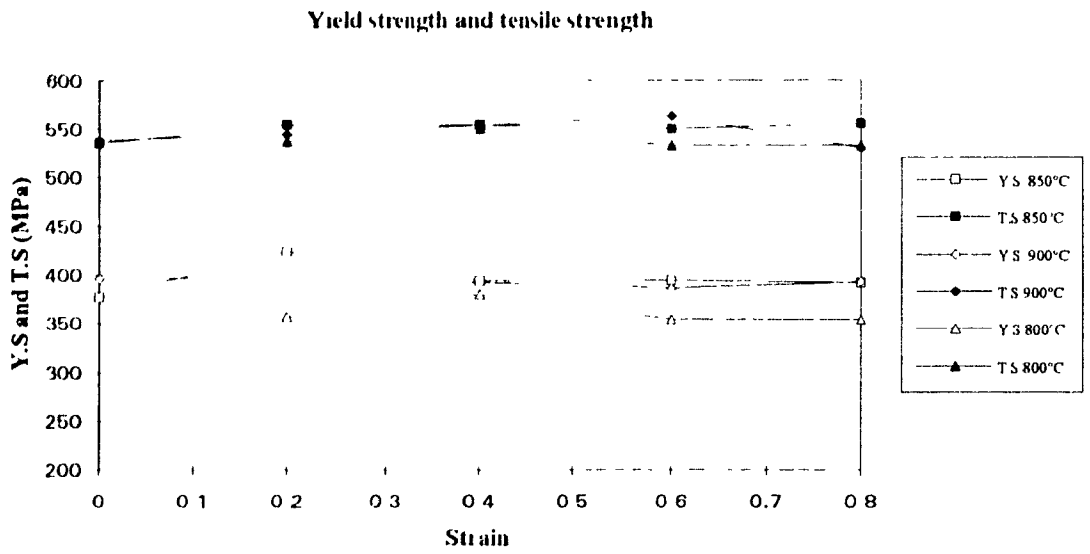

Figure 4 29 Influence of strain on the yield and tensile strengths.

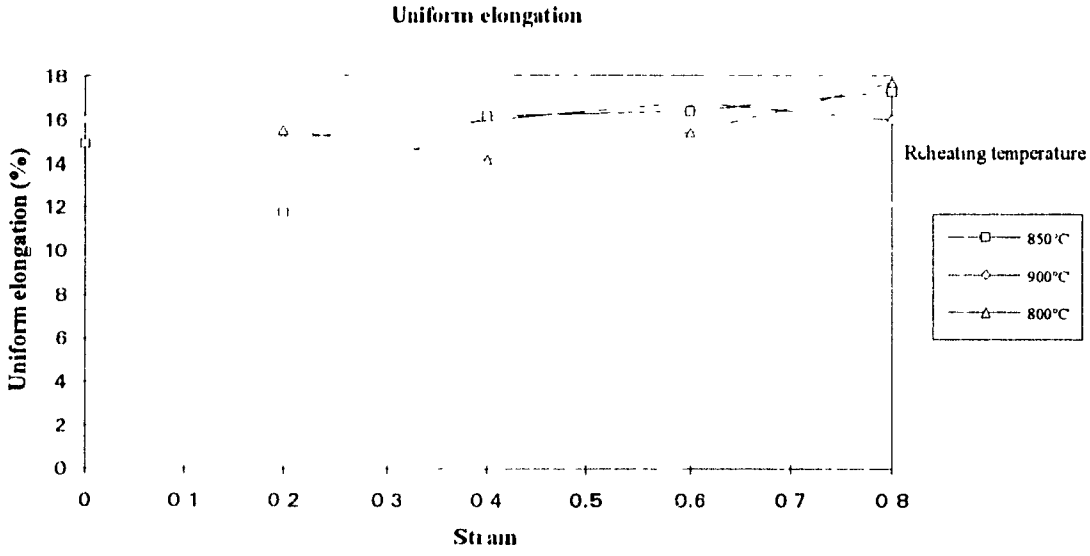

Figure 4 30 Influence of strain on the uniform elongation

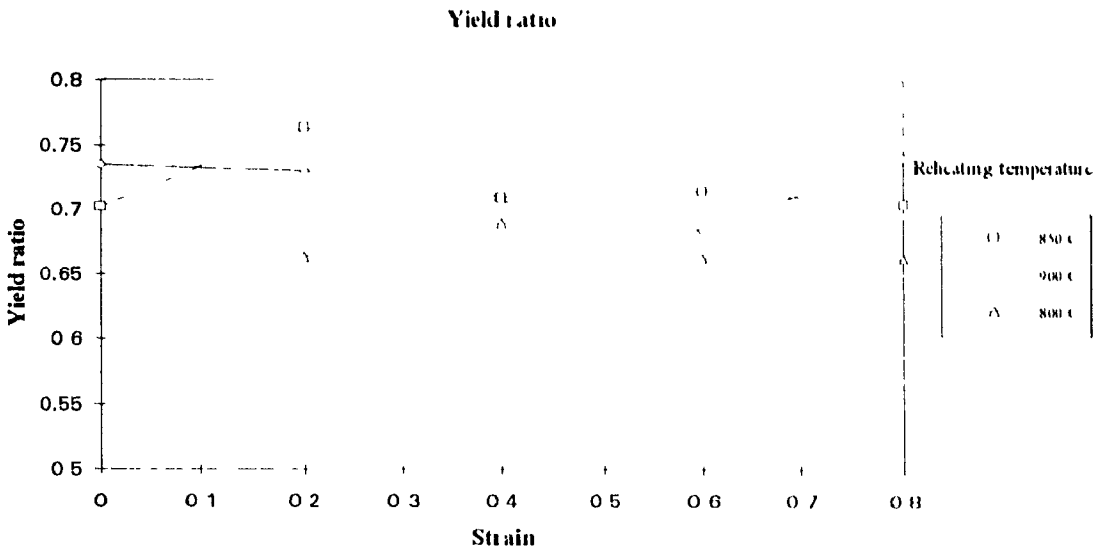

Figure 4 31 Influence of strain on the yield ratio

CHAPTER V

DISCUSSION

The results presented in Chapter IV were obtained by laboratory simulation. Nevertheless, they were intended to provide information about events taking place during the processing of HR55 steels in an industrial environment The link between the experiment and the industrial process is not necessarily an easy one to establish It will be the object of the first part of this discussion, where the influence of the various process parameters is described In the second part, a theoretical approach will be taken to explain the metallurgical phenomena observed during this study For this purpose, the cooling curves will be analysed in detail and a method, developed during this investigation, of deducing the transformation kinetics from the cooling data will be presented In the last part, a synthesis will be carried out, which leads to recommendations for rolling and cooling practices that should have beneficial consequences on the quality of this product

V.1 Microstructures

Various microstructures were observed and presented in Chapter IV The objective was to identify them in order to be able to interpret the metallographic results in an industrial context To begin the discussion, these microstructures will be summarized briefly This will permit the different cases to be related more clearly to the process conditions Then the consequences of these microstructural characteristics on quality control will be discussed

Three main microstructures were found

1 A mixture of polygonal and/or acicular ferrite, very fine pearlite and some degenerate pearlite This microstructure was observed in all specimens cooled from a fine austenite grain size (10 to 20μm) at the lowest cooling rate, 55°C/s Optical microscopy was insufficient in this case to make out the lamellar structure of the pearlite.

2 A mixture of polygonal and/or acicular ferrite, and a second phase containing B_2 bainite, and another component composed of ferrite containing a non-uniform distribution of carbides This microstructure was observed in all specimens cooled from a fine austenite grain size (10 to 20μm) at a high cooling rate, 90°C/s Under an optical microscope, the appearance of this mixture was similar to that of the previous microstructure, differentiated from the latter only by a higher fraction of second phase

3 A mixture of strongly acicular ferrite, and a second phase containing B_2 bainite, and another component composed of ferrite containing a non-uniform distribution of carbides This microstructure was observed in specimens cooled at 55°C/s from a coarse austenite grain size (150μm) The proportion of the ferrite plus carbide phase seemed to increase when the coiling temperature was decreased

The lack of information about the appearance of the second phase from other sources makes it difficult to compare these results with those of other workers The main information found indicates that, in the case of the specimens cooled at 90°C/s from a fine austenite grain size (10 to 20μm) and at 55°C/s from a coarse austenite grain size, the second phase is not composed of a single component but of two different components One is easily identifiable as bainite The second does not correspond readily to any classical nomenclature It does not possess a lamellar structure attributable to pearlite nor

a clear lath structure, such as those encountered in bainites or martensites At this point, it is not even possible to conclude whether the second component is a low temperature product, related to lower bainite, or a high temperature product, such as a form of degenerate pearlite The frequently observed high dislocation density could be a sign that it is a low temperature product So would the observation that the proportion of this unidentified component tends to increase as the coiling temperature is decreased. However, TEM observations are not necessarily representative of the bulk material as far as the proportions of the phases are concerned The massive appearance of the carbides and their alignment could indicate that this phase was formed at high temperatures as a result of the decomposition of pearlite This would be in agreement with the fact that pearlite was also observed in the specimens cooled at 55°C from a coarse austenite grain size

From an industrial point of view, the fact that the second phase is composed of two elements that cannot be distinguished solely by optical microscopy limits the use of the latter for quality control of the so-called ferrite-bainite grades Moreover, the optical microstructures produced by slow cooling differed from the ones obtained by fast cooling only by the amount of second phase During this research, several etchants were tried (nital, picral, Le Pera's reagent), all of which led to the same type of contrast between the second phase and the matrix In all cases, the distinction between the former and the latter was complicated by the morphology and composition of the second phase, which resulted in large darkness variations within the second phase grains It appears that areas containing a high concentration of carbides are much darker than the lath-bainite that is almost free of precipitates For this reason, the attempts to use image analysis for quantitative characterization of the microstructure resulted in only limited success. This is another difficulty with regard to the industrial context, where image analysis now tends to be used extensively for quality control

V.2 Influence of the process parameters

The second objective of this work was to identify the influence of process parameters such as cooling rate, coiling temperature and finish rolling temperature The results displayed in Chapter IV were all obtained under conditions intended to represent possible variations of the actual process parameters In what follows, the major tendencies will be outlined. In the next section, the physical mechanisms involved in the phenomena observed will be examined more closely

V.2.1 Coiling temperature

As mentioned in the literature review, coiling temperature is considered by many authors as the most influential parameter with regard to the microstructure and mechanical properties [29-32]. Most authors distinguish three different temperature ranges between which large differences are observed: regime I for temperatures above 500°C, leading to the formation of ferrite-pearlite microstructures, regime II for temperatures between 500°C and 300°C, in which ferrite-plus-bainite is found, and regime III corresponding to temperatures below 300°C, where martensite is sometimes produced

In the present context, the idea was not to develop a new steel, but rather to investigate the possible variations in microstructure and properties likely to be induced by processing parameter fluctuations during the manufacture of HR55 strip For this reason, all the investigations were carried out within the regime II temperature range, i e between 500°C and 300°C, with exception of a few tests at 550°C

The results can be classified according to the state of the austenite before accelerated cooling. For specimens reheated to low temperatures, i e 800°C, 850°C and 900°C, the coiling temperature did not seem to have an influence on the microstructure The mechanical properties were subject to some variations, which remained, however,

limited in amplitude For example, the specimens cooled at 55°C/s from reheating temperatures of 800°C and 900°C displayed an increase in tensile strength of approximately 20MPa when the coiling temperature was decreased from 500°C to 300°C (Figure 4 24) This can be considered as a variation of limited importance

The yield strength did not display the same evolution It was relatively stable over the entire coiling temperature range or, rather, it exhibited fluctuations that could not be related to changes in coiling temperature The specimens cooled at 90°C/s from fine austenite microstructures also displayed very uniform yield and tensile strengths over the coiling temperature range. In their cases, the uniform elongation was subject to larger variations than for the other specimens But, again, it was not possible to deduce any clear tendency from these results Putting together all the observations, it can be said that coiling temperature has very little influence on the mechanical properties for specimens which have fine austenite grain sizes before accelerated cooling; this confirms what was already observed for the microstructures

For the specimens reheated at 1050°C, which exhibited a coarse austenite grain size before accelerated cooling, some variations were observed in the microstructure with decreasing coiling temperature The mechanical properties also displayed large variations with decreasing coiling temperature The tensile strength increased as much as 100MPa when the coiling temperature was lowered from 550°C to 300°C The yield strength was also affected, with an increase of about 70MPa between 550°C and 400°C A further decrease to 300°C resulted in a decrease in yield strength that can be attributed to the appearance of martensite, which was observed at that temperature Similar diminutions of yield strength because of the appearance of martensite have been observed by many workers and are at the origin of the outstanding work hardening properties of dual-phase steels Consequently, we can say that coiling temperature has a strong influence on the

microstructure and mechanical properties in the case of specimens reheated at 1050°C before accelerated cooling

V.2.2 Cooling rate

As mentioned in the literature review, few studies have concentrated on the influence of cooling rate on the properties of ferrite-bainite steels and, when this was done, it was the pattern of cooling that was changed and not the cooling rate itself The cooling rates used were also often much lower than the cooling rates encountered in hot strip mills. The intention of the present study was thus to determine the role of cooling rate, when it is situated in a range comparable with industrial ones Two cooling rates were used for this work 90°C/s and 55°C/s, as measured in the austenite temperature range

Figure 4 24 above illustrated the influence of cooling rate on tensile strength For the same initial conditions, an increase in cooling rate from 55°C/s to 90°C/s resulted in an increase in tensile strength by an average of 30MPa The yield strength displayed similar behavior, as it increased by approximately 30MPa, while the uniform elongation decreased by 3 to 4% (Figure 4.27)

The microstructures were also greatly affected by the increase in cooling rate The proportion of second phase rose from 35% to nearly 50% and its morphology changed from lamellar pearlite to lath-like B_2 bainite and/or ferrite containing a fairly high density of carbides. This evolution explains the observed variation in the mechanical properties, although such a strong influence on the microstructure was not expected

V.2.3 State of the austenite

The last factor studied in this investigation was the state of the austenite before accelerated cooling. It is related to the finish rolling temperature employed in the hot strip mill. In the present study, the state of the austenite was changed by changing the reheat

temperature as well as the amount of strain before cooling This resulted in variations in austenite grain size from 10 to 20μm

The last section of Chapter IV revealed that the state of the austenite had no noticeable effect on the mechanical properties in the case of the specimens cooled at 90°C/s (Figures 4 29 to 4 31) This was also evident from Figures 4 24 to 4 28, where the mechanical properties of the specimens reheated at 850°C (13μm) and those of the specimens reheated at 900°C (20μm) were identical Furthermore, the microstructure was little affected by such a change in austenite grain size, the only variation being a slight decrease in final grain size

These results are in apparent contradiction with the observations of various authors, who found that larger strains applied prior to accelerated cooling promoted the formation of higher temperature second phase products such as pearlite, leading to a decrease in the strength of the steel

In the case of the specimens cooled at 55°C/s, a slight increase in tensile strength (10MPa) was noticeable when the reheating temperature was increased from 850°C to 900°C However, the extent of this variation is limited and is not likely to be significant

The case of intercritical rolling was also studied While the second phase formed by cooling at 90°C/s looked like bainite, the mechanical properties obtained were those of a specimen cooled at 55°C/s from a fine (10 to 20μm) austenite structure. For these specimens again, the strain did not seem to have any influence on the mechanical properties, even when very large variations in grain size and ferrite/second phase distribution were involved

Additional results were obtained by reheating at 1050°C. In this case, the behavior of the steel was completely different, because it displayed a strong sensitivity to coiling temperature and because very high strength levels were attained However, the austenite

grain size resulting from reheating was extremely coarse, 150μm, i e about 10 times the grain size of the specimens mentioned earlier

V.3 Interpretation of the results

In the previous sections, the influence of the process parameters on the microstructure and mechanical properties was described It can be summarized as follows there is a strong influence of cooling rate and little influence of coiling temperature or state of the austenite before accelerated cooling In order to understand these results, it is of interest to know something about the progress of transformation during accelerated cooling Such information is usually obtained from dilatometer measurements But the equipment was not available at McGill For this reason, a new and different method was developed. It is based on work published by IRSID and uses changes in the thermal properties of steel during cooling

In what follows, the principles of the IRSID method will first be explained Then, the limitations attributable to the configurations of the specimen and of the machine will be dealt with. The assumptions made and the experimental verifications carried out will also be the object of a section Finally, the results will be summarized and presented together with the transformation mechanisms that are considered to occur on the runout table

V.3.1 Principles of the IRSID method

The method was described briefly during the 29th Conference of Metallurgists in Hamilton[15] It is based on performing a thermal balance during cooling During cooling, heat is removed from the specimen at a rate that can be calculated, provided that laws of cooling for the relevant medium are known If the specific heat of the material is known, the temperature changes induced by such heat removal can be calculated in the absence of transformation When transformation occurs, heat is generated (or absorbed, depending on the direction of the reaction) It results in a lower cooling rate (see Figure 5 1) This heat being proportional to the amount of primary phase transformed into the secondary phase,

it is possible to deduce this quantity from the deviations from the original cooling rate This phenomenon is described formally by the following equation

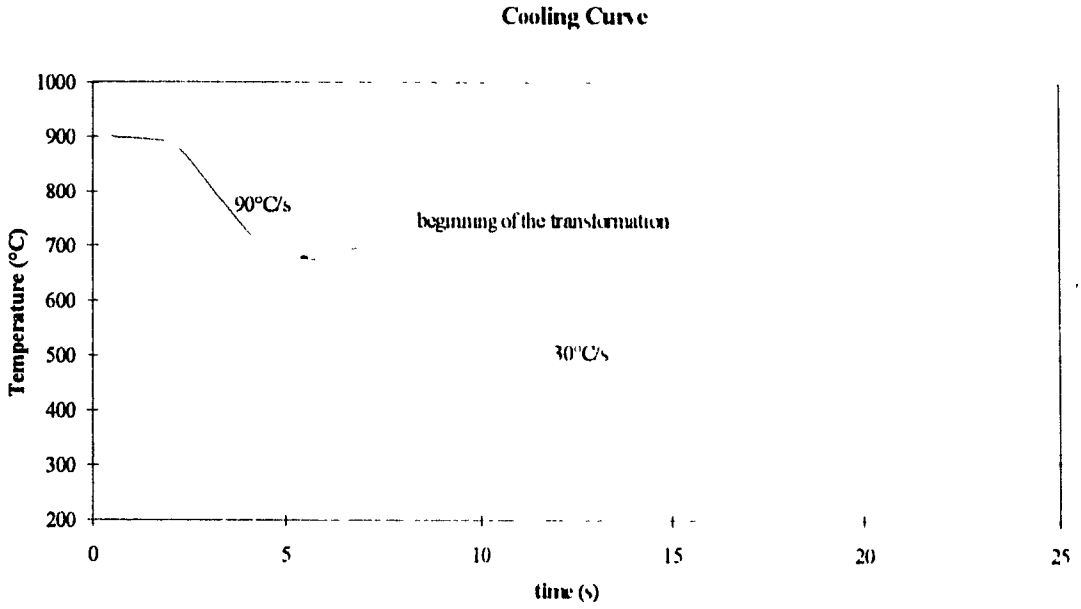

Figure 5.1 Cooling curve illustrating the influence of the transformation on the cooling rate.

The general heat balance can be written as:

$$\Phi . A . dt = -m\, C_p\, dT + m . \Delta H_{\gamma \to \alpha} . dz \qquad (5\ 1)$$

where Φ is the flux of heat removed by the coolant per unit area, A is the surface area of the specimen, dT is the temperature increase in time dt, m is the mass of the specimen, C_p is the specific heat of the material at instant t, $\Delta H_{\gamma \to \alpha}$ is the heat generated by the austenite to ferrite transformation per unit mass, and dz is the fraction of austenite transformed in time dt.

When this method was first used at IRSID, small dilatometer specimens were used with compressed helium as the coolant. In this case, the heat flux Φ was known with precision. The rate of heat transfer obeyed Newton's law,

$$\Phi = \lambda(T - T_{gas}) \qquad (5\ 2)$$

where T is the temperature of the specimen surface, T_{gas} is the temperature of the cooling gas, and λ is a constant that depends on the thermal conductivity of the gas, the geometry of the specimen, and the pressure and rate of flow of the gas around the specimen.

The temperature of the specimen was measured during cooling, and the thermal properties, C_p and $\Delta H_{\gamma\to\alpha}$ were known It was thus possible to calculate the amount of transformation dz from.

$$dz = \frac{\Phi . A.dt + m\ Cp.dT}{m\ \Delta H_{\gamma\to\alpha}} \qquad (5.3)$$

V.3.2 Modification of the method to torsion specimens

In the present case, the specimens were much more massive than for dilatometry and the temperature was measured at the interior. In Chapter III, computer simulations showed that, during cooling, gradients of temperature were generated between the center and the skin of the specimen. This implied that Newton's law could not be used directly by replacing the surface temperature by the center temperature.

In order to determine the relation between the heat flux and the temperature at the center, a computer simulation of cooling was performed assuming that no transformation occurs. Figure 5 2 shows the curve of cooling rate versus temperature at the center obtained from this simulation. A linear relationship is observed over the major part of the curve. To check this result, a ferritic stainless steel sample, which does not transform when the temperature is decreased, was cooled in our testing apparatus. The same type of relationship was obtained (Figure 5.3). The cooling rate measured at the center of the specimen in the absence of transformation can thus be expressed as:

$$\frac{dT}{dt} = aT + b \qquad (5.4)$$

where a and b are constants.

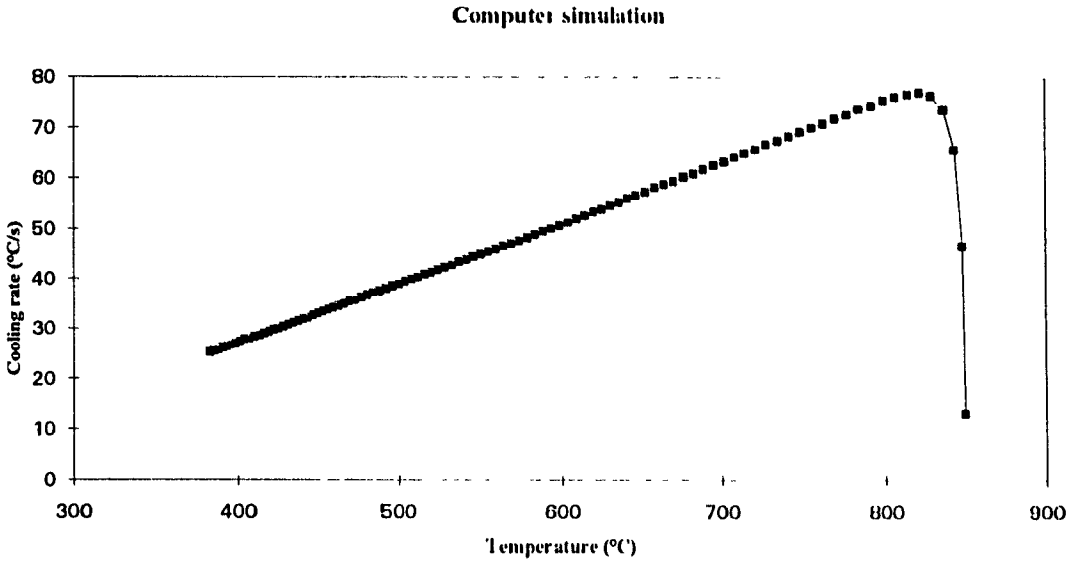

Figure 5.2 Cooling rate versus temperature obtained by computer simulation assuming that no transformation takes place

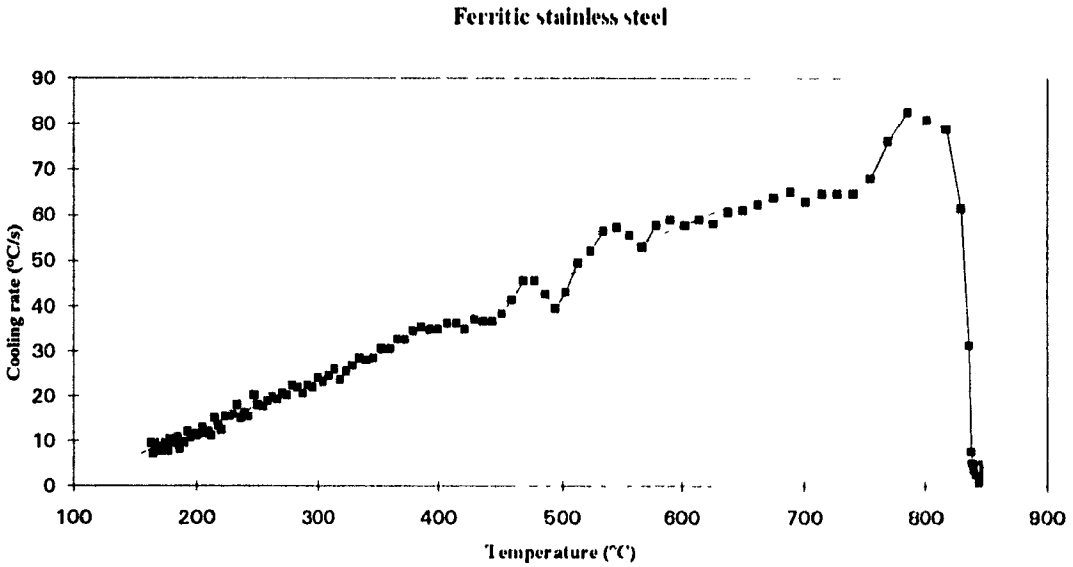

Figure 5.3 Cooling rate measured on a ferritic stainless steel specimen cooled with compressed helium.

For a cylindrical cell of radius r and length l located in the center of the specimen, the heat balance can be written, in the absence of transformation, as

$$2\pi r l.\Phi.dt = -\pi r^2 l.\rho.C_p.dT \qquad (5.5)$$

where ρ is the mass per unit volume. When combined with equation (5.4), this yields:

$$\Phi = \frac{r\rho}{2} C_p(aT+b) \qquad (5.6)$$

It is convenient to express Φ in a form similar to Newton's law, which is done by defining a function λ(T) such that:

$$\Phi = \frac{r\rho}{2} \lambda(T)(T - T_{gas}) \qquad (5.7)$$

The general heat balance becomes:

$$\lambda(T).(T - T_{gas}).dt = -C_p\, dT + \Delta H_{\gamma\to\alpha} dz \qquad (5.8)$$

From equation (5 7) and assuming that no transformation takes place (equation 5.6), the general form of λ(T) can be deduced.

$$\lambda(T) = C_p\left(\frac{aT+b}{T - T_{gas}}\right) \qquad (5.9)$$

In what follows, it is assumed that λ(T) retains the same form throughout the transformation. In other words, this is equivalent to assuming that heat transfer from a cell within the specimen is not greatly affected by the transformation. This neglects possible changes attributable to modification of the thermal conductivity of the material due to the transformation. However, computer simulations have shown that such variations are not very large, which permits use of the assumption as a first approximation.

To determine the transformation kinetics, one only has to know the values of a and b. They are obtained by fitting the function λ(T) to the curve relating $\frac{C_p}{(T-T_{gas})}\frac{dT}{dt}$ to the temperature at temperatures where the state of the material is known. This is illustrated in Figure 5.4. $\frac{C_p}{(T-T_{gas})}.\frac{dT}{dt}$ was calculated for the two values of C_p corresponding to austenite and ferrite. At high temperatures, λ(T) is fitted to the curve for austenite and at low temperatures it is fitted to the curve for ferrite. dz is then obtained using equation (5.8) through an incremental process. After each time increment, dz is calculated along with C_p, which is expressed as

$$C_p = z\, C_{p_\alpha} + (1-z)\, C_{p_\gamma} \qquad (5\ 10)$$

where $C_{p\alpha}$ and $C_{p\gamma}$ are the specific heats of ferrite and austenite, respectively

The kinetic curve obtained by this method is illustrated in Figure 5 5, together with the cooling rate versus temperature curve for the specimen for which λ(T) was fitted in Figure 5.4. The correspondence between the linear portions of the cooling rate curve and the beginning and end of the detected transformation is readily observable

A computer program which performs all these calculation steps was written. The flow chart is shown in Figure 5.6. The listing is given in Appendix III. The results obtained by this method were compared with those reported by A. Hurkmans et al.[11], who employed a similar method on a 0.11%C-1%Mn steel. Good agreement was observed for the shapes and positions of the curves.

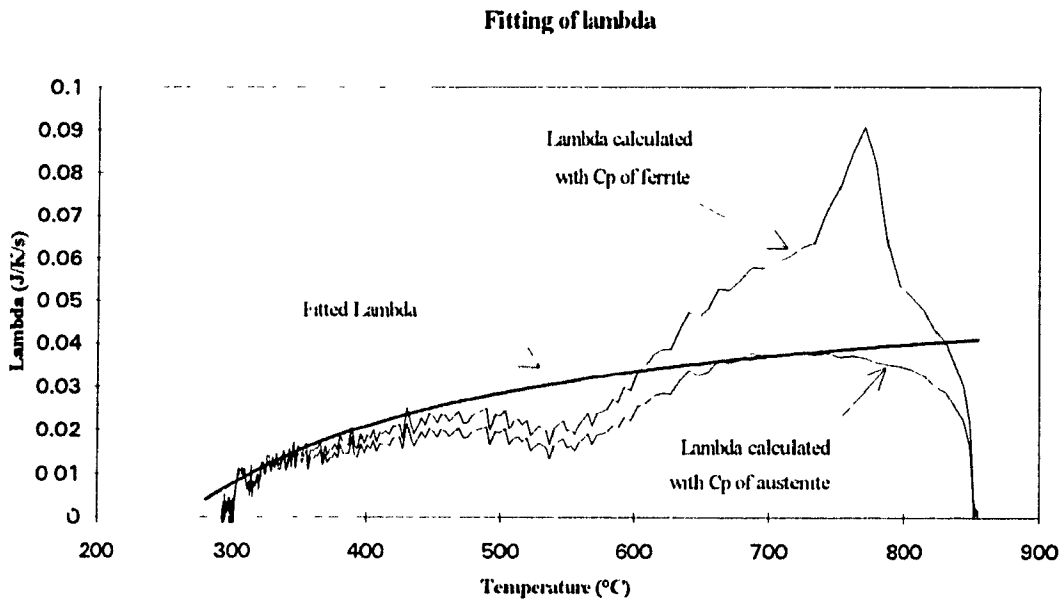

Figure 5.4 Fitting of the function for λ to the cooling data.

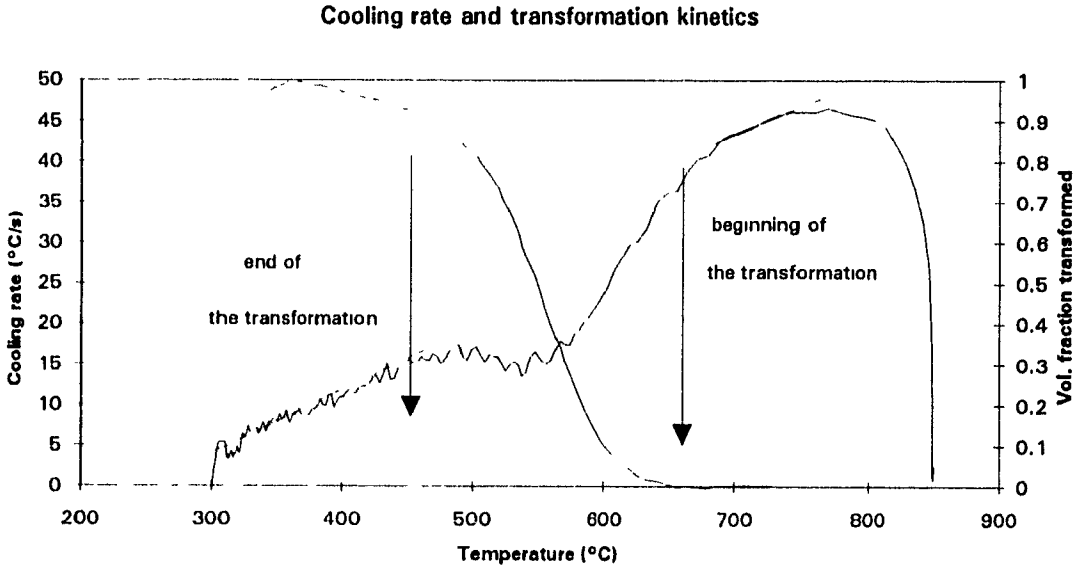

Figure 5.5 Transformation curve obtained by the IRSID method and the corresponding cooling rate.

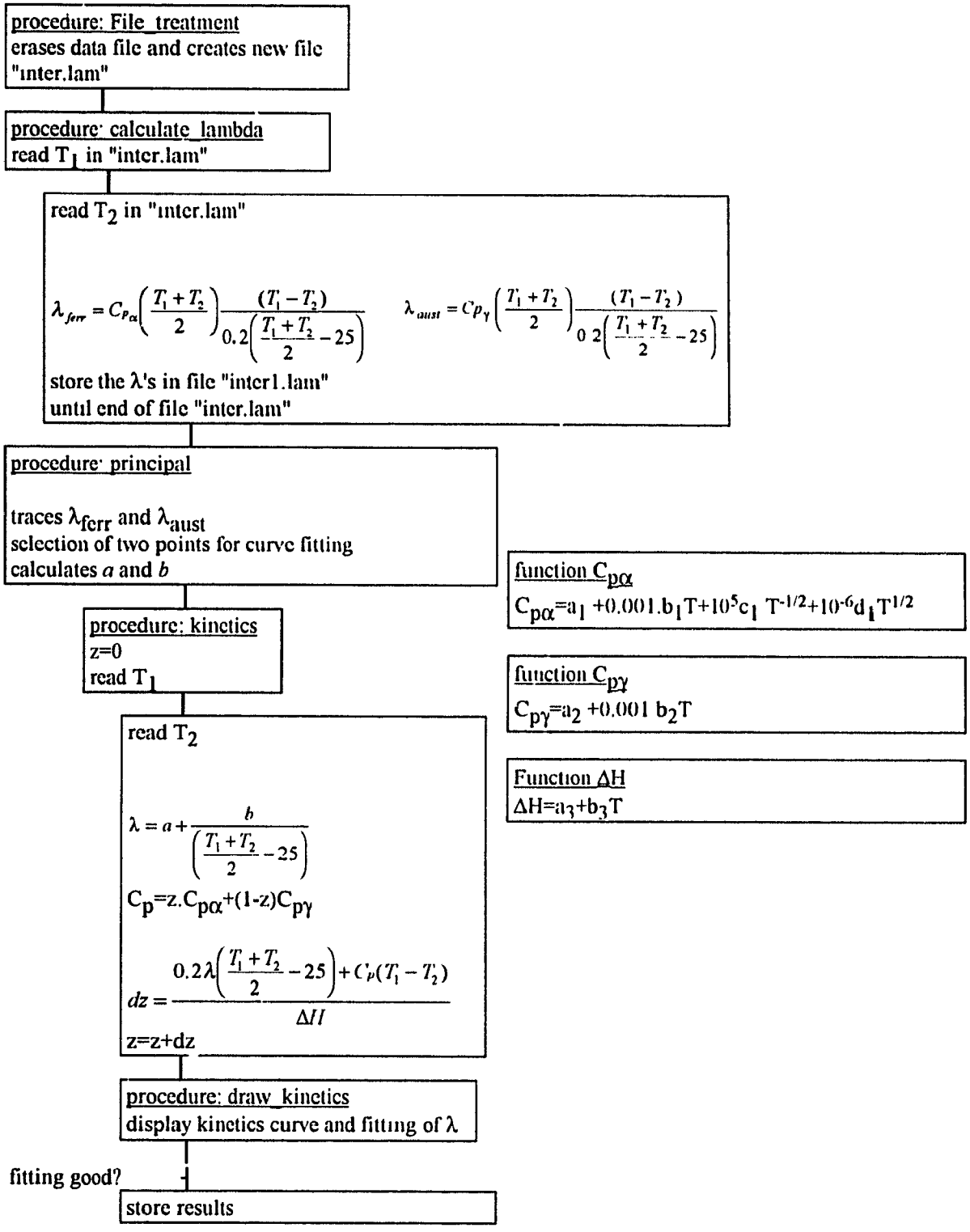

Figure 5.6 Simplified flow chart of the computer program used for the calculation of the transformation kinetics by the IRSID method

V.3.3 Transformation kinetics

Using the method described above, the transformation kinetics were calculated for several specimens reheated, deformed and cooled under various conditions. In order to have a large range of temperatures for the fitting of $\lambda(T)$ at low temperatures, only the specimens coiled at 300°C or below were used. The results are displayed in Figure 5 8.

Three different behaviors are observed. The specimens cooled at 55°C/s from 900°C or 850°C begin their transformation at the highest temperature (730°C) and are completely transformed above 500°C. When the cooling rate is increased, the transformation curved is moved by approximately 25°C towards lower temperatures. When reheating is performed at 1050°C (leading to coarser austenite grain sizes), the transformation is further delayed by 75°C

The negligible influence of coiling temperature on the microstructure and mechanical properties can be readily interpreted with the aid of Figure 5.7. For both the specimens cooled at 55°C/s and those cooled at 90°C/s from a fine austenite microstructure, the transformation was 95 % complete above 500°C The majority of the coiling temperatures employed were situated below 500°C, i.e. in a range where the transformation was over. The only possible alterations that could result from decreasing the temperature would be changes in the carbon or nitrogen concentration, as described by Kunishige[16].

The effect of nitrogen is related to the precipitation of AlN, which occurs only very slowly at low temperatures, leading to an increased level of solute nitrogen in the matrix. In the present case, the amount of isothermal holding after the end of accelerated cooling was probably insufficient for any significant AlN precipitation. This is amplified by the fact that the present nitrogen content was approximately half that used by Kunishige.

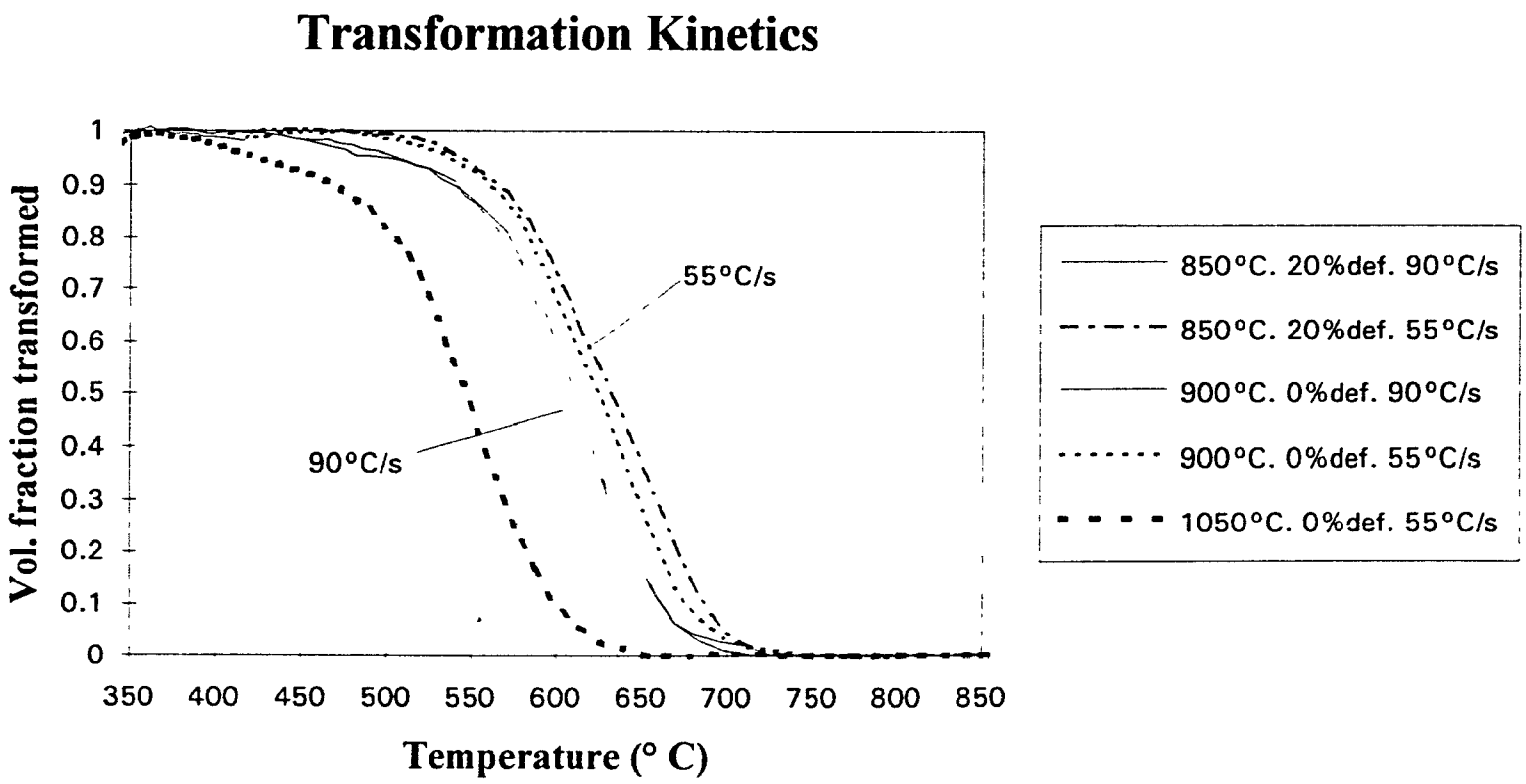

Figure 5 7 Transformation kinetics calculated by means of the IRSID method

Variations of solute carbon content were observed by Kunishige after coiling at temperatures between 200°C and room temperature. In the present study, the coiling temperatures were above 300°C. Little influence of coiling temperature can thus be expected

For the specimens cooled at 55°C/s from a reheating temperature of 1050°C, corresponding to a large austenite grain size, a strong influence of coiling temperature was observed. This can be interpreted with the aid of Figure 5.7. In this case, the transformation is delayed to much lower temperatures. It is incomplete at most of the coiling temperatures used for this study, leading to the possibility that different types of transformation products can form after the end of cooling.

The M_S temperature was calculated to be 432°C for the steel studied, using a formula from the literature[6]. In the case of the large austenite grain size specimens cooled at 55°C/s, when this temperature is reached, there is still a large volume fraction of untransformed austenite, which explains the presence of martensite in the specimens coiled at 300°C. In the finer grain size materials, by the time the M_S temperature is reached, the austenite has already completely transformed into ferrite plus second phase. This explains why no martensite was observed in these specimens, even when low coiling temperatures were employed.

V.3.4 Influence of cooling rate on transformation temperature.

From Figure 5.7, it can be observed that, when the cooling rate is increased from 55°C/s to 90°C/s, the A_{r3} temperature is lowered by 23°C. The measured values of A_{r3} are 675°C for the specimen cooled at 90°C/s and 698°C for the specimen cooled at 55°C/s. For better representativity, A_{r3} was taken as the temperature for 5% transformation.

Studies at IRSID have shown that the A_{r3} temperature is related to the cooling rate by the following formula:

$$A_{r3} = A_{r3}^{0}.C_r^{-a} \qquad (5.11)$$

where A_{r3}^{0} is the temperature of the beginning of the austenite-to-ferrite transformation when cooling takes place at 1°C/s, C_r is the cooling rate, and a is a positive constant.

Two specimens were tested at lower cooling rates, 2.5°C/s and 15°C/s. The transformation kinetics were deduced and are displayed in Figure 5.8. Both curves display

an inflection point which can be attributed to the beginning of the pearlite transformation The measured A_{r3}'s are 714°C for a cooling rate of 15°C/s and 747°C for a cooling rate of 2.5°C/s. These values are plotted against cooling rate in Figure 5 9, together with the curve fitted using equation (5 11). The parameters a and $A_{r3}°$ were found equal to 0.025 and 768°C, respectively. This last figure is in good agreement with the value of 7.'1°C calculated using formula (2.13).

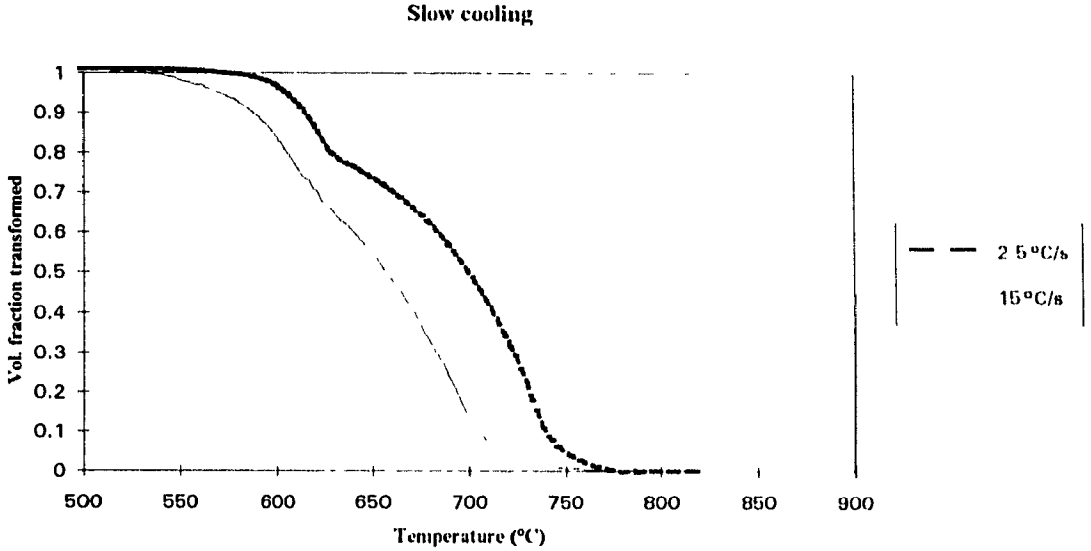

Figure 5.8 Kinetics curves for slow cooling

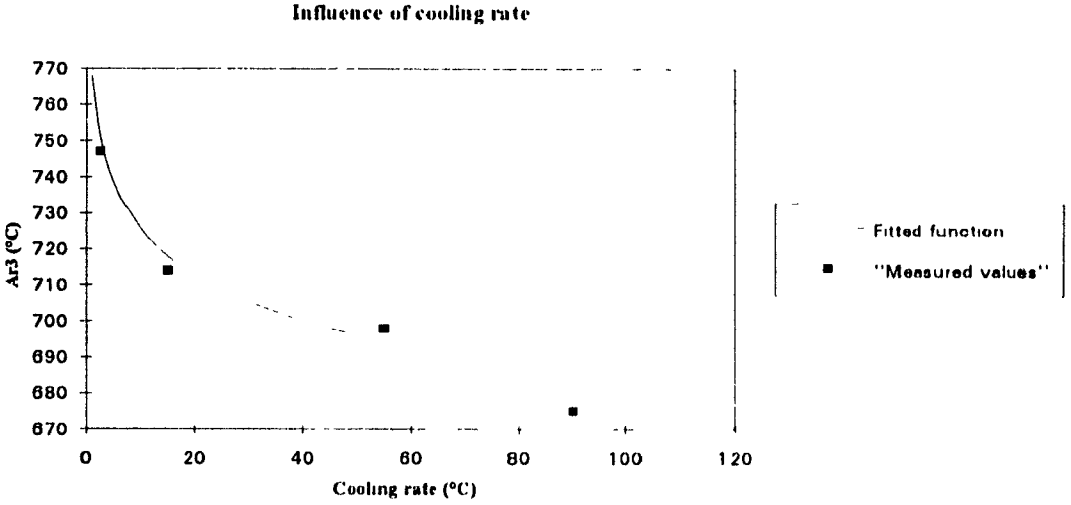

Figure 5.9 Dependence of A_{r3} on cooling rate.

The above results concerning the kinetics of transformation can be used to construct a CCT diagram for the steel studied The temperature for the beginning of the austenite-to-pearlite transformation is detectable on the slow cooling kinetics curves. For 2 5°C/s, A_{r1} is about 635°C At 15°C/s, it decreases to 625°C. At the faster cooling rates, the temperature of the beginning of the austenite-to-second phase (either fine pearlite or bainite) transformation is deduced from the proportion of second phase measured by metallography For a cooling rate of 55°C/s, the second phase represents 35% of the total volume For the same cooling rate, the temperature at which 35% of the austenite remains untransformed is 610°C For a cooling rate of 90°C/s, the volume fraction of second phase was 48%, which also corresponds to a temperature of 610°C The CCT diagram obtained in this way is given in Figure 5 10

The role of cooling rate is also clarified by the evolution of the shape of the transformation kinetics curve At low cooling rates, the curve is composed of two S-shaped portions corresponding, respectively, to ferrite and pearlite. This means that the ferrite has already finished transforming when the pearlite reaction occurs In other words, the critical composition for austenite-to-pearlite decomposition is reached before the critical temperature is attained When the cooling rate is increased, the temperature interval between these two events decreases, leading to a smoother curve. A further increase in cooling rate results in a completely smooth kinetics curve The ferrite is still transforming at its fastest rate when the critical temperature for pearlite transformation is reached. This is the case for the specimens cooled at 55°C/s. In this case, pearlite was observed, which means that the critical composition was attained at temperatures very close to the critical temperature At still faster cooling rates, the curve remains smooth. The critical composition for the pearlite reaction is no longer reached in the vicinity of the critical temperature, instead, another type of transformation takes place, leading to bainite as the second phase

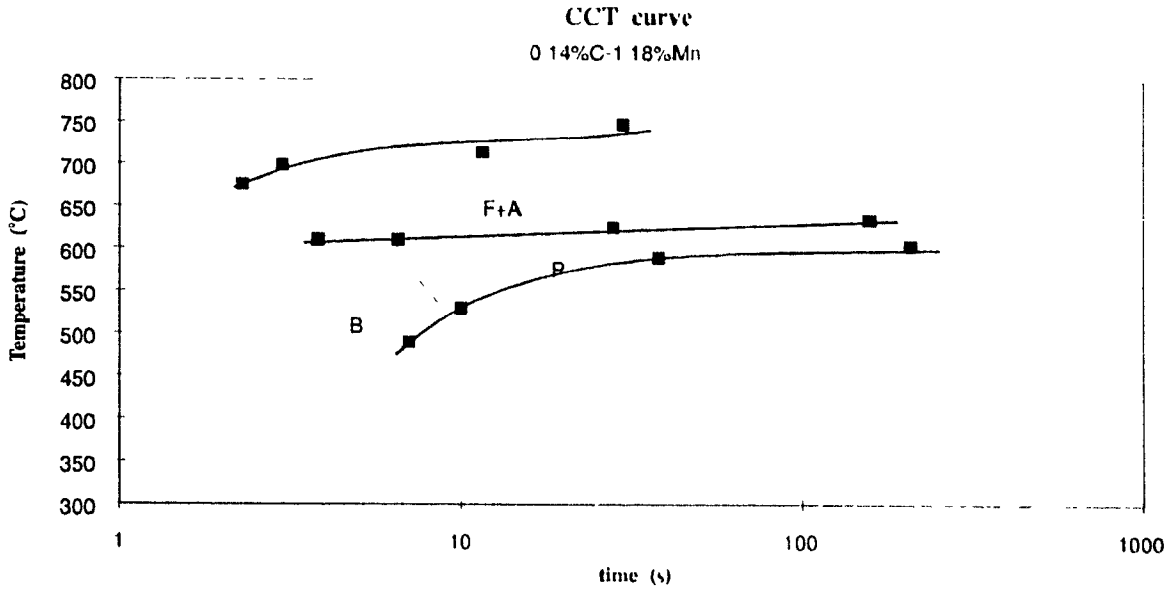

Figure 5 10 CCT diagram obtained from the kinetics data obtained by means of the IRSID method. F=Ferrite, A=Austenite, P=Pearlite and B=Bainite

V.3.5 Influence of the state of the austenite before cooling

The mechanical results (Chapter IV) showed that the state of the austenite before cooling had little influence in the case of the specimens cooled at 90°C/s This was confirmed by the transformation kinetics, which were unaffected by a change in reheating temperature from 850°C to 900°C The latter leads to an increase in austenite grain size from 13µm to 20µm Furthermore, when the strain was increased for the same cooling rate, no variation in mechanical properties was observed On the other hand, when a cooling rate of 55°C/s was employed, some influence could be detected, resulting in a delay of the transformation (Figure 5 6), and an increase in tensile strength when the reheating temperature was increased from 850°C to 900°C The amplitude of these variations remained small and could have been simply due to errors in measurement However, this phenomenon can also have a physical origin, as will be explained in what follows

As already mentioned in the literature review, Amano et al [13,18] studied the influence of strain and supercooling on ferrite nucleation for various steel compositions,

including a 0 15%C, 1 3%Mn, 0 3%Si steel They observed that, for limited supercooling, the strain increase resulted in a rapid increase in the amount of nucleation at grain boundaries, which reached saturation at a true strain of 0.2 (Figure 5.11). At the same time, the number of nuclei in the grain interiors increased steadily from zero at a strain of 0.1 to a maximum at a strain of 0.8 (Figure 5.12). Thus, for low supercooling and small strains, nucleation at grain boundaries was the dominant mechanism. On the other hand, when the supercooling was high, nucleation at both grain interiors and grain boundaries was maximized, even at low strains, resulting in little influence of the strain on ferrite nucleation. In this case, the number of nuclei in the grain interiors per unit volume was similar to that at the grain boundaries, so that nucleation in the grain interiors had a role equivalent to that of nucleation at the grain boundaries.

In the present study, reheating at different temperatures resulted in variations of the austenite grain size, which should lead to variations in the number of nuclei at the grain boundaries. In the case of slow cooling, which corresponds to low supercooling, nucleation at grain boundaries is dominant. This explains the observed variations in the transformation kinetics and mechanical properties In the case of fast cooling, corresponding to appreciable supercooling, there is substantial nucleation in the grain interiors For this reason, variations in the number of nuclei at the grain boundaries have a lesser influence on the subsequent transformation. This explains the absence of variations associated with changes in reheating temperature. The fact that, for large supercooling, both nucleation in the grain interiors and at grain boundaries are maximized, even at low strains, explains why no variations were observed when the strain was increased for a cooling rate of 90°C/s.

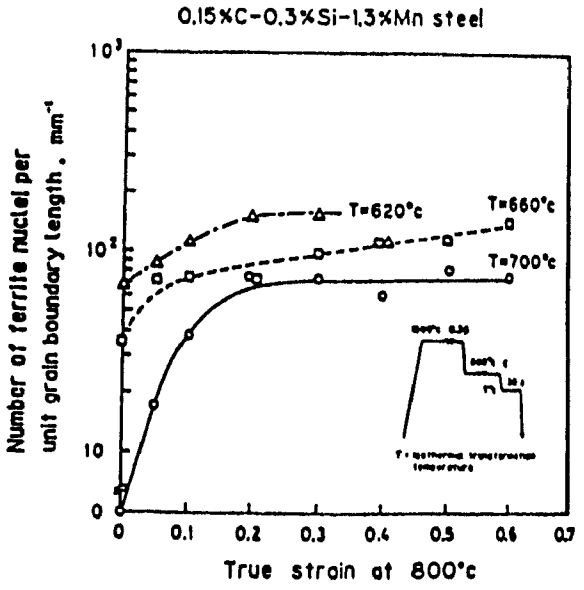

Figure 5.11 Number of ferrite nuclei per unit grain boundary length vs. true strain at 800°C as a function of isothermal transformation temperature.[18]

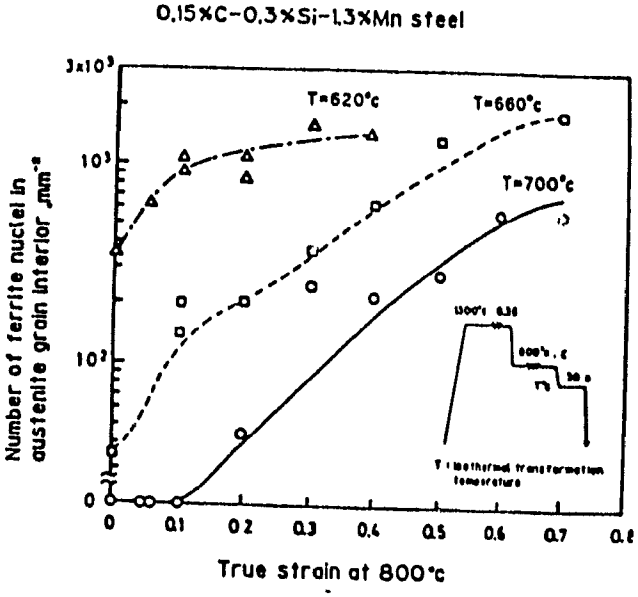

Figure 5.12 Number of ferrite nuclei in the grain interiors per unit area vs. true strain at 800°C as a function of isothermal transformation temperature.[18]

V.4 Consequences with respect to industrial practice

This study has shown that when the cooling rate is increased from 55°C/s to 90°C/s, an increase in tensile strength is obtained, with limited decrease in uniform elongation and little variation in yield ratio. This phenomenon is used to produce a direct as-hot-rolled high strength sheet steel with high strength and good formability. Its microstructure is composed of a mixture of a first phase consisting of polygonal and/or acicular ferrite, and a second phase composed of lath-like bainite and ferrite containing a fairly high density of carbides. It was shown that the cooling rate was the main factor affecting the microstructure and mechanical properties. Coiling temperature had no effect, provided it was below 500°C, because the transformations took place above this temperature. The state of the austenite before cooling had some effect when the cooling rate was low but none when it was high.

In a hot strip mill, the finish rolling temperature, cooling rate and coiling temperature are interrelated parameters. Depending on the type of cooling unit or on the operating conditions, the cooling rate can be adapted to allow the coiling temperature to be reached at the exit of the runout table, or the cooling rate is fixed and the number of water banks used is varied in order to attain the target coiling temperature. The first configuration certainly represents the most flexible solution. It is the type of cooling system used presently at SOLLAC for the production of HR55.

One consequence of this arrangement, however, is that detrimental variations in cooling rate can take place during the cooling of a single coil or between two coils of the same grade. This is particularly true if regulation of the runout table is based on the coiling temperature. To attain the cooling rate required to produce the desired microstructure and mechanical properties, it is necessary to aim for a low coiling temperature. The average cooling rate can be expressed as:

$$C_r = \frac{RT - CT}{t}$$

where RT is the finish rolling temperature, CT is the coiling temperature, and t is the time spent by the strip on the runout table.

If the finish rolling temperature is lowered but the coiling temperature is held constant by the controller, the cooling rate is decreased. This also happens when the speed of the strip is lowered, which results in an increase in the time spent on the runout table. In both cases, the microstructure and mechanical properties may be affected adversely.

The solution to this would be a control system that monitors the cooling rate rather than the coiling temperature This could be accomplished by taking variations in finish rolling temperature and rolling speed into account for the regulation of the water banks.

CHAPTER VI

CONCLUSIONS

This study had two objectives: 1) to identify the microstructures formed in a 0.14%C-1.18%Mn steel when it is hot rolled and cooled under conditions similar to those found industrially; 2) to understand the influence of the process parameters on the final microstructure and mechanical properties. For this purpose, torsion specimens were reheated to various temperatures, deformed to different strain levels, and cooled at either 55°C/s or 90°C/s, as measured in the austenite. Coiling temperatures ranging from 550°C to 300°C were employed. Metallographic investigations were carried out by means of optical and transmission electron microscopy. Tensile tests were also performed to measure the mechanical properties. Thermal analysis of the cooling curves provided information about the transformation kinetics. The following conclusions can be drawn from this work.

1. Standard hot rolling and cooling conditions, simulated by reheating at 850°C followed by the application of a strain of 0.2 and accelerated cooling at 90°C/s, result in a complex microstructure composed of polygonal and/or acicular ferrite, and a second phase consisting of lath-like bainite, together with ferrite containing a non-uniform distribution of carbides. This microstructure is associated with a tensile strength close to 560 MPa, a uniform elongation of about 14%, and a yield ratio falling between 0.7 and 0.75.

2. The lower cooling rate of 55°C/s results in the formation of pearlite instead of the bainite and ferrite containing a non-uniform distribution of carbides produced when the cooling rate of 90°C/s is employed. In this case, the tensile strength is decreased by approximately 30MPa. The uniform elongation is increased, but the yield ratio does

not change From this result, it is evident that the cooling rate has a strong influence on both the microstructure and mechanical properties. Its effect on the transformation temperatures conforms to the behavior described in the literature. The influence of cooling rate can be readily interpreted in terms of the CCT diagram derived from the transformation kinetics calculations.

3. For both the specimens cooled at 90°C/s and at 55°C/s from a fine austenite microstructure (obtained by reheating at 850°C or 900°C), the coiling temperature has no influence on the microstructure or on the mechanical properties. This is explained by the fact that the transformations all take place at temperatures above the highest coiling temperature.

4. When a very coarse austenite microstructure, atypical of hot strip mills and obtained by reheating at 1050°C, is present before accelerated cooling, the transformations are delayed to much lower temperatures. This results in a greater influence of coiling temperature on the microstructure and mechanical properties. The increased supercooling can be attributed to the large decrease in the number of nucleation sites available at grain boundaries.

5. When lower reheating temperatures are used, for which the austenite grain size remains between 10 and 20μm, the strain and austenite grain size have no influence on the microstructure and mechanical properties of the specimens cooled at 90°C/s and only limited influence on the specimens cooled at 55°C/s. This can be interpreted in terms of the greater importance of nucleation in the grain interiors for the higher cooling rate as opposed to nucleation at grain boundaries for the lower cooling rate.

6. As a consequence of these results, it is concluded that a regulation system which controls the cooling rate should have a beneficial effect on the quality of the product in comparison with a system that controls the coiling temperature.

References

[1] G. Diry, 'Solmer's 90-in. hot strip mill', Iron and steel engineer, vol.54, 1977, pp 33-38.

[2]R.I.L. Guthrie and J.J. Jonas, "Steel processing technology", Metals Handbook, ASM International, Materials Park, Ohio 44073, 1989, pp. 107-125.

[3] H B. Bowman, Handbook of Precision Sheet, Strip and Foil, ASM International, Metals Park, Ohio 44073, 1980.

[4] R.W.K. Honeycombe, The Plastic Deformation of Metals, Edward Arnold, Bedford Square, London, 1984.

[5] W.J. McG. Tegart and A. Gittins, "The hot deformation of austenite", The Hot Deformation of Austenite, ed. John B.Ballance, (Metallurgical Society of AIME,Warrendale, PA, 1977), pp.1-30

[6] A.K. Sinha, Ferrous Physical Metallurgy, Butterworths, 80 Montvale ave., Stoneham, MA 02180, 1989, p. 616.

[7]C.M. Sellars, "Modelling microstructural development during hot rolling", Materials Science and Technology, vol.6, nov. 1990, pp. 1072-1081

[8] J. H. Beynon and C M Sellars, "Modelling microstructure and its effects during multipass hot rolling", ISIJ International, vol. 32 (1992), No. 3, pp. 359-367.

[9]Christine Roucoules, "Dynamic and Metadynamic Recrystallization in HSLA Steels", Ph. D thesis, McGill University, Montreal, Canada, 1992

[10] C.M. Sellars, Hot Working and Forming Processes, ed. C.M Sellars and G J. Davies, The Metals Society, London, 1980, pp. 3-15.

References

[11] W. Roberts, A. Sandberg, T. Siwecki and T. Werlefors, HSLA Steels Technology and Applications, Proc Int. Conf., Philadelphia, ASM, (1984), p. 67.

[12]A. Hurkmans, G.A. Dutt, Th.M. Hoogendoorn, F. Hollander, "Accelerated cooling and the transformation of steel", Int. Symposium on Accelerated Cooling of Steel, Ed. P.D. Southwick, (Metallurgical Society of AIME,Warrendale, PA, 1985), pp. 481-499.

[13]J.W Christian, Transformations in Metals and Alloys, Pergamon Press, Oxford, U.K., 1975, p. 450.

[14]K Amano, T. Hatomura, M. Koda, C. Shiga, and T. Tanaka, "Moderation of controlled-rolling by accelerated cooling", Int. Symposium on Accelerated Cooling of Steel, Ed. P.D. Southwick, (Metallurgical Society of AIME,Warrendale, PA, 1985), pp. 349-365.

[15]M. Umemoto, "Mathematical modelling of phase transformation from work-hardened austenite", Mathematical Modeling of Hot Rolling of Steel", Ed S Yue, (Montreal, Que, Canada: The Canadian Institute of Mining and Metallurgy, 1990) pp. 404-423.

[16] P. Choquet, P. Fabrègue, J Giusti, B. Chamont, J.N. Pezant and F. Blanchet, " Modelling of forces, structure and final properties during the hot rolling process on the hot strip mill", Mathematical Modeling of Hot Rolling of Steel", ed. S Yue, (Montreal, Que, Canada: The Canadian Institute of Mining and metallurgy, 1990) pp. 34-43.

[17] M. Umemoto, H. Ohtsuka and I.Tamura, "Estimation of ferrite grain size from work-hardened austenite", Int. Conference on Physical Metallurgy of Thermomechanical Processing of Steel, THERMEC 88., ed. Imao Tamura, (Tokyo, Japan: ISIJ, 1988), pp. 791-799.

[18]K. Amano, T. Hatomura, C. Shiga and T Enami, "Effects of accelerated cooling on ferrite nucleation rate and second phase transformation behavior from deformed austenite", Int. Conference on Physical Metallurgy of Thermomechanical Processing of steel, THERMEC 88., ed. Imao Tamura, (Tokyo, Japan: ISIJ, 1988), pp. 368

References

[19]C. M. Vlad, "The effect of cooling rate on the transformation behaviour of deformed austenite", Int. Symposium on Accelerated Cooling of Steel, ed. P D. Southwick, (Metallurgical Society of AIME, Warrendale, PA, 1985), pp. 435-445.

[20] Sun Benrong, Zheng Xiuzhen, Zhu Ronglin and Sun Fuyu, "Effect of hot deformation on CCT curves", Int. Conference on Physical Metallurgy of Thermomechanical Processing of Steel, THERMEC 88., ed Imao Tamura, (Tokyo, Japan: ISIJ, 1988), pp. 412-419.

[21] M. Mizui, T. Sekine and M. Ejima, "Application of high-strength steel sheets to automotive wheels", Nippon Steel Technical Report, No. 23, June 1984, pp. 19-30.

[22]C. Lang and Th. Heidelauf, "Steels for passenger-car wheel fabrication", La revue de metallurgie, mai 1989, pp. 440-446.

[23]M.S. Rashid, "Relationship between steel microstructure and formability", Formable HSLA and Dual-Phase Steels, ed. A.T. Davenport, (New York, NY, The Metallurgical Society of AIME, 1977), pp. 57-63.

[24]R.G. Davies, "On the ductility of dual-phase steels", Formable HSLA and Dual-Phase Steels, ed. A.T Davenport, (New York, NY, The Metallurgical Society of AIME, 1977), pp 92-99.

[25]A.K. Sinha, Ferrous Physical Metallurgy, Butterworths, 80 Montvale ave., Stoneham, MA 02180, 1989, p. 629.

[26] A. Tivolle, A. Tardif and M. Perin, Revue de metallurgie CIT, 81 (décembre 1984), pp 925-930.

[27]A.P. Coldren and G. Tither, Journal of Metals, 30 (1978), pp. 6-9.

[28] S. Hanai, K. Watanabe and K. Esaka, "The manufacture of Si-Mn as-hot-rolled dual phase steel sheets", Journal of ISIJ, Tetsu to Hagane, vol.68, 1982, p.1306-1312.

[29] S. Hashimoto, M. Sudo and K. Mimura, "Effect of microstructures on mechanical properties of C-Mn high strength hot rolled sheet steel", Trans ISIJ 26 (1986), pp. 985-992.

References

[30] M. Sudo, M. Higashi, H. Hori, T Iwai, S. Kambe and Z. Shibata, "Effects of microstructures on the mechanical properties of multi-phase sheet steels", Trans ISIJ. 21 (1981), pp.820-827.

[31]M. Sudo, T. Iwai, S Hashimoto, T Hosoda and K. Hirata, "Effect of control cooling on the mechanical properties of as-hot-rolled multi-phase steel sheets, Int. Symposium on Accelerated Cooling of Steel, Ed. P.D Southwick, (Metallurgical Society of AIME,Warrendale, PA, 1985), pp. 501-519.

[32] M. Sudo, S. Hashimoto and S. Kambe, "Niobium bearing ferrite-bainite high strength hot-rolled sheet steel with improved formability. Trans ISIJ. 23 (1983), pp. 303-311.

[33] I.S. Kim, U. Reichel and W. Dahl, "Effect of bainite on the mechanical properties of dual phase steels", Steel Research, April 1987, pp. 186-190.

[34] N. Nagao, K. Kunishige, S. Hamamatsu and T. Nunokawa, "Hot rolled high strength steel sheet for automotive use produced by controlled cooling", Int Symposium on Accelerated Cooling of Steel, Ed. P.D. Southwick, (Metallurgical Society of AIME,Warrendale, PA, 1985), pp. 463-479.

[35]K. Kunishige and N. Nagao, "Microstructures and mechanical properties of high strength steel sheets taking full advantage of thermomechanical treatments on hot strip mills", The Sumitomo Search, No. 31 (1985), pp. 53-62.

[36] K Kunishige, "Strengthening mechanism in low temperature coiling and its application to the development of high-strength sheet-steels", Int. Conference on Physical Metallurgy of Thermomechanical Processing of Steel, THERMEC 88., ed. Imao Tamura, (Tokyo, Japan: ISIJ, 1988), pp. 480-486.

[37] C. Ouchi, T. Sampei and I. Kozasu; Trans. ISIJ, v.22, 1982, pp. 214-222.

[38] T. Kunitake and T Okada, "Continuous cooling transformation characteristics of some low alloy steels", Tetsu to Hagane Overseas, 5, (1965), pp. 27-33.

[39] B.L. Bramfitt and J.G Speer, "A perspective on the morphology of bainite", Metallurgical Transactions A, vol 21A, 1990, pp. 817-829.

[40]D. V. Edmonds and R.C. Cochrane, "Structure property relationships in bainitic steels", Metallurgical Transactions A, vol 21A, 1990, pp. 1527-1540.

[41] W.L. Roberts, Hot Rolling of Steel, Marcel Dekker, New York, 1983, p.641.

[42]M. Suehiro et al. "Mathematical model for predicting microstructural changes and strength of low carbon steels in hot strip rolling", Int. Conference on Physical Metallurgy of Thermomecanical Processing of Steel, THERMEC 88., ed. Imao Tamura, (Tokyo, Japan: ISIJ, 1988), pp 791-799.

[43] A. Hurkmans, G. Duit, T.M. Hoogendoorn, F. Hollander, "Accelerated cooling and the transformation of steel", Int. Symposium on Accelerated Cooling of Steel, Ed. P D. Southwick, (Metallurgical Society of AIME,Warrendale, PA, 1985), pp 481-499.

[44]A.J. Chapman, Heat Transfer, Macmillan Publishing, New York, 1974.

[45]G.M. Dusinberre, Heat-Transfer Calculations by Finite Differences, International Textbook Company, Scranton, PA, 1961.

[46]F.S. Le Pera, "Improved etching technique for the determination of percent martensite in high-strength dual-phase steels", Metallography, 12, 1979, pp. 263-268.

[47]Standard methods of tension testing of metallic materials, ASTM Designation E8-69, "Annual Book of ASTM Standards,' American Society for Testing and Materials, Philadelphia.

[48]M.J. Barba, Memoires de la Société des Ingénieurs Civils, pt.1, p 682, 1880.

APPENDIX I

Computer program for the calculation of the temperature gradients on cooling of a torsion specimen

```
var i,j,n:integer;
   typ:array[0..10,0..29] of integer;
   T1,T2:array[0..10,0..29] of real;
   k,k1,h,t,deltat,dr,dL,v,r,a,x,Long,s,rho,cp,lambda,Tout,Tbar,Tini:real;
   result,donne:text;
   nomfich:string[20];


procedure comon;
   begin
    r:=i*dr;
    if i=0 then v:=pi*sqr(dr/2)*dL
    else
    v:=pi*(sqr(r+dr/2)-sqr(r-dr/2))*dL;
    a:=-2*pi*dL/(v*rho*Cp);
    s:=-1/(dL*rho*Cp);
   end;


function Tnoeud1(u,v:integer):real;
   var q1,q2,q3,q4:real;

   begin
   q1:=k*(T1[u,v]-T1[u-1,v])/dr;
   q2:=k*(T1[u,v]-T1[u,v-1])/dL;
   q3:=k*(T1[u,v]-T1[u+1,v])/dr;
   q4:=k*(T1[u,v]-T1[u,v+1])/dL;
   Tnoeud1:=a*(q3*(r+dr/2)+q1*(r-dr/2))*deltat+s*(q4+q2)*deltat+T1[u,v];
   end;

function Tnoeud9(u,v:integer):real;
   var q1,q2,q3,q4:real;

   begin
   q1:=0;
   q2:=k*(T1[u,v]-T1[u,v-1])/dL;
   q3:=k*(T1[u,v]-T1[u+1,v])/dr;
   q4:=k*(T1[u,v]-T1[u,v+1])/dL;
   Tnoeud9:=a*(q3*(r+dr/2)+q1*(r-dr/2))*deltat+s*(q4+q2)*deltat+T1[u,v];
   end;

function Tnoeud2(u,v:integer):real;
   var q1,q2,q3,q4:real;

   begin
```

```
    q1:=k*(T1[u,v]-T1[u-1,v])/dr;
    q2:=k*(T1[u,v]-T1[u,v-1])/dL;
    q3:=-lambda*(Tout-T1[u,v]);
    q4:=k*(T1[u,v]-T1[u,v+1])/dL;
    Tnoeud2:=a*(q3*(r+dr/2)+q1*(r-dr/2))*deltat+s*(q4+q2)*deltat+T1[u,v];
    end;

function Tnoeud3(u,v:integer):real;
    var q1,q2,q3,q4:real;

    begin
    q1:=k*(T1[u,v]-T1[u-1,v])/dr;
    q2:=-lambda*(Tout-T1[u,v]);
    q3:=k*(T1[u,v]-T1[u+1,v])/dr;
    q4:=k*(T1[u,v]-T1[u,v+1])/dL;
    Tnoeud3:=a*(q3*(r+dr/2)+q1*(r-dr/2))*deltat+s*(q4+q2)*deltat+T1[u,v];
    end;


function Tnoeud4(u,v:integer):real;
    var q1,q2,q3,q4:real;

    begin
    q1:=k*(T1[u,v]-T1[u-1,v])/dr;
    q2:=k*(T1[u,v]-T1[u,v-1])/dL;
    q3:=k*(T1[u,v]-T1[u+1,v])/dr;
    q4:=-lambda*(Tout-T1[u,v]);
    Tnoeud4:=a*(q3*(r+dr/2)+q1*(r-dr/2))*deltat+s*(q4+q2)*deltat+T1[u,v];
    end;


function Tnoeud5(u,v:integer):real;
    var q1,q2,q3,q4:real;

    begin
    q1:=k*(T1[u,v]-T1[u-1,v])/dr;
    q2:=-lambda*(Tout-T1[u,v]);
    q3:=-lambda*(Tout-T1[u,v]);
    q4:=k*(T1[u,v]-T1[u,v+1])/dL;
    Tnoeud5:=a*(q3*(r+dr/2)+q1*(r-dr/2))*deltat+s*(q4+q2)*deltat+T1[u,v];
    end;

function Tnoeud6(u,v:integer) real;
    var q1,q2,q3,q4:real;

    begin
    q1:=0;
    q2:=-lambda*(Tout-T1[u,v]);
    q3:=k*(T1[u,v]-T1[u+1,v])/dr;
    q4:=k*(T1[u,v]-T1[u,v+1])/dL;
    Tnoeud6:=a*(q3*(r+dr/2)+q1*(r-dr/2))*deltat+s*(q4+q2)*deltat+T1[u,v];
    end;

function Tnoeud7(u,v:integer).real;
```

```
    var q1,q2,q3,q4:real;

    begin
    q1:=k*(T1[u,v]-T1[u-1,v])/dr;
    q2:=k*(T1[u,v]-T1[u,v-1])/dL;
    q3:=-lambda*(Tout-T1[u,v]);
    q4:=-lambda*(Tout-T1[u,v]);
    Tnoeud7:=a*(q3*(r+dr/2)+q1*(r-dr/2))*deltat+s*(q4+q2)*deltat+T1[u,v];
    end;

function Tnoeud8(u,v:integer):real;
    var q1,q2,q3,q4:real;

    begin
    q1:=k*(T1[u,v]-T1[u-1,v])/dr;
    q2:=k*(T1[u,v]-T1[u,v-1])/dL;
    q3:=k*(T1[u,v]-T1[u+1,v])/dr;
    q4:=k*(T1[u,v]-Tbar)/dL;
    Tnoeud8:=a*(q3*(r+dr/2)+q1*(r-dr/2))*deltat+s*(q4+q2)*deltat+T1[u,v];
    end;

function Tnoeud10(u,v:integer):real;
    var q1,q2,q3,q4:real;

    begin
    q1:=0;
    q2:=k*(T1[u,v]-T1[u,v-1])/dL;
    q3:=k*(T1[u,v]-T1[u+1,v])/dr;
    q4:=-lambda*(Tout-T1[u,v]);
    Tnoeud10:=a*(q3*(r+dr)+q1*r)*deltat+s*(q4+q2)*deltat+T1[u,v];
    end;

procedure initialisation;
var typ1:integer;
  begin
  i:=0;
  j:=0;
  while i<9 do
    begin
    j:=0;
     while j<19 do
     begin
     read(donne,typ1);
     typ[i,j]:=typ1;
     if typ1=0 then T1[i,j]:=0
     else
     T1[i,j]:=Tini;
     T2[i,j]:=0;
     j:=j+1;
     end;
   i:=i+1;
  end;
end;
```

```
procedure ecritresult;
var ii,jj:integer;
  begin
  ii:=0;
  jj:=0;
  while ii<9 do
   begin
   jj:=0;
   writeln(result,' ');
   While jj<19 do
    begin
    write(result,T2[ii,jj] 3:0,' '),
    jj:=jj+1;
    end;
   ii:=ii+1;
  end;
 end;
procedure echresult,
var ii,jj:integer;
  begin
  ii:=0;
  while ii<9 do
   begin
   jj:=0;
   While jj<19 do
    begin
    T1[ii,jj]:=T2[ii,jj];
    jj:=jj+1;
    end;
   ii:=ii+1;
  end;
 end;

begin
   n:=0;
   t:=0;
   k:=28;
   k1:=0.143;
   deltat:=0.001;
   dr:=0.91/1000,
   dL:=3.171/1000
   h:=0.0002;
   lambda:=k1/h,
   rho:=7900;
   Cp:=585;
   Tout:=20;
   Tbar:=850;
   Tini:=850;

   assign(donne,'d:\bd\donne dat');
   reset(donne);
   initialisation,
   close(donne);
   assign(result,'d.\bd\result.dat');
```

```
    rewrite(result);
    i:=0;
    j:=0;
    while t<10 do
     begin
     i:=0;
     while i<9 do
       begin
       comon,
       j:=0;
       While j<19 do
        begin
        if typ[i,j]=0 then T2[i,j]:=0;
        if typ[i,j]=1 then T2[i,j]:=Tnoeud1(i,j);
        if typ[i,j]=2 then T2[i,j]:=Tnoeud2(i,j);
        if typ[i,j]=3 then T2[i,j]:=Tnoeud3(i,j);
        if typ[i,j]=4 then T2[i,j]:=Tnoeud4(i,j);
        if typ[i,j]=5 then T2[i,j]:=Tnoeud5(i,j);
        if typ[i,j]=6 then T2[i,j]:=Tnoeud6(i,j);
        if typ[i,j]=7 then T2[i,j]:=Tnoeud7(i,j);
        if typ[i,j]=9 then T2[i,j]:=Tnoeud9(i,j),
        if typ[i,j]=11 then T2[i,j]:=Tini;
        j:=j+1;

       end;
      i:=i+1;
    end;
  echresult;
  n:=n+1,
  if n/1000-trunc(n/1000)=0 then
  begin
   ecritresult;
   writeln(n,t);
  end;
  t:=t+deltat;
  end;
 close(result);
 end.
```

APPENDIX II

Computer program based on Sellar's model for the calculation of the austenite grain sizes and fraction recrystallized after each pass in the hot strip mill.

```
{$N+}{$E+}
program sellars;
uses crt;
var i,j,k,n:integer;
   tpass,davant,epsilon,t05,z,r:array[1..10] of real;
   interpass,epspoint,epspeak,epsetoile,epsres:array[1..10] of real;
   q,glop,v,t95,dmoy:real;
   nomdat,answer:string[20];
   dpass,donpass,resim:text;

function puiss(a,b:real):real;
      begin
      puiss:=exp(b*ln(a));
      end;
{-------------------------------------------------------------------------}
procedure torsion(n:integer);
var k:integer;
   temp,strain,interp,strainrate:real;
begin
for k:=1 to n do
begin
 writeln('temperature of pass',k);
 readln(temp);
 writeln('strain?');
 readln(strain);
 writeln('interpass');
 readln(interp),
 writeln('strain rate?');
 readln(strainrate);
 writeln(donpass,temp,' ',strain,' ',interp,' ',strainrate);
 end;
end;
{-------------------------------------------------------------------}
procedure entredonne;       {input the data}
var v1,v,r,h0,hcalc,h1,tpass,epsilon,interpass,epsilonpoint,hfin:real,
   k,L,tempini,davant,tpassnew.real,
   answer1,i,n:integer;
begin
writeln('you want to enter the strain,temperature conditions (1)'),
writeln('or to enter a rolling schedule (thicknesses and mill conditions) (2)');
readln(answer1);
K:=0.16317;                    {the data ie  strain per pass}
L:=1500;                      {temperatures,strain rate}
writeln('name of file');          {interpass time will be stored}
read(nomdat);                  {in file c.\bd\tp\nomdat.dat  }
nomdat:='d:\bd\tp\'+nomdat+'.dat';
assign(donpass,nomdat);
```

```
rewrite(donpass);
writeln('n'),
readln(n);
writeln(donpass,n),
writeln('initial grain size');
readln(davant),
if answer1=1 then torsion(n)
else
begin
 writeln('radius of the rolls');
 readln(r);
 writeln('final thickness');
 readln(hfin);
 v1:=28000/hfin,
 writeln('initial thickness');
 readln(h0);
 writeln(' initial temperature');
 readln(tempini);
 tpass:=tempini;
 i:=1;
 while i<n+1 do
 begin
 writeln('final thickness of pass',i);
 readln(h1);
 epsilon.=-ln(h1/h0);
 hcalc:=(h0+h1)/2,
 epsilonpoint:=2*v1*hfin*sqrt(-sqr(h1)-sqr(hcalc)-4*r*h1+4*r*hcalc+2*h1*hcalc)/(2*r+h1-
hcalc)/sqr(hcalc);
 writeln('strain rate',epsilonpoint),
 v:=v1*hfin/h1;
 interpass:=7000/v;
 writeln('temperature',tpass);
 tpassnew:=tpass-K*(h1+L)*tpass*interpass/h1/L;
 h0:=h1;
 end;
writeln(donpass,tpass,' ',epsilon,' ',interpass,' ',epsilonpoint);
i:=i+1;
end;
writeln(donpass,davant);
close(donpass);
end;
{-------------------------------------------------------------}


procedure initialisation;
        begin
        i =1,
        while i<n+1 do
        begin
        readln(dpass,tpass[i],epsilon[i],interpass[i],epspoint[i]);
        davant[i]:=0;
        t05[i]:=0;
        {t95[i]:=0;}
        z[i]:=0;
```

```
        epspeak[i]:=0;
        epsetoile[i]:=0;
        epsres[i]:=0;
        i:=i+1;
        end;
        read(dpass,davant[1]);
        epsilon[n+1]:=0;
        end;

{-------------------------------------------------------------------}
{ Main programm: performs the calculations of Sellars model        }
{-------------------------------------------------------------------}
begin
    clrscr;
    writeln('do you want to enter new rolling schedule');
    readln(answer);
    if answer='yes' then
     entredonne
    else
     begin
     writeln('filename for old schedule');
     read(nomdat);
     nomdat:='d:\bd\tp\'+nomdat+'.dat';
    end;
    assign(dpass,nomdat),
    reset(dpass);
    read(dpass,n);
    initialisation;
    write('nombre de passe');
    write(n);
    writeln(davant[1]);
    epsres[1]:=epsilon[1];
    i:=1;
    writeln('davant eps  epsres interp epspoint epsp  t05  ri+1  epsresi+1 epsetoile'),
    while i<n+1 do
    begin
    q:=3.12e5/(8.14*(tpass[i]+273));
    z[i]:=epspoint[i]*exp(q);
    epspeak[i]:=4.9e-4*puiss(davant[i],0.5)*puiss(z[i],0.15);
    if epsres[i]<=0.8*epspeak[i] then
    t05[i]:=2.5e-19*sqr(davant[i])*puiss(epsres[i],-4)*exp(3e5/8.14/(tpass[i]+273))
    else
    t05[i]:=1.06e-5*puiss(z[i],-0.6)*exp(3e5/8.14/(tpass[i]+273)),
    t95:=t05[i]*puiss(-ln(0.05)/0.693,1/1.5);
    epsetoile[i]:=2.8e-4*puiss(davant[i],0.67)*puiss(z[i],0.15);
    if epsres[i]<epsetoile[i] then
    davant[i+1]:=0.5*puiss(davant[i],0.67)/epsres[i]
    else
    davant[i+1]:=1.8e3*puiss(z[i],-0.15);
    v:=ln(0.5)*puiss(interpass[i]/t05[i],1.5);
    if v<-88 then r[i]:=1
    else
    r[i]:=1-exp(v);
    davant[i+1]:=davant[i]*davant[i+1]/puiss(r[i]*puiss(davant[i],3)+(1-r[i])*puiss(davant[i+1],3),1/3);
```

```
if interpass[i]>t95 then
begin
 davant[i+1]:=puiss(davant[i+1]/1000,10);
 davant[i+1].=davant[i+1]+5.02e23*(interpass[i]-t95)*exp(-914000/8.14/(tpass[i]+273));
 davant[i+1]·=1000*puiss(davant[i+1],0.1);
end;
epsres[i+1]:=epsilon[i+1]+(1-r[i])*epsres[i];
write(davant[i]:5:2,' ',epsilon[i]:5:3,' ',epsres[i]:5:3,' ',interpass[i]:5:3,'  ',epspoint[i]:5:3);
writeln('   ',epspeak[i]:5:2,' ',t05[i]·5 2,' ',r[i]:5·3,' ',(1-R[I])*epsres[i]:5:3,' ',epsetoile[i]:5:3 );
i:=i+1;
end;
write(davant[i]:5:2,'          ',epsres[i].5·3);
readln;
readln,
end.
```

APPENDIX III

Computer program for the deduction of the transformation kinetics from the cooling data by the IRSID method.

```
uses Graph,crt;


var donne,result,inter:text;
   str1:string[1];
   reponse:string[4];
   nomfich,namefile:string[30];
   time,temp1,temp2,T,lam1,lam2,ls1,ls2,ts1,ts2,ts3.real,
   alam,blam,nlam,cor:real;
   key:char;
   xf1,yf1,ya1:integer;
{************************************************************************}
function puiss(x,y:real):real,                  {power function which does}
begin                                           {not exist in pascal     }
puiss:=exp(y*ln(x));
end;
{************************************************************************}


 procedure traitement_fichier;                  {to get rid of the useless text}
                                                {in the source file          }
 begin                                          {the destination file is named }
 readln(nomfich);
 namefile:='d:\bd\'+nomfich+'.dat';              {inter lam                   }
 writeln(namefile);
 assign(donne,namefile);                        {it only contains the time and }
 assign(inter,'d:\bd\inter.lam');               {real temperature data       }
 reset(donne);
 rewrite(inter);
 str1:='a';
 while (str1<>'1') and (str1<>'0') do
  begin
   readln(donne,str1);
   write(str1);
  end;
 While not eof(donne) do
  begin
  readln(donne,time,temp1,temp2);
  writeln(inter,time:6:3,' ',temp2:3:2);
  end;
  close(inter);
  close(donne);
```

```
 end;

{ ************************************************************************}

function Cpa(T:real):real;                    { calculates Cp of alpha phase }
var a1,b1,c1,d1:real;                         { at the temperature T        }
begin                                         { Cp expressed in kJ/g/K      }
if T<527 then
 begin
 a1:=28.175;
 b1:=-7.318;
 c1:=-2.895;
 d1:=25.041;
 end;
if (T>527) and (T<727) then
 begin
 a1:=-263.454;
 b1:=255.810;
 c1:=619.232;
 d1:=0;
 end;
if (T>727) and (T<769) then
 begin
 a1:=-641.905; b1:=696.339; c1:=0; d1:=0,
 end;
if (T>769) and (T<787) then
 begin
 a1:=1946.255; b1:=-1787.497; c1:=0; d1.=0;
 end;
if (T>787) then
 begin
 a1:=-561 932; b1:=334.143; c1:=2912.114; d1:=0;
 end;
cpa:=(a1+0.001*b1*(T+273)+1e5*c1/sqr(T+273)+1e-6*d1*sqr(T+273))/55.847;
end;

{************************************************************************}
function Cpg(T:real).real;          {calculates Cp of the gamma phase}
var a1,b1:real;
begin
a1:=23.991; b1:=8.360;
cpg:=(a1+0.001*b1*(T+273))/55.847;
end;
{************************************************************************}


function deltaH(T:real):real,                 { calculates the delta H for the }
var a1,b1:real;                               { gamma to alpha transformation  }
begin
 if (T>700) then
 begin a1:=-0.03473; b1.=33.075988; end;
 if (T<700) and (T>500) then
 begin a1:=-0.02176; b1:=23 935988; end;
 if (T<500) then
```

```
 begin a1:=-0.0134; b1:=18.34; end;
 deltah:=a1*T+b1;
end;
{ ************************************************************************}
procedure calcul_lambda;
var T1,T2,time,Cpfer,Cpaust,lamfer,lamaust:real;
                                        { this calculates values of }
 begin                                  { lambda in the case of a   }
 write('coucou');
 assign(donne,'d:\bd\inter.lam');       { completely ferritic or    }
 assign(inter,'d:\bd\inter1.lam');      { completely austenitic     }
 reset(donne);                          { specimen                  }
 rewrite(inter);                        { values are stored in a new}
 readln(donne,time,T1);                 { file: inter1.lam          }
 while not eof(donne) do
  begin
  readln(donne,time,T2);
  Cpfer:=Cpa(T1/2+t2/2);
  Cpaust:=Cpg(T1/2+t2/2);
  lamfer:=Cpfer*(T1-T2)/(T1/2+t2/2-25)/0.2;
  lamaust:=Cpaust*(T1-T2)/(T1/2+t2/2-25)/0.2;
  writeln(inter,time:3:3,' ',T1:4:2,' ',lamfer:3:4,' ',lamaust:3:4);
  T1:=T2;
  end;
 close(donne);
 close(inter);
 end;
{ ************************************************************************}
procedure trace;                                { this draws a line between two }
var time:real;                                  { successive values of lambda   }
   xf2,yf2,ya2:integer;
    begin
    readln(donne,time,T,lam1,lam2);
    Xf2:=trunc(320*(T-300)/600)+320;
    Yf2:=-trunc(240*lam1/0.1)+256;
    ya2:=-trunc(240*lam2/0.1)+256;
    line(xf1,yf1,xf2,yf2);
    line(xf1,ya1,xf2,ya2);
    xf1:=xf2; yf1:=yf2; ya1:=ya2;
    end;

{************************************************************************}
procedure draw_lambda;                  { this makes a graph of the values of lambda}
                                        { then it allows to chose the first and last}
                                        { value of lambda which will be used in the }
 var                                    { calculation of a theoretical curve for lambda}
   Gd, Gm : Integer;
   touche:char;
   time:real;
   xf2,yf2,xa2,ya2,x1,x2,y1,y2,n.integer;
   text:string[4];
   p:pointer;
   size:word;
```

```
begin
 n:=0;
 assign(donne,'d.\bd\inter1.lam');
 reset(donne);
 Gd:=0;
 InitGraph(Gd,gm, 'c:\tp\bgi');
 bar(320,16,639,256);
 setcolor(2);
 Rectangle(320,16,639,256);
 readln(donne,time,T,lam1,lam2);
 Xf1:=trunc(320*(T-300)/600)+320;
 Yf1:=-trunc(240*lam1/0.1)+256;
 ya1:=-trunc(240*lam2/0.1)+256;

 while not eof(donne) do
  trace;
            {***}
  reset(donne);
  setcolor(4);
  x1:=320;y1:=16;x2:=639;y2:=256;
  while not eof(donne) do
  begin
   trace;
   touche:=readkey;
    if touche='a' then
    begin
     Ts1:=T;
     ls1:=lam2;
    end;
   if touche='b' then
    begin
     Ts2:=T;
     ls2:=lam1;
    end;
   if touche='c' then
   begin
   close(donne);
   Ts3:=T;
    exit;
   end;
    n:=n+1;
  end;
  ReadLn;

 close(donne);
 end;

{ ************************************************************************}
procedure lacalc;                { this calculates the parameters in the theoretical }
 begin                           { curve for lambda                      }
 nlam:=0.28;
 blam:=(ls1-ls2)/(1/(ts1-25)-1/(ts2-25));
 alam:=ls1-blam/(ts1-25);
 writeln(alam:3:4,blam:3:4);
```

```
  end;
{*************************************************************************}
procedure kinetics;                    { this calculates the kinetics of}
  var time,z,Cp,dz,deltH,T1,T2:real;   { decomposition from austenite  }
      lambda:real;                     { to ferrite                    }


  begin
  assign(donne,'d:\bd\inter.lam');
  namefile:='d:\bd\'+nomfich+'.lam';
  assign(result,namefile);
  reset(donne);
  rewrite(result);
  z:=0;
  readln(donne,time,T1);
  while not eof(donne) do
   begin
    readln(donne,time,T2);
    if T2>ts1 then z:=0
     else
    begin
     if T2<ts3 then
      begin
      close(donne);
      close(result);
      exit;
      end
     else
      begin
       lambda:=alam+blam/(T1/2+t2/2-25);
        Cp:=(1-z)*Cpg(T1/2+t2/2)+z*Cpa(T1/2+t2/2);
       dz:=(lambda*(T1/2+t2/2-25)*0.2-Cp*(T1-T2))/deltah(T1/2+t2/2)/cor;
       z:=z+dz;
      end;
    end;
   writeln(result,time:4:4,'   ',T2:4:4,'   ',z:4:4);
   T1:=T2;
   end;
 close(donne);
 close(result);
 end;

{*************************************************************************}
procedure draw_kin;
 var                                   { calculation of a theoretical curve for lambda}
   Gd, Gm : Integer;
   time,z:real;
   xf2,yf2,xa2,ya2,x1,x2,y1,y2,n:integer;
   xl1,xl2,yl1,yl2,n1:integer;
   text:string[4];
   p:pointer;
   size:word;

 begin
```

```
    n:=0;
    assign(donne,namefile),
    reset(donne),
    bar(320,240,639,480);
    setcolor(2);
    Rectangle(320,240,639,480),
    readln(donne,time,T,z);
    line(320,260,639,260);
    Xf1:=trunc(320*(T-300)/600)+320;
    Yf1:=-trunc(240*z)+480;
    yl1:=-trunc((alam+blam/(T-25))/0.1*240)+256,
    while not eof(donne) do
    begin
    readln(donne,time,T,z);
    Xf2:=trunc(320*(T-300)/600)+320;
    Yf2:=-trunc(220*z)+480;
    yl2:=-trunc((alam+blam/(T-25))/0.1*240)+256;
    line(xf1,yf1,xf2,yf2);
    line(xf1,yl1,xf2,yl2);
    xf1:=xf2; yf1:=yf2,yl1:=yl2;
    end;
    close(donne);
    end;

{ ************************************************************************}

 procedure principale;
 var cortex.string[5];
 begin
 draw_lambda;
 lacalc;
 cor:=4.184;
 repeat
  begin
   kinetics,
   draw_kin;
   key:=readkey;
   if key='+' then
   cor:=cor+0.05;
   if key='-' then
   cor:=cor-0.05;
   end;
   str(cor:2:2,cortex);
   outtext(cortex);
 until key='o';
 closegraph;
 end;
 {************************************************************************}
  begin
 traitement_fichier;
 calcul_lambda;
 repeat
 begin
 principale;
```

```
writeln('satisfait');
readln(reponse);
end;
until reponse=('oui');

end.
```